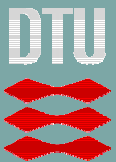


Simon Furbo  
Elsa Andersen  
Jørgen M. Schultz

Advanced storage concepts for solar  
thermal systems in low energy buildings  
Slutrapport

DANMARKS  
TEKNISKE  
UNIVERSITET



Sagsrapport  
BYG· DTU SR-06-01  
2006  
ISSN 1601 - 8605



## **FORORD**

Denne rapport udgør slutrapporten for EFP 2003 projektet “Advanced storage concepts for solar thermal systems in low energy buildings”, j.nr. 1213/03-0001.

Projektet, som er finansieret af Energistyrelsen, er den danske del af IEA Task 32 projektet “Advanced storage concepts for solar thermal systems in low energy buildings” i perioden 2003-2005.

IEA Task 32 projektet gennemføres i perioden 2003-2007. Forhåbentlig vil der ved hjælp af et nyt projekt blive mulighed for dansk deltagelse i Task 32 projektet, også i perioden 2006-2007.

## INDHOLDSFORTEGNELSE

<b>1. Projektsammenfatning .....</b>	<b>5</b>
<b>2. Smeltevarmelagre.....</b>	<b>5</b>
2.1. Forsøgsopstilling .....	6
2.2. Forsøgsresultater.....	7
<b>Bilag 1</b>	
Insulation materials for advanced water storages.....	11
<b>Bilag 2</b>	
Heat of fusion storage systems for combined solar systems in low energy buildings. ....	29
<b>Bilag 3</b>	
Investigation of heat of fusion storage for solar low energy buildings. ....	41
<b>Bilag 4</b>	
Theoretical and Experimental investigations of Inlet stratifiers for Solar Storage Tanks.....	49
<b>Bilag 5</b>	
Investigations of the SOLVIS stratification inlet pipe for solar storage tanks.....	65
<b>Bilag 6</b>	
Investigations of solar combi systems.....	77
<b>Bilag 7</b>	
Investigations of fabric stratifiers for solar tanks.....	85
<b>Bilag 8</b>	
Performance improvement by discharge from different levels in solar storage tanks. ....	93
<b>Bilag 9</b>	
Investigations of medium sized solar combi systems.....	105

## Projektsammenfatning

Task 32 projektets formål er, i et internationalt samarbejde, at udvikle nye/avancerede varmelagertyper, som er økonomisk og teknisk velegnede som langtidsvarmelagre til solvarmeanlæg med høje dækningsgrader.

Den danske deltagelse i projektet har været fokuseret om subtask A, C og D:

I subtask A er der ydet bidrag til en statusrapport på varmelagerområdet. Det danske bidrag fremgår af bilag 1.

I subtask C er der arbejdet med smeltevarmelagre baseret på salthydratet  $\text{NaCH}_3\text{COO}\cdot 3\text{H}_2\text{O}$  med smeltepunktet  $58^\circ\text{C}$ . En blanding bestående af 98,0-99,9% natriumacetat og 0,1-2,0% xanthangummi har den attraktive egenskab at den underafkøler stabilt. For denne blanding kan man styre, hvornår størkningen sættes i gang, for eksempel ved at påføre den smeltede blanding en stor forskydningsspænding eller et salthydratkrystal. Blandingen kan benyttes som varmeakkumulerende materiale i langtidsvarmelagre med meget små varmetab, idet lagrene kun taber varme til omgivelserne under opladning og afladning samt i den første del af underafkølingsperioden indtil omgivelsestemperaturen er nået. I den periode, hvor lageret henstår underafkølet ved omgivelsestemperaturen, er lageret tabsfrit.

Der er gennemført teoretiske og eksperimentelle undersøgelser for at klarlægge hvorledes lageret bedst udformes. Undersøgelserne viste, at et solvarmeanlæg med et relativt lille solfangerareal med et modulopbygget smeltevarmelager, der udnytter underafkølingsprincippet, kan dække hele varmebehovet og varmtvandsforbruget i et lavenergihus, mens et tilsvarende solvarmeanlæg med et traditionelt vandlager, uanset hvor stort lagervolumenet er, ikke kan dække varmebehovene fuldstændigt på grund af vandlagerets varmetab. Det er således i huse med et solvarmeanlæg med et smeltevarmelager muligt at undvære andre varmeanlæg.

I subtask D er der gennemført teoretiske og eksperimentelle undersøgelser af hvorledes avancerede vandlagre til solvarmeanlæg til kombineret rumopvarmning og brugsvandsopvarmning bedst udformes. Forskellige lagertyper, inklusive en markedsført varmelagerunit med et indbygget supplerende energianlæg, er inkluderet i undersøgelserne. Desuden er de ydelsesmæssige fordele ved at benytte stratifikationsindløbsrør og aftapning af varme fra lageret fra forskellige niveauer i lageret klarlagt. Forskellige stratifikationsindløbsrør er undersøgt eksperimentelt. Blandt andet er et nyudviklet billigt stratifikationsindløbsrør bestående af flere lag stof undersøgt. Dette stratifikationsindløbsrør har vist sig at fungere lige så godt som det bedste langt dyrere markedsførte stratifikationsindløbsrør. Undersøgelserne fremgår af bilag 4-8.

## 2. Smeltevarmelagre

De teoretiske undersøgelser, som kort er omtalt i kapitel 1, fremgår af bilag 2 og 3. Desuden er der gennemført eksperimentelle undersøgelser af et forsøgssmeltevarmelager i laboratoriet med natriumacetat-trihydrat. Saltets vigtigste egenskaber er beskrevet i bilag 2 og 3 og er gengivet i tabel 1.

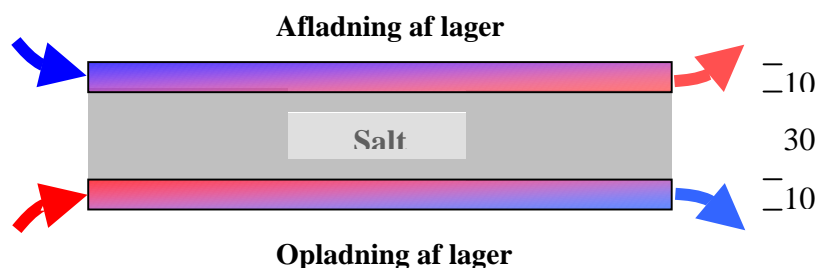
Tabel 1. Oversigt over de termiske egenskaber for natriumacetat-trihydrat.

<b>Navn</b>	Natriumacetat-trihydrat
<b>Kemisk beskrivelse</b>	$\text{NaCH}_3\text{COO}\cdot 3\text{H}_2\text{O}$
<b>Massefylde (smeltet ved 58°C)</b>	1301 kg/m <sup>3</sup>
<b>Varmekapacitet (størknet)</b>	2540 J/(kg K)
<b>Smeltepunkt</b>	58 °C
<b>Smeltevarme</b>	265 kJ/kg
<b>Vandindhold</b>	40 vægt-%

De varmeoverføringsmæssige forhold er undersøgt både for et opvarmnings- og et afkølingsforløb.

## 2.1. Forsøgsopstilling

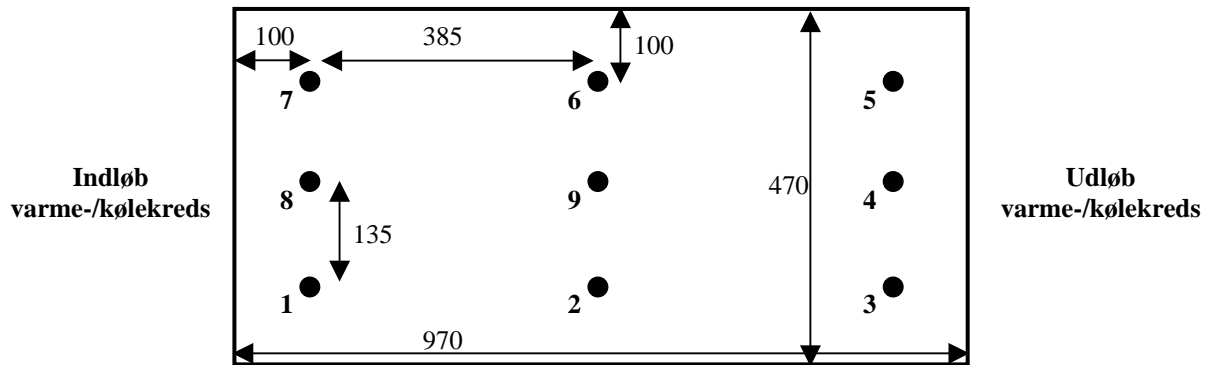
Ved design af smeltevarmelageret er det forsøgt at opnå størst mulig varmeoverføring i saltet ved at opvarmningen (opladningen) af lageret sker nedefra og afkølingen (afladningen) af lageret sker ovenfra. På denne måde skabes der en naturlig intern konvektion i lageret under både op- og afladning. Saltet er placeret i en lav lukket bakke (højde  $\times$  bredde  $\times$  længde: 0,03  $\times$  0,47  $\times$  0,97 m), hvilket giver et stort varmeoverføringsareal set i relation til lagervolumenet. Forsøgssmeltevarmelageret er vist skematisk i figur 1.



Figur 1. Skematisk tegning (lodret snit) af forsøgssmeltevarmelageret.

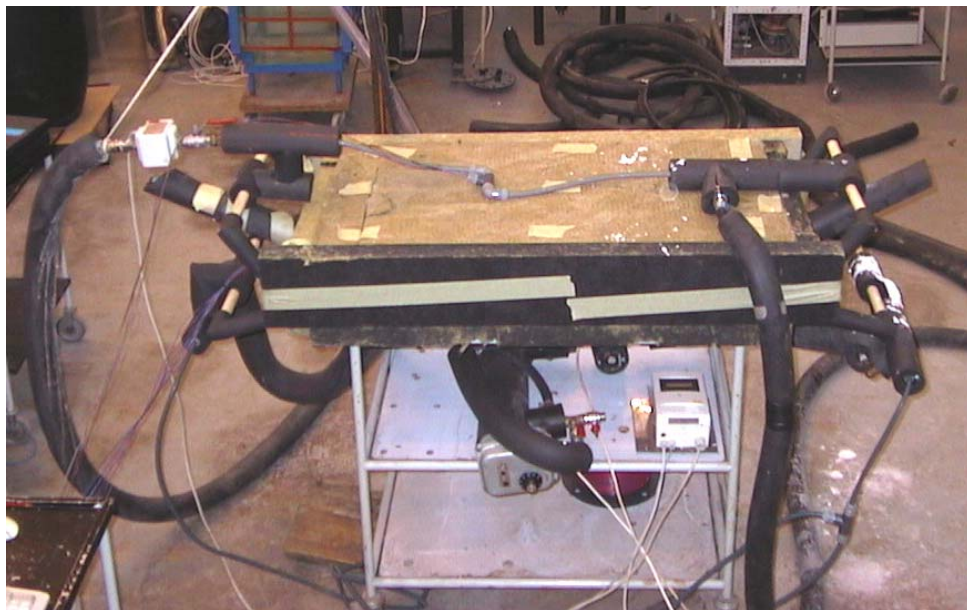
I smeltevarmelageret er der placeret 9 temperaturfølere (figur 2) til registrering af lager-temperaturen. Derudover måles indløbs- og udløbstemperaturen samt volumenstrøm i hhv. opladnings- og afladningskredsen. Saltlagerets volumen er 13,7 liter. Hele opstillingen er isoleret med 50 mm mineraluld. På figur 3 ses et foto af opstillingen.

Opladning af lageret sker ved cirkulation af varmt vand, der opvarmes af en elpatron i vandkredsen. Den maksimale temperatur, der kan opnås i vandkredsen ved denne opstilling, er ca. 75°C. Afladning af lageret sker med koldt vand fra vandforsyningen, hvor volumenstrømmen reguleres med en ventil. Koldt vandstemperaturen er ca. 12°C.



Figur 2. Dimensioner af forsøgsmeltevarmelager samt placering af temperaturmålepunkter i saltet. Alle mål i mm.

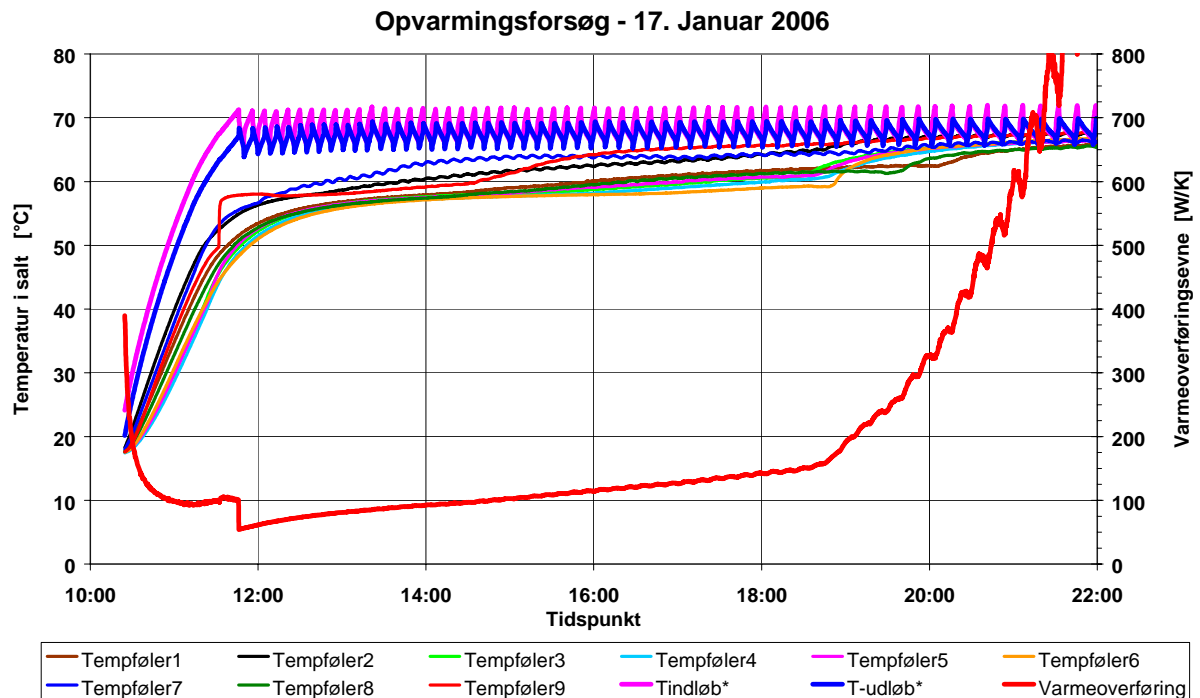
Natriumacetat-trihydrat er kendetegnet ved at volumenet under størkning formindskes i forhold til i flydende form, hvorfor fyldning af lageret er sket ved at hælde smeltet salt ved ca. 80°C ned i lageret, der inden påfyldning var opvarmet til ca. 70°C. Herved sikredes det, at der ikke skete en krystallisation af saltet under påfyldningen.



Figur 3. Foto af forsøgsopstilling.

## 2.2. Forsøgsresultater

Der er udført en række opvarmnings- og afkølingsforsøg med forskellige volumenstrømme i hhv. opladnings- og afladningskreds. Figur 4 viser et typisk opladningsforsøg med en volumenstrøm på 5,9 liter/minut.



Figur. 4 Eksempel på målte temperaturer i lageret samt beregnet varmeoverføringsevne for forsøgssmeltevarmelageret under opvarmning fra krystalliseret kold tilstand til smeltet tilstand.

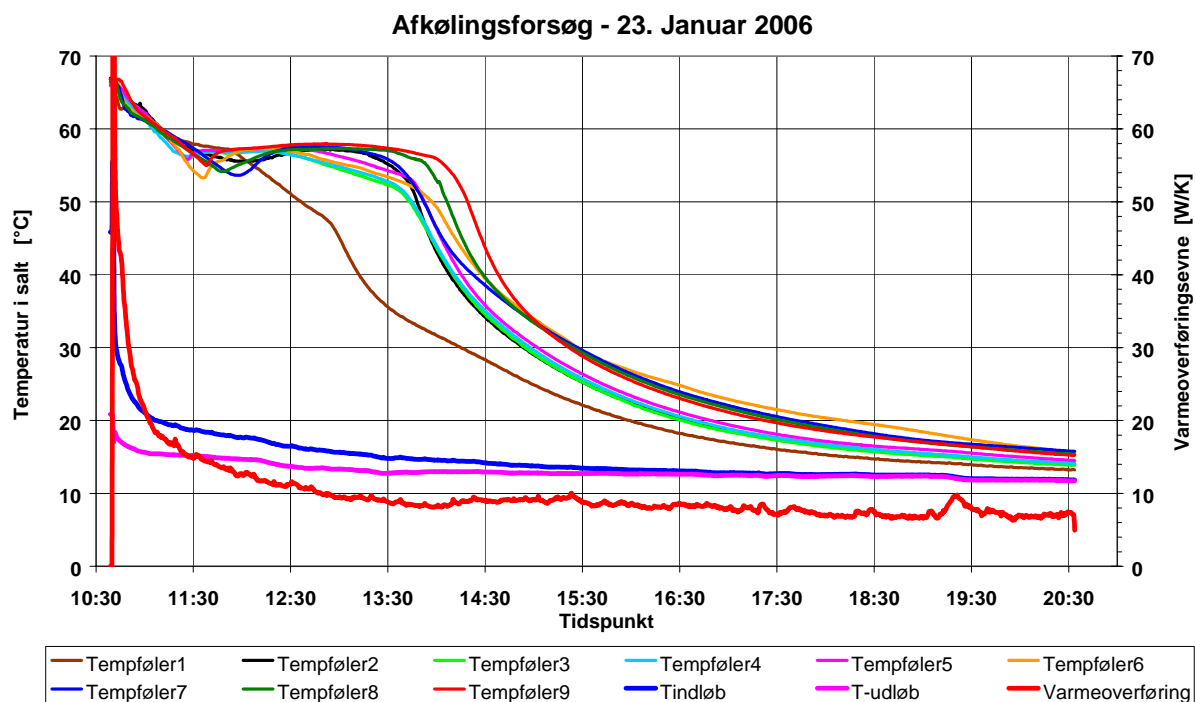
Figur 4 viser tydeligt, at temperaturen i lageret først stiger hurtigt indtil smeltepunktet er nået, hvorefter temperaturen forbliver nogenlunde konstant omkring 58°C indtil saltet er fuldt smeltet, hvorefter temperaturen atter stiger.

Den fede røde kurve viser varmeoverføringsevnen fra ladekreds til lageret beregnet ud fra lagerets middeltemperatur og ladekredsens indløbs- og udløbstemperatur ( $\dot{q}$  er massestrømmen i ladekredsen og  $C_p$  er varmekapaciteten af vand):

$$H = -\dot{q} C_p \ln \left( 1 - \frac{T_{\text{indløb}} - T_{\text{udløb}}}{T_{\text{indløb}} - \bar{T}_{\text{lager}}} \right) \quad [\text{W/K}]$$

Efter at hele lageret er smeltet, stiger lagertemperaturen til et niveau, der ligger mellem varmelegemets termostats ind- og udkoblingstemperatur, hvorfor den beregnede varmeoverføring ikke mere har nogen mening, hvilket afspejler sig i den kraftigt stigende varmeoverføring efter kl. 18.00. I starten af opvarmningsperioden stiger indløbstemperaturen op mod termostats udkoblingspunkt, hvorefter indløbstemperaturen vil svinge svarende til termostats hysteres. Derfor er der efter dette punkt anvendt en rullende middelværdi af indløbstemperatur og udløbstemperatur ved beregning af varmeoverføringen. Denne overgang i beregningsmetoden fremgår af figur 4 som et lille fald i varmeoverføringen lidt før kl. 12.00.

Figur 5 viser tilsvarende et typisk afladningsforsøg fra fuld smeltet tilstand til krystalliseret kold tilstand. Volumenstrøm var i dette forsøg 2,4 liter/minut.



Figur. 5 Eksempel på målte temperaturer i lageret samt beregnet varmeoverføringssevne i forsøgssmeltevarmelageret under afkøling fra smeltet tilstand til afkølet krystalliseret tilstand.

Under afladning af lageret falder temperaturen i lageret hurtigt til omkring smeltepunktet, hvorefter temperaturen forbliver næsten konstant indtil hele lageret er størknet, hvorefter temperaturen atter falder til niveauet for koldt vandstemperaturen.

Det bemærkes at de enkelte målepunkter generelt registrerer, at temperaturen kortvarigt falder til under smeltepunktet i begyndelsen af afkølingsperioden for derefter atter at stige til ca. 58°C. Dette indikerer, at der optræder en kortvarig underafkøling af det smeltede salt, inden det begynder at størkne.

Det fremgår også af figur 5, at der er en relativ stor spredning mellem målingerne fra de enkelte følere. En forklaring kan være, at følerne under monteringen ikke er kommet til at sidde i fuldstændig samme højde i varmelageret. Når saltet begynder at størkne fylder det mindre, og der er dermed en risiko for, at nogle af følerne reelt kommer til at sidde i en lomme uden at være omgivet af saltblandingen.

Der er udført 3 afkølingsforsøg og 3 opvarmningsforsøg med lageret ved forskellige volumenstrømme på hhv. den kolde og varme side af lageret. Ud fra målingerne er varmeoverføringssevnen samt varmeoverføringskoefficienten bestemt baseret på det varmeoverførende areal på 0.456 m<sup>2</sup>. Resultatet af forsøgene er vist i tabel 2.

Tabel 2. Resultat af opvarmnings- og afkølingsforsøg med 13,7 liter natriumacetat-trihydrat ved variende volumenstrøm på hhv. den varme og kolde side af lageret.

Forsøg	Volumenstrøm		Gennemsnitlig varmeoverførings- evne	Gennemsnitlig varmeoverførings- koefficient
	Varm side	Kold side		
	l/min	l/min	W/K	W/m <sup>2</sup> K
Opvarmning	1,1		92	202
Opvarmning	2,4		78	171
Opvarmning	5,9		101	221
Afkøling		1,1	16	35
Afkøling		2,4	10	22
Afkøling		5,4	21	46

Resultaterne i tabel 2 viser at der ved opvarmning af lageret nedefra kan opnås en varmeoverføring på ca. 100 W/K mens varmeoverføringen ved afkøling af lageret kun er ca. 20% af varmeoverføringen ved opvarmning. Den væsentligste forklaring er, at varmeledningsevnen for salthydratkrystaller er lille. Derudover kan forklaringen også skyldes, at saltet under størkning fylder mindre, hvorved der dannes et isolerende hulrum mellem salt og den varmeoverførende overflade af lagerbeholderen.

De udførte forsøg viser også, at der kan opnås den samme varmeoverføringsevne ved enten et relativt lille laminart flow eller ved et relativt højt turbulent flow. Ved praktisk anvendelse af smeltevarmelageret må det tilstræbes at anvende så lille flow som muligt for opnåelse af den maksimale afkøling/opvarmning af væsken.

I de teoretiske beregninger af solvarmesystemer med smeltevarmelagere er der anvendt en væsentlig højere varmeoverføringskoefficient end, der er målt i forsøgsvarmelageret for opnåelse af en tilstrækkelig afkøling/opvarmning i hhv. solfangerkredsen og brugsvand/rumvarmekredsen. Resultatet af de udførte forsøg viser dermed, at en simpel overskylning af lagerdelens under-/overside ikke giver en tilstrækkelig varmeoverføring, hvorfor der skal arbejdes videre med løsninger til at forøge denne.

Det har under forsøgene ikke været muligt at opnå en stabil underafkøling i lageret på trods af, at dette har været praktiseret i små prøver af saltet forud for de egentlige forsøg. Da en stabil underafkøling er baggrunden for de positive resultater fra de teoretiske beregninger, kræves der videre undersøgelse for at klarlægge, hvorledes stabil underafkøling opnås i praksis..

# **Bilag 1**

## **Insulation materials for advanced water storages.**

Kapitel 7 i IEA SH&C Task 32 state of the art report:  
*Thermal energy storage for solar low energy buildings*,2005.  
Jørgen M. Schultz.



## 7. Insulation materials for advanced water storages

by Jørgen M. Schultz

### 7.1 Introduction

This chapter gives an overview of different insulation materials that may be of interest for insulation of solar storage tanks. In order to understand the special characteristics of the different insulation materials the heat transfer mechanisms involved are shortly described. In the following sections different insulation materials are described with respect to material characteristics and some comments on the easiness of application for tank insulation.

The material properties listed in this paper are typical values, which gives an idea of the possibilities but in case of a specific design a more detailed survey of the market is required.

### 7.2 Heat transfer in insulation products

In general insulation products are made up of a skeleton of solid material with a lot of cavities in between the solid parts (Fig. 1). The heat transfer takes place as thermal conduction in the solid material in parallel with thermal radiation and conduction in the cavities.

#### 7.2.1 Conduction in the solid

The conduction through the solid part of the material depends mainly on the thermal conductivity of the solid material, the effective contact areas in the skeleton and the overall solid distance between the two surfaces of the material.

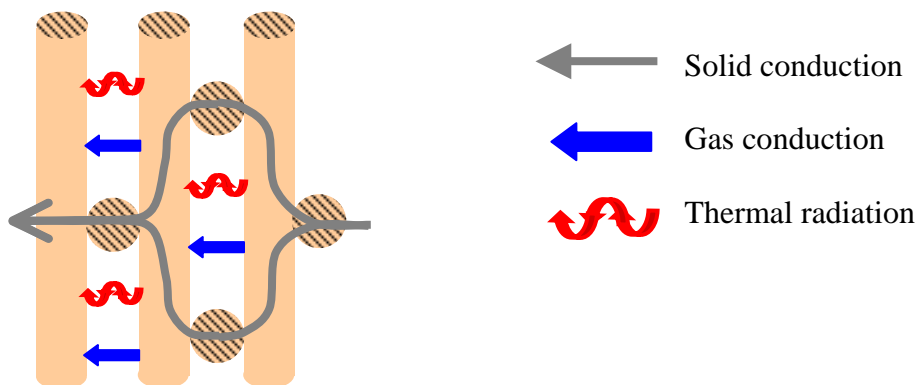


Fig 1. Illustration of heat transport in a fibrous insulation material e.g. mineral wool. Heat flow perpendicular to the fibres.

## 7.2.2 Thermal radiation in the cavities

The thermal radiation in the cavities depends on the emissivity and absorptance of the solid surfaces surrounding the cavity. Most materials have an absorptance close to 100% for thermal radiation leaving the emissivity as the governing parameter. The emissivity of typical building materials is in the range of 80 - 90%. This means "only" 80 - 90% of the absorbed thermal radiation is reemitted. This phenomenon is important, as the heat transfer by thermal radiation will be reduced each time the radiation has to be absorbed and reemitted. In porous materials the thermal radiation will be absorbed and reemitted many times reducing the heat transfer by thermal radiation through the material.

The radiative heat transfer can also be reduced using materials with a low-emissive surface or by coating the material with a low-emissive coating. The most well known low-emissive material is probably aluminium foil with an emissivity in the range of 4 - 20%. Fig. 2 illustrates the effect of low-emissive surfaces as well as several radiation blocking layers.

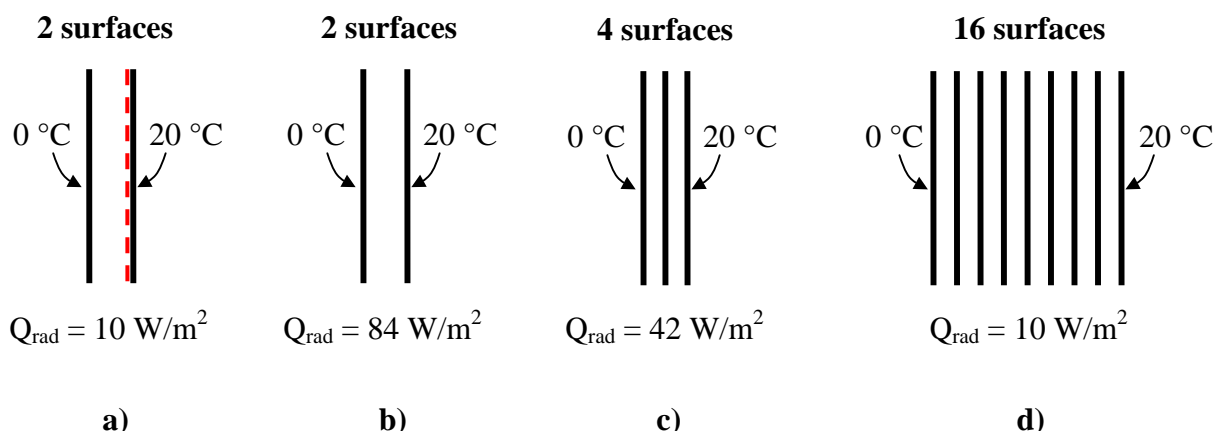


Fig. 2. Calculated heat transfer by radiation.

- One surface with an emissivity = 0.9 and one coated surface with an emissivity = 0.1.
- Two surfaces all with an emissivity = 0.9.
- Four surfaces, all with an emissivity = 0.9.
- Sixteen surfaces, all with an emissivity = 0.9.

The example in figure 2 shows that subdividing one cavity into 8 cavities by means of radiation blocking layers with an emissivity of 0.9 equals the effect of having one surface in the cavity coated with an emissivity of 0.1.

## 7.2.3 Conduction in the cavities

The conduction in a gas-filled enclosure takes place due to internal collisions between the gas molecules. In a large volume at atmospheric pressure the distance one molecule can move before colliding with another is very limited. By the collision heat is exchanged between the molecules and through successive collisions the heat are

transferred from the warm to the cold side of the enclosure. The average distance one molecule can travel before colliding with another molecule is called the *free mean path* and is calculated as:

$$\lambda = \frac{1}{\pi \times D^2 \times n} \quad [\text{m}] \quad (1)$$

where  $\lambda$  is the free mean path [m]  
 $D$  is the molecule diameter [m]  
 $n$  is the number of molecules per  $\text{m}^3$  [ $\text{m}^{-3}$ ]

If average values for gaseous molecules at atmospheric pressure are used the free mean path can be calculated to approximately  $10^{-7}$  meter. If the dimensions of the cavity holding the gas is significant larger than  $10^{-7}$  meter the probability for a molecule to hit another molecule is much larger than hitting the walls of the cavity and an undisturbed heat transfer takes place.

The speed of the molecules governs the thermal conductivity and depends of the molecular weight, which explains the difference in thermal conductivity of different gases (table 1).

Table 1 Overview of molecular weight and thermal conductivity for different gasses.

Gas	Molecular weight	Thermal conductivity (20 °C, 1 atm)
	g/mole	W/mK
Oxygen (O <sub>2</sub> )	32	0.026
Nitrogen (N <sub>2</sub> )	28	0.026
Argon (Ar)	40	0.017
Dry atmospheric air	29	0.026
Krypton (Kr)	84	0.010
Xenon (Xe)	131	0.006
Cyclopentane* (C <sub>5</sub> H <sub>10</sub> )	70	0.012

\*Cyclopentane is a widely used blowing gas for polyurethane foam.

If the cavities in the insulation material is smaller than the free mean path a reduced thermal conductivity in the cavities are observed. In this case the probability for a molecule hitting another molecule is lower than that of hitting the walls of the void and the heat transfer is reduced.

Finally the thermal conduction in the cavities can be lowered or eliminated by removal of the molecules by establishing a vacuum in the pores. Reducing the number of molecules per volume increases the free mean path - see equation (1). If the free mean path becomes larger than the cavity dimension the thermal conductivity is decreased. This means that no effect of evacuation on the thermal conductivity will be seen before the gas pressure has been decreased to a level where the equivalent free mean path has a value comparable with the cavity dimension. Table 2 shows the free mean path for atmospheric air as function of the pressure in the cavity. Further decrease of the number of molecules in the cavity reduces the thermal conduction, as fewer molecules are present to transport the heat. At absolute vacuum the conduction in the gas is eliminated.

Table 2 Free mean path as function of gas pressure (atmospheric air) in the cavities

Pressure in the cavity		Free mean path
Atm	hPa (mbar)	mm
1	1000	0.0001
0.5	500	0.0002
0.1	100	0.0010
0.01	10	0.0100
0.001	1	0.1000
0.0001	0.1	1.0000
0.00001	0.01	10.0000

Fig. 3 below illustrates the different heat transport phenomena described above.

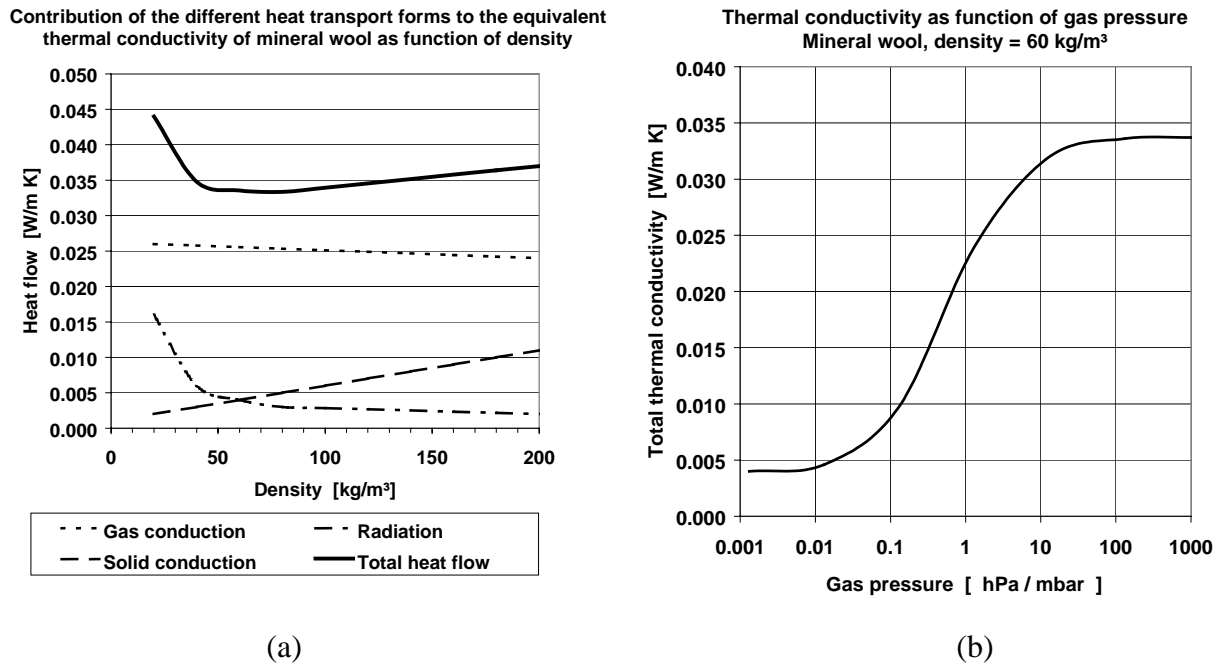


Fig. 3. Example on contribution of heat transport forms to the total thermal conductivity of mineral wool as function of density (a) and the total thermal conductivity as function of gas pressure (b).

Fig. 3 (a) shows that the gas conduction at atmospheric pressure is almost independent of the density though with a slightly lower value for the high-density products due to smaller cavity dimensions. The solid conduction is proportional to the density as expected. The heat transfer by radiation for low-density products is significant due to the limited number of radiation blocking surfaces and perhaps even areas without any blocking surface. For densities higher than 50 kg/m<sup>3</sup> the thermal radiation is almost fully blocked.

Fig. 3 (b) shows the three phases during evacuation.

1. In the range from 1000 – 10 hPa almost no effect of the evacuation is seen on the thermal conductivity, which indicates that the average cavity dimension is larger than 0.01 mm (table 2).
2. In the range from 10 – 0.01 hPa a significant decrease in thermal conductivity is seen, while the number of molecules in the cavities becomes lower.
3. Below 0.01 hPa the thermal conductivity becomes stable, i.e. the gas conduction has been eliminated. The remaining heat transport is due to radiation and conduction in the solid material.

## 7.3 Description of common insulation materials

The most common insulation products used in the building sector has pores or cavities filled with air. The pores or cavities can be open or closed towards the ambient. In the following the most common products are briefly described.

### 7.3.1 Mineral wool

Mineral wool is made from fibres of glass or stone. The fibres forms an open air-filled network kept together by means of an added bonding material. The production process can be controlled to get different density of the mineral wool for different use. High-density mineral wool products are used for situations where high compression strength is required, e.g. in slab on ground floor constructions and external insulation of foundations etc. Mineral wool is flexible, compressible and partly elastic, which makes it easy to fit to odd shapes, e.g. around pipes, heat stores etc.

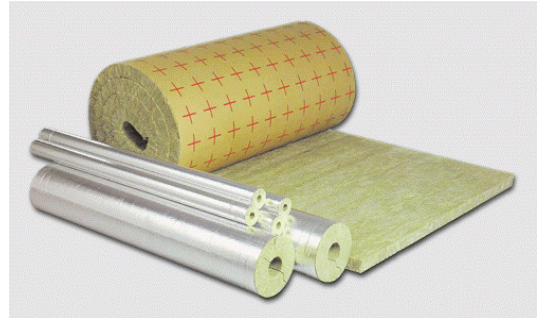


Fig. 4 Example of technical insulation products of mineral wool (Rockwool).

Thermal conductivity in praxis ( $T_{\text{mean}} = 10 \text{ }^{\circ}\text{C}$ ):	0.036 - 0.050 W/mK (density dependant)
Temperature dependency:	0.4 - 0.8 %/K
Maximum temperature:	Glass wool: 250 - 400 $^{\circ}\text{C}$
	Stone wool: 250 - 1000 $^{\circ}\text{C}$
	(bonding material is destroyed at 250 $^{\circ}\text{C}$ )

### 7.3.2 Polystyrene foam

Polystyrene is a plastic product extracted from fossil oil. Two different kind of polystyrene foam is common on the market: Expanded polystyrene (EPS) and extruded polystyrene (XPS).

Expanded polystyrene is initially formed as pellets of polystyrene foam, which further can be joined and formed into insulation boards or specific forms. The pellets can also be used directly for insulation of cavities. Special care should be given to avoid settling of the pellets, but it is possible to fill even very irregular cavities with insulation material and avoid thermal bridges due to areas without insulation. This is difficult to achieve with the boards.

Extruded polystyrene is made from the styrene raw material by adding different chemicals and the cell structure is formed during extrusion by means of a special gas. In earlier XPS products the cells were formed by means of CFC-gasses but now these environmental harmful gasses have been substituted with non-CFC gasses. XPS-products are coloured in order to distinguish them from EPS products.

XPS-foam has a more uniform cell structure than EPS-foam leading to higher compression strength and lower water vapour diffusion properties than EPS-products. However, both EPS- and XPS-foam can be manufactured with a wide range of compression strengths.

Thermal conductivity in praxis ( $T_{\text{mean}} = 10 \text{ }^{\circ}\text{C}$ ):

Boards: 0.034 – 0.050 W/mK (density dependant)

Pellets: 0.050 W/mK

Temperature dependency: 0.4 – 0.5 %/K

Maximum temperature: Approx. 80 °C



Fig. 5 Expanded polystyrene (Sundolitt)



Fig. 6 Expanded polystyrene (Dow Corning)

### 7.3.3 Polyurethane foam (PUR)

The combination of very good insulating properties, good gluing properties, good compressive strength and the possibility of in-situ foaming has probably made polyurethane foam the most widely used insulating foam outside the building sector. Polyurethane is foamed with a blow gas, which previously has been of the CFC kind - harmful to the environment - but now other gasses as cyclopentane is used. Polyurethane is highly porous material with closed cells holding the blowing gas. The low thermal conductivity of cyclopentane (table 1) reduces the gas conduction in the cells compared to air filled foams. The actual thermal conductivity of polyurethane depends on how well the blowing process is controlled, the density of the polyurethane foam and the age of the foam. Polyurethane foam is not completely tight against diffusion and the insulating gas will slowly diffuse out of the cells during time if the polyurethane foam is not equipped with a barrier material. However the barrier material only need excellent barrier properties against the blow gas and not for wide range of gasses.



Fig. 7. Examples of PUR foam used in blocks sandwich elements and pipe insulation (Elliott®)

Thermal conductivity in praxis ( $T_{\text{mean}} = 10 \text{ }^{\circ}\text{C}$ ):	0.024 - 0.035 W/mK (density dependant)
Temperature dependency:	0.4 - 0.5 %/K (Temp. > 0 °C)
Maximum temperature:	140 °C

## 7.4 Description of highly porous insulation materials

### 7.4.1 Micro-porous insulation materials

Micro porous insulation materials make use of having pore sizes smaller than the free mean path of atmospheric air. The composition of the materials varies but in general a mixture of ceramic powder and fibres are compressed to form a rigid highly insulating block. The blocks are normally sealed with a glass fibre cloth to prevent ceramic dust to be released. The blocks can also be cast in specific forms, e.g. for pipe insulation etc. Finally, the micro porous insulation material can also be found in a flexible version in form of blankets to wrap around irregular shapes.



Fig. 8 Examples on micro porous insulation. (Microtherm)

Thermal conductivity ( $T_{\text{mean}} = 10 \text{ }^\circ\text{C}$ ):	0.020 – 0.025 W/mK
Temperature dependency:	0.1%/K
Maximum temperature:	900 – 1500 $^\circ\text{C}$

### 7.4.2 Nano-porous insulation materials

A further decrease in the average pore size leads to even lower thermal conductivities without introducing insulating gasses or the use of vacuum. Examples of such materials are the silica gels, which have pore sizes in the range of 5 – 300 nm. Fumed and precipitated silica gels are powders that primarily are used for vacuum insulation panels.

Silica aerogels that has the lowest thermal conductivity can be made in both a monolithic (tiles) and a granular form.

The monolithic gels are very fragile and would only be applicable if protected against mechanical stresses. The most promising application for tank insulation will also in this case be in evacuated form. The granular form has the same advantages as the polystyrene pellets that it can fill out irregular cavities if special care is taken to avoid settling. However, the voids between the pellets increase the overall thermal conductivity.



Fig. 9. Examples of granular aerogel (Cabot – Nanogel)

Thermal conductivity ( $T_{\text{mean}} = 10 \text{ }^\circ\text{C}$ ):

Fumed and precipitated silica gel	~ 0.020 W/mK
Monolithic silica aerogel	0.016 – 0.018 W/mK
Monolithic silica aerogel (IR-blocked)*	0.012 – 0.014 W/mK
Granular silica aerogel	0.020 – 0.025 W/mK

Temperature dependency:

Monolithic and fine powders:	0.1 %/K
Granular silica aerogel:	0.3 – 0.5 %/K

\*IR-blocked: Carbon black added for efficient blocking of thermal radiation

Maximum temperature: Approximately 500  $^\circ\text{C}$

## 7.5 Vacuum insulation

### 7.5.1 Vacuum definitions

Vacuum means in fact that no molecules at all are present, but more general vacuum refers to gas pressure lower than the atmospheric pressure. Depending on the level of depressurisation different regions of vacuum are defined, table 3 [1].

Evacuation in the rough vacuum region is almost straightforward due to the viscous flow, i.e. the pressure difference created by the vacuum pump makes the gas flow to the pump and rough vacuum can be obtained without large costs. In the high and ultra-high regions the evacuation becomes more difficult as the evacuation is based on trapping of single molecules eventually reaching the vacuum pump. The molecules travel freely and are not influenced by a pressure gradient guiding them towards the pump.

Table 3 Definition of vacuum regions [1].

Region	Pressure level	Flow
Rough vacuum	1000 – 1 hPa	<i>Viscous flow:</i> Interactions between the molecules dominates the flow which can be laminar or turbulent. The free mean path is smaller than the diameter of the conducting tube
Medium vacuum	1 – 10 <sup>-3</sup> hPa	<i>Knudsen flow:</i> Transition from viscous to molecular flow. The free mean path is of same size as the diameter of the conducting tube
High vacuum	10 <sup>-3</sup> – 10 <sup>-7</sup> hPa	<i>Molecular flow:</i> The molecules move freely independent of each other. The free mean path is larger than the diameter of the conducting tube
Ultra-high vacuum	< 10 <sup>-7</sup> hPa	

### 7.5.2 The "Dewar flask" principle

The ideal vacuum insulation would be an enclosure with low emissive surfaces with vacuum in between. This solution can only be realised in cylindrical geometries, which have the potential for withstanding the external atmospheric pressure acting on the outer surfaces if a reasonable material thickness should be considered. The most well known example is the Dewar flask or better known as the thermos bottle with a double-walled glass cylinder, which is silver coated on the surfaces facing the evacuated enclosure. The emissivity of silver is 0.02 – 0.03 reducing the heat transfer by radiation with 97-98 %. Further reduction of the heat loss by radiation could be achieved by adding more radiation blocking layers in the enclosure, but fixing of the layers may be difficult without creating thermal bridges that may eliminate the effect of the reduced heat transfer by radiation.

In the thermos bottle the main heat loss is due to the thermal bridge where the glass walls are joined and through the bottle lid, which both are at the top of the bottle where the temperature is highest. Looking at water storage tanks for solar heating systems, where thermal stratification is a key issue in order to keep the lower part of the tank as cold as possible the "thermos bottle" should be turned upside down in which case the thermal bridge due to the wall joining and the poor "lid insulation" will be located in the coldest part of the tank. The main drawbacks are the need for a double shell with a relatively large wall thickness to withstand the atmospheric pressure and the need for a high vacuum due to the wall distance compared to the free mean path of the air molecules.

For example if the distance between the cylindrical walls is 1 mm the pressure should be lower than 0.1 hPa before a significant decrease in gas conduction as function of gas pressure starts (see table 2) and a 99% decrease in gas conduction is achieved at a pressure of  $10^{-6}$  hPa (the high vacuum region).

### 7.5.3 Vacuum insulation filler materials

To avoid the drawbacks of thermos bottle principle with respect to establishing the high vacuum and the need for a thick and strong outer cylinder wall an open-pored filler material with a sufficient compressive strength can be applied between an outer and the inner wall of the storage. In this case the external load from the atmospheric pressure is transferred through the filler material to the inner wall that initially has the sufficient strength to withstand not only the atmospheric pressure but also the much higher internal pressure from the pressurised water in the tank. The filler material should have a high porosity with small pore sizes in which case the solid conduction will be limited and reduced gas conduction can be achieved at a pressure in the rough or medium vacuum region. The filler material also eliminates the need for low emissive surface coating of the storage walls. Table 4 shows some of the most common materials used for vacuum insulation products.

Table 4 Internal pore gas pressure and corresponding thermal conductivity for different open celled materials used in vacuum insulation products

Material	Pressure	Thermal conductivity ( $T_{\text{mean}} = 10 \text{ }^{\circ}\text{C}$ )	Temperature dependency*
	hPa	W/mK	%/K
Polystyrene foam (open pored)	0.1	0.004	?
Polyurethane foam (open pored)	0.1	0.006	?
Precipitated silica gel	1	0.006	0.1
Fumed silica gel	10	0.004	0.1

\*The thermal dependency of the thermal conductivity has not been reported, but the dependency would be lower than in the un-evacuated state due to the small amount of gas molecules in the pores.

In general vacuum insulation has a thermal conductivity of 0.005 W/mK at a mean temperature of 10 °C. The difference in pressure related to the thermal conductivity is due to differences in the average pore size for the different materials, i.e. polyurethane and polystyrene foams has pore sizes in the range of 40 – 70  $\mu\text{m}$  while silica gels have pore sizes in the range of 0.01 – 1  $\mu\text{m}$ .

The requirements to the level of vacuum is decreased due to the small pore sizes of the filler materials but the small pore sizes increases the diffusion coefficient, which means that evacuation through a single connection in the vacuum insulation enclosure becomes very time consuming (weeks) if a common storage size is considered.

It should be noted that no examples on direct foaming of e.g. open pored polyurethane foam in a large enclosure has been found, which might be due to technical difficulties or due to the evacuation problem for large volumes.

### 7.5.4 Vacuum insulation panels (VIP)

Vacuum insulation panels are commercial available products. A highly porous filler or core material is evacuated and encapsulated in a shell to keep the vacuum. Only metals with a thickness  $> 0.1$  mm and glass is 100% gas and water vapour tight, but both materials has a relatively high thermal conductivity. This leads to a significant thermal bridge at the edges of the panel and the benefits of the vacuum insulation is more or less eliminated. Therefore all VIP's are made with a barrier film with a high but not 100% resistance against gas and water vapour diffusion.

Most barrier films consist of several different plastic layers with different orientations and one or two metallized layers to get the very high barrier properties. In some cases thin aluminium foils laminated between two layers of plastic is used, which results in excellent barrier properties but also increased edge heat losses Fig. 10, [2].

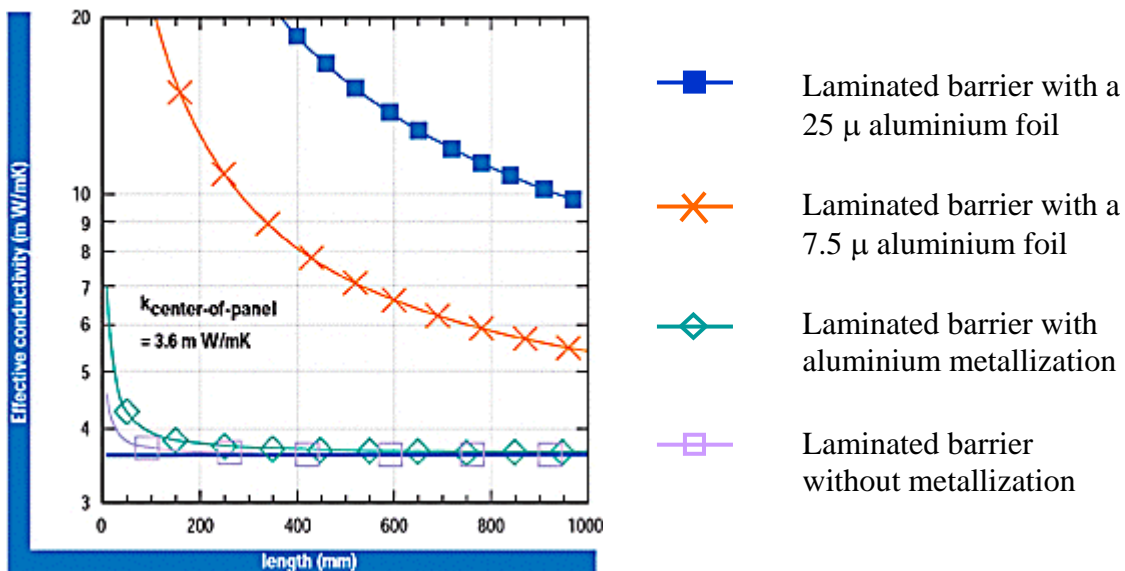


Fig. 10. Effective thermal conductivity ( $T_{\text{mean}} = 10$  °C) of vacuum insulation panels as function of size (side length) and type of barrier for square 25 mm thick VIP's. The thermal conductivity at the centre is 0.0036 W/mK. [2].

The effect of the thermal bridges at the edges can be reduced if more layers of VIP's are applied in which case the different layers can be mounted with displaced joints.

As the laminated barrier films without foils are not 100% tight a slow pressure increase will take place in the VIP over time. Depending on the filler material even a small pressure increase could lead to significant increase in the thermal conductivity. Fig. 11 [2] shows the relation between internal gas pressure and equivalent thermal conductivity of VIP's with different filler materials.

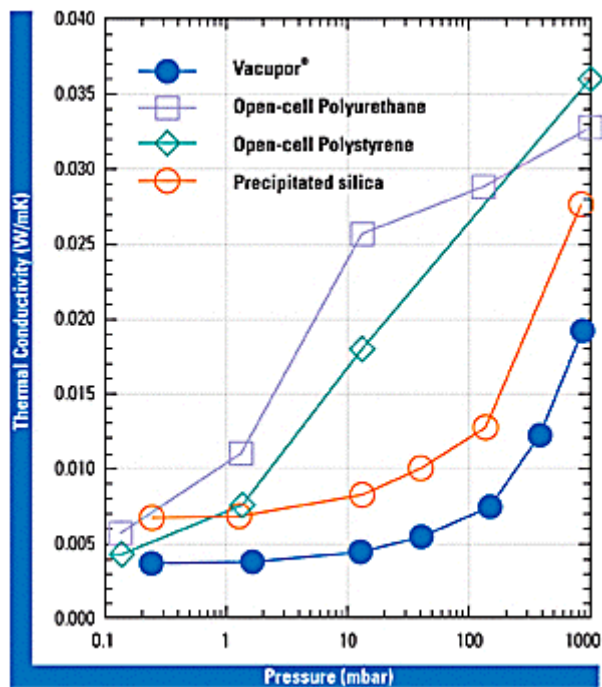


Fig. 11 Thermal conductivity ( $T_{\text{mean}} = 10\text{ }^{\circ}\text{C}$ ) as function of internal gas pressure in different VIP filler materials [2]. The Vacupor is based on fumed silica gel. (1 mbar  $\sim$  1hPa).

Due to the nanostructure of silica gels a pressure increase from 1 to 100 hPa only doubles the thermal conductivity, while the same pressure increase would increase the thermal conductivity of polyurethane and polystyrene foams with a factor 5. Therefore foam based VIP's includes a so-called getter capsule that holds a material designed to adsorb gas and water vapour molecules.

The lifetime of VIP's with respect to thermal conductivity depends beside the capacity of the getter material and the effective barrier properties also on the panel volume relative to the surface area. A large volume relative to the surface area increases the panel lifetime. However a lifetime of 10 – 20 years should be expected.

*Application for storage insulation*

Even though vacuum insulation panels can be made in a variety of forms (Fig. 12) the most efficient way of use is to encapsulate the panels in polyurethane foam often used as insulation material for storage units. The polyurethane foam protects the vacuum barrier film against mechanical damages and furthermore reduces the gas and moisture diffusion into the VIP.



Fig. 12 Example of vacuum insulation panels [3].

The overall reduction of the storage heat loss depends of course on the total area with VIP's and their thickness, but large savings are possible:

If 50 mm thick polyurethane insulation (thermal conductivity  $\lambda = 0.028 \text{ W/mK}$ ) is exchanged with a sandwich of 20 mm polyurethane – 10 mm VIP ( $\lambda = 0.005 \text{ W/mK}$ ) – 20 mm polyurethane, this will reduce the heat loss coefficient with approximately 50% from  $0.6 \text{ W/m}^2\text{K}$  to  $0.3 \text{ W/m}^2\text{K}$ .

Use of vacuum panels alone makes it difficult to obtain a continuous insulation layer on curved surfaces. If only vacuum insulation panels should be used the best solution would be to place the storage in a rectangular box with a plane layer of VIP panels.

## 7.6 Summary

Table 5 lists the thermal characteristics of the different insulation types described in this paper as well as references to some manufacturer of the materials. The list of manufacturers is not at all meant to be a complete list but only as a help to find additional information on some of the product types.

Use of polyurethane foam with the lowest possible thermal conductivity would probably be the most economic first step for improvement of the tank insulation. Table 5 shows that further significant improvement of the tank insulation can only be achieved with vacuum insulation. From a production angle of view the most applicable way is to have vacuum insulation panels embedded in polyurethane foam as already practised in freezers and refrigerators [4]. This principle protects the vacuum insulation panel against mechanical damage and the PU foam fills out all irregular shapes.

Table 5. Overview of insulation materials and their typical thermal characteristics

Material	Thermal conductivity ( $T_m = 10\text{ }^\circ\text{C}$ ) W/mK	Maximum temperature $^\circ\text{C}$	References
Mineral wool Stone wool Glass wool	0.036 – 0.050 0.036 – 0.050	250 – 1000 250 – 400	<a href="http://www.rockwool.com">www.rockwool.com</a> <a href="http://www.isover.com">www.isover.com</a>
Polystyrene EPS granular EPS blocks XPS blocks	~ 0.050 0.034 – 0.050 0.034 – 0.050	80 80 80	<a href="http://plymouthfoam.com/index.html">http://plymouthfoam.com/index.html</a> <a href="http://www.dow.com/styrofoam/index.htm">www.dow.com/styrofoam/index.htm</a>
Polyurethane	0.024 – 0.050	140	<a href="http://www.elliottfoam.com/features.html">http://www.elliottfoam.com/features.html</a>
Micro porous insulation	0.020 – 0.025	800 – 1200	<a href="http://www.microtherm.uk.com/prod.html">http://www.microtherm.uk.com/prod.html</a>
Nano porous insulation Silica gels Silica aerogels monolithic Silica aerogels granular	~ 0.020 0.012 – 0.018 0.020 – 0.025	500 500 500	<a href="http://w1.cabot-corp.com/index.jsp">http://w1.cabot-corp.com/index.jsp</a> <a href="http://www.airglass.se">www.airglass.se</a>
Vacuum insulation Open pored polystyrene Open pored polyurethane Precipitated silica gel Aerogels	0.004 at 0.1 hPa 0.005 at 0.1 hPa 0.006 at 1.0 hPa 0.004 at 10 hPa	80 140 500 500	<a href="http://www.microtherm.uk.com/prod7.html">http://www.microtherm.uk.com/prod7.html</a> <a href="http://www.glacierbay.com/ultra-r.asp">http://www.glacierbay.com/ultra-r.asp</a> <a href="http://www.porextherm.com/en/">http://www.porextherm.com/en/</a> <a href="http://www.nanopore.com/vip.html">http://www.nanopore.com/vip.html</a>

The thermal dependency of the thermal conductivity is in the range of 0.4 – 0.8 %/K for mineral wool and foams and approximately 0.1 %/K for microporous and nanoporous materials. Vacuum insulation will show less thermal dependency due to the reduction of gas molecules in the pores.

## References

- [1] Vacuum Technology - its Foundations, Formulae and Tables. Leybold-Heraeus Vacuum Components and Standard Systems Division, Köln, Germany
- [2] <http://www.porextherm.com/en/>
- [3] <http://www.nanopore.com/vip.html>
- [4] <http://www.electrolux.com/index.asp>

## **Bilag 2**

### **Heat of fusion storage systems for combined solar systems in low energy buildings.**

Jørgen M. Schultz og Simon Furbo.  
Proceedings of EuroSun 2004 Congress,  
Freiburg, Tyskland.



# Heat of fusion storage systems for combined solar systems in low energy buildings

Jørgen M. Schultz, Simon Furbo. Department of Civil Engineering, Technical University of Denmark, Brovej, Building 118, DK-2800 Kgs. Lyngby, Denmark. Email: [js@byg.dtu.dk](mailto:js@byg.dtu.dk)  
Fax: +45 45 88 32 82

## Introduction

Solar heating systems for combined domestic hot water and space heating has a large potential especially in low energy houses where it is possible to take full advantage of low temperature heating systems. If a building integrated heating system is used – e.g. floor heating - the supply temperature (and the the return temperature) would only be a few degrees above room temperature due to the very low heating demand and the large heat transfer surface area.

One of the objectives in a newly started IEA Task 32 project is to investigate and develop improved thermal storages for combined solar systems through further improvement of water based storages and in parallel to investigate the potential of using storage designs with phase change materials, PCM.

The advantage of phase change materials is that large amounts of energy can be stored without temperature increase when the material is going from solid to liquid form (Fig. 1). Keeping the temperature as low as possible is an efficient way to reduce the heat loss from the storage. Furthermore, the PCM storage might be smaller than the equivalent water storage as more energy can be stored per volume. If the PCM further has the possibility of a stable super cooling, i.e. the material is able to cool down below its freezing point ( $T_{\text{fusion}}$ ) and still be liquid, the possibility exist for a storage with a very low heat loss. When energy is needed from the storage the solidification is activated and the temperature rises almost instantly to the melting point.

The work within the IEA Task 32 project focuses on the phase change material Sodium Acetate with xanthan rubber. This material melts at 58 °C, which means that low temperature heating systems could make full use of such a storage system. Energy to a large extent can be withdrawn even when the storage is in its super cooled phase without activation of the phase change.

This paper presents an initial simulation model of a PCM storage for implementation in TRNSYS 15 [1] as well as the first test results achieved with the model.

## Sodium acetate with xanthan rubber

For the moment only one material, Sodium Acetate with Xanthan rubber, is considered for the PCM storage. Sodium Acetate has a melting point of 58 °C and a heat of fusion capacity of 265 kJ/kg. Addition of xanthan rubber to the hydrate makes it very stable when super cooled [2].

Fig. 1 shows that the PCM storage compared to water has a slightly lower storage capacity in the solid phase below the melting point of 58 °C, but when the sodium acetate begins to melt the heat storage capacity increases dramatically due to the heat of fusion. It is also seen that the amount of energy stored at a temperature of 58 °C is about twice the amount of stored energy in traditional water storage even if this was heated to near 100 °C. This shows one of the advantages of a PCM storage: A very large amount of energy can be stored at a moderate temperature.

Figure 1 also shows the advantage of super cooling as the storage can be allowed to cool down to room temperature and still contain large amounts of latent energy (the dotted thick line in figure 1). If the storage has reached a temperature equal to the room temperature no further heat losses occur before the phase change is activated. When the super cooled PCM is activated the temperature increases almost instantly to 58 °C. However, some of

the heat of fusion is used to heating up the PCM to the melting point as indicated with the dashed arrow in figure 1.

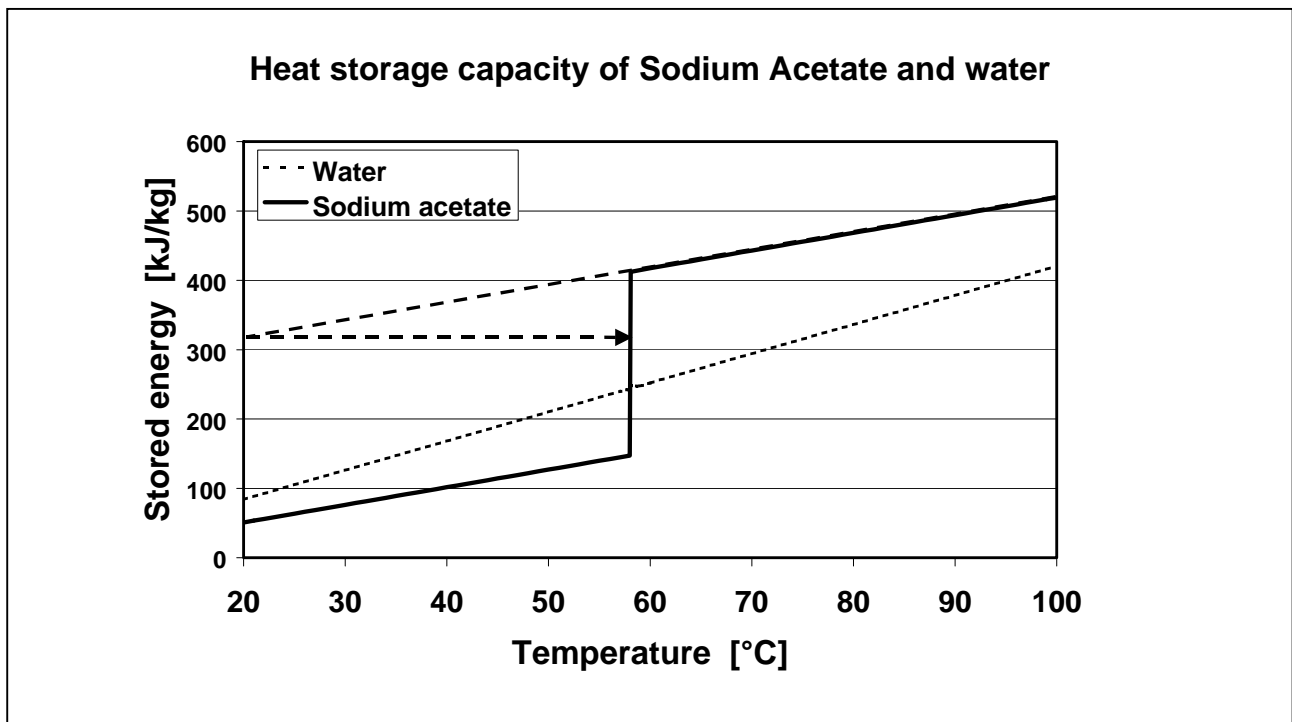


Fig. 1. Heat storage capacity of Sodium Acetate hydrate and water. The thick dashed line shows the sub cooling effect.

One of the critical questions is how to activate the phase change in the super cooled material. One method is to make contact between the super cooled material and a solid crystal of the same material. This method is however not feasible in case of thermal storages. Other methods are to apply a sudden force on the solution e.g. mechanically or acoustically [3].

The question on how to activate the super cooled phase change material has not been considered so far in the project and for the energetic potential evaluation it is anticipated that the PCM can be activated on demand.

### Description of the PCM storage model

The solar system under consideration is outlined in Fig. 2. The system consists of a solar collector, a domestic hot water tank and the PCM storage. The use of two separate storages is due to the idea of extensive use of the super cooling effect of the PCM storage, which would be impossible if a combined storage for domestic hot water and space heating is used. The system is designed to give priority to the domestic hot water tank.

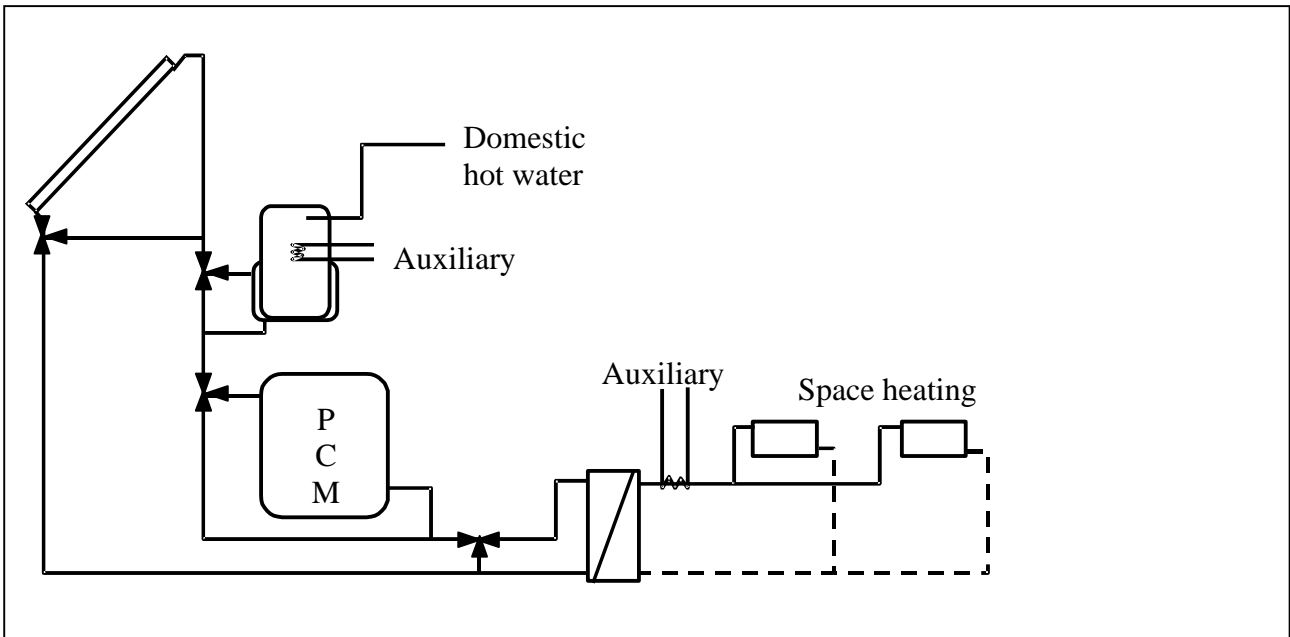


Fig. 2. Schematic illustration of solar combi system taken into account.

The PCM storage design for the first investigation is made without any thoughts on economy or practical problems as the first objective is to evaluate the potential of using a PCM storage compared to traditional water storages. If full benefit of the super cooling effect with respect to reduced heat loss should be achieved a multi-sectioned storage design is needed. By sub-dividing the storage into many separate layers or sections it will be possible only to activate the phase change in the storage volume needed to match the energy demand, and this will be the only part of the storage that will be heated up to the PCM melting point. This has been the main idea behind the design outlined in figure 3.

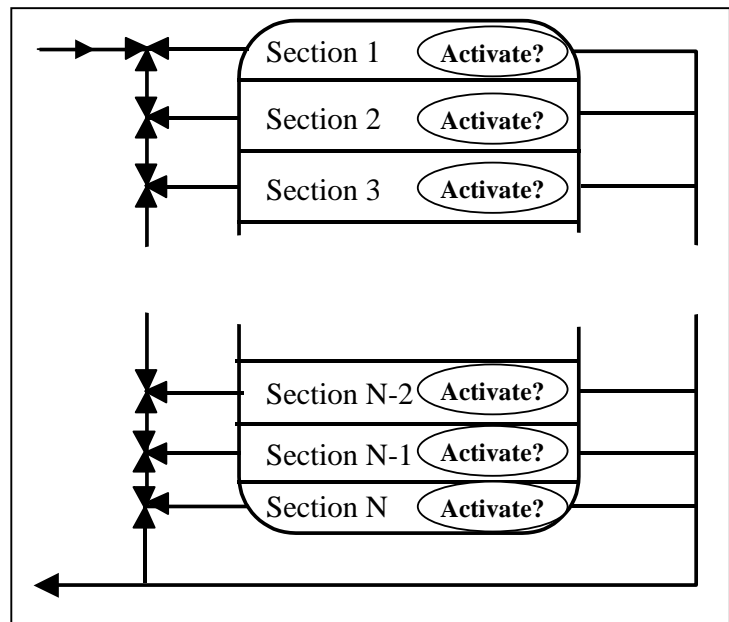


Fig. 3. Outline of multi-layered PCM storage. The phase change can be activated in each separate layer.

A first draft of a TRNSYS type model has been developed. The model subdivides the simulation time step in smaller time steps in order to achieve a sufficient accuracy. The following takes place in each of the small time steps (Fig. 4).

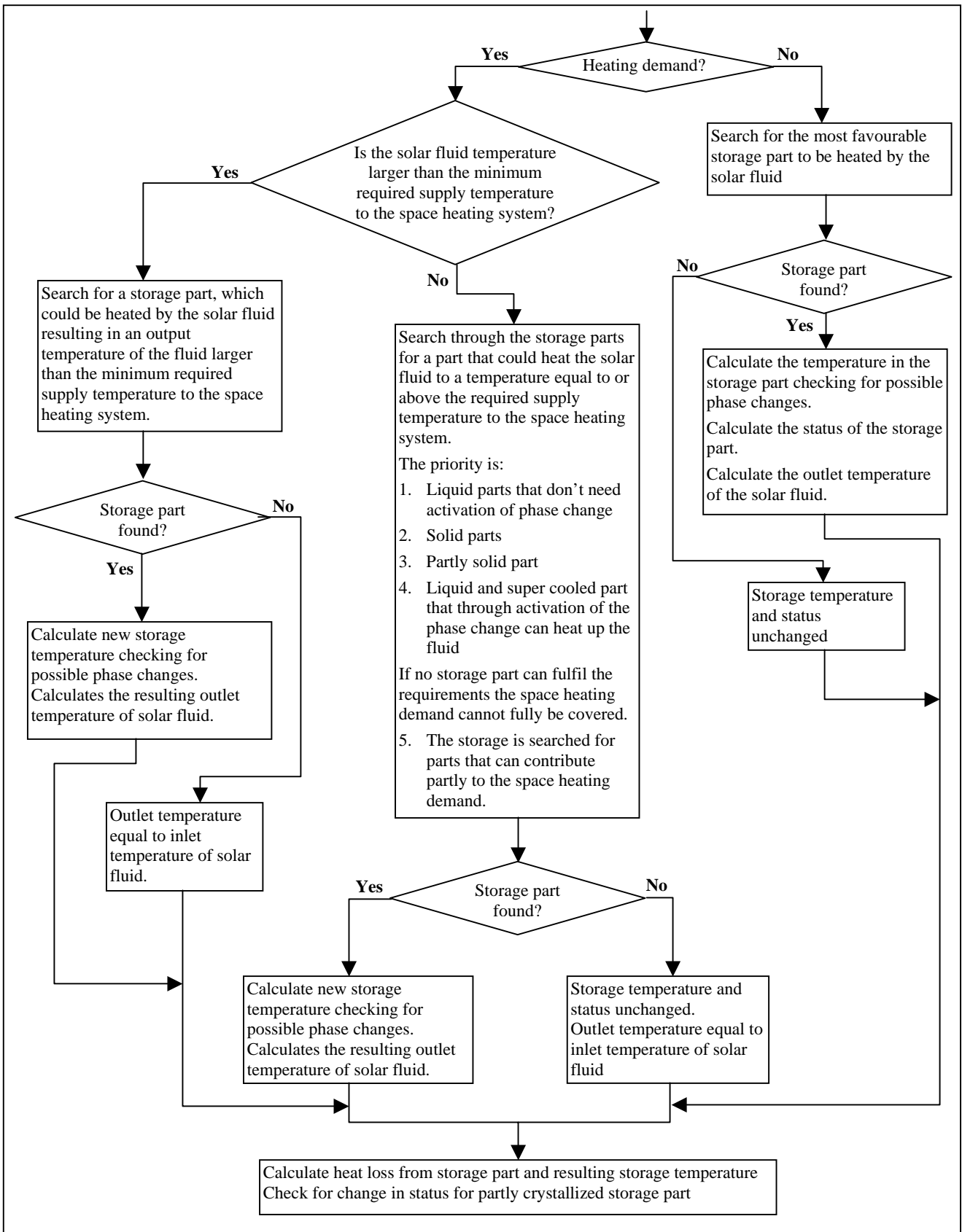


Fig. 4 Flow chart showing the main structure of the model.

Based on the input parameters the most favourable section of the storage is chosen for storage of solar energy or - in case of a space heating demand - heating of the solar fluid to cover the space heating demand. The strategy is always to minimise the storage mean temperature and to avoid activation of phase change in a super cooled section as long as possible.

In each time step the transfer of energy between the solar fluid and the PCM storage is calculated. Next the heat loss to the surroundings is calculated and the final temperature of each section is found. This first model does not take internal heat exchange between the different storage sections into account.

The inputs, parameters and outputs are shown in table 1.

*Table 1. Inputs, parameters and outputs of the model.*

Input	Supply temperature Supply flow rate Required supply temperature to the heat exchanger for covering the space heating demand Required space heating demand Return temperature in the space heating system to the heat exchanger
Parameters	Number of layers (sections) in the storage Volume of each layer Surface area of each layer U-value of the storage insulation (uniform) Number of internal time steps Initial temperature (uniform) Initial status (uniform) Melting point Heat of fusion
Output	Outlet temperature from the storage Average storage temperature Average status of the storage (liquid, partly liquid or solid) Heat loss

Each section is simulated as a lumped model, i.e. the section is supposed to have a uniform temperature. Figure 5 shows the model of one section.

Of special interest is the STATUS parameter, which is the measure of the state of the PCM material. If the storage section is liquid STATUS equals 1 and if the storage section is solid STATUS equals 0. When a fully solid PCM layer reaches the melting point continuous supply of energy will make the PCM begin to melt and a mixture of solid and liquid PCM material will be present. In the simulation model this is registered in the STATUS parameter, which increases proportional to the fraction of melted PCM from a value of 0 to the value of 1, when an energy amount equal to the heat of fusion has been supplied to the storage section.

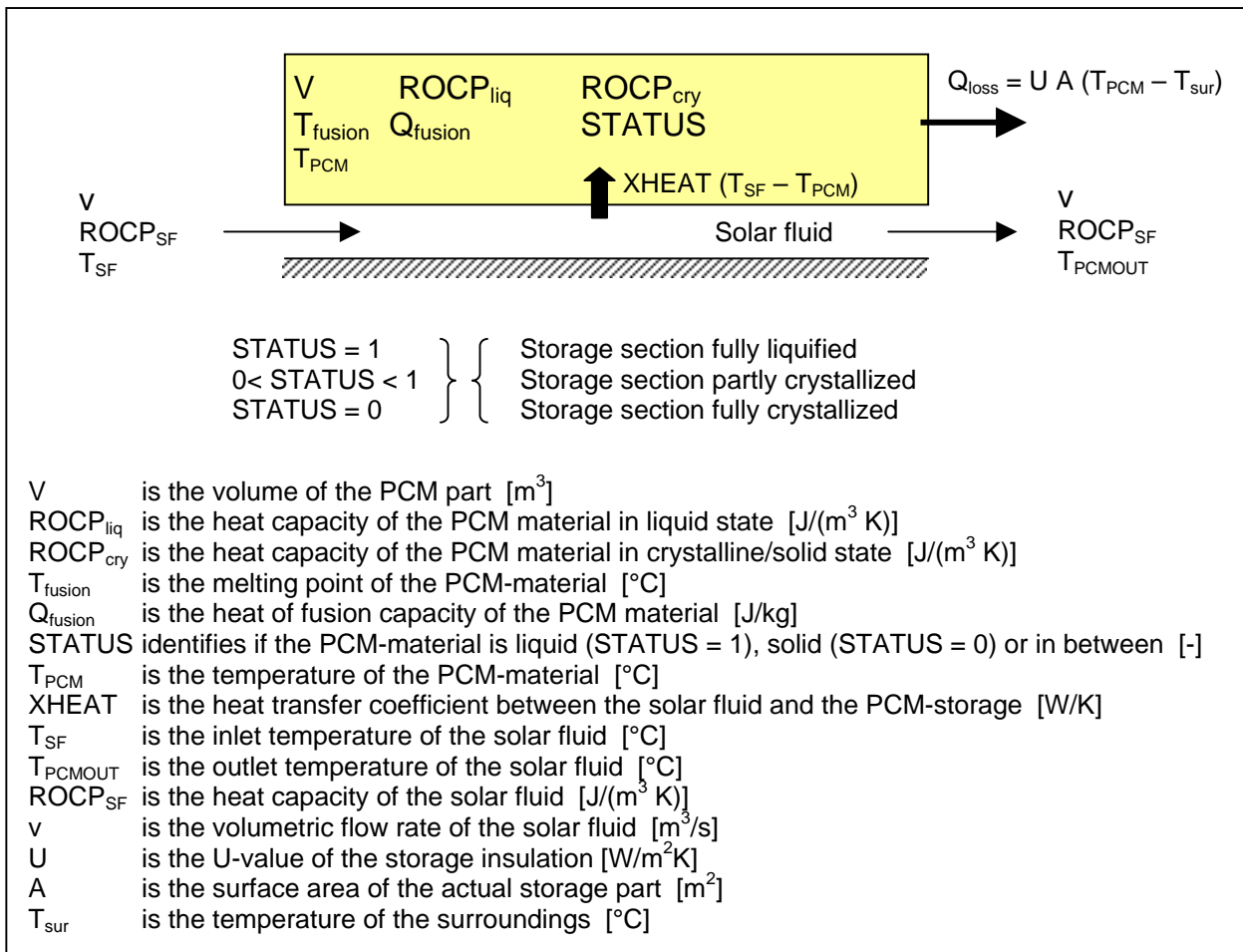


Fig. 5 Lumped model of one section of the PCM storage

## Preliminary simulation results

The model has been implemented in TRNSYS 15. Data for the main components is shown in table 2. For the reason of simplicity and the fact that the model is purely theoretical no pipes have been modelled, i.e. no pipe heat loss. The flow in the solar collector loop is constant all year round. If the outlet temperature from the solar collector is lower than the supply temperature to the collector + 10 K the controlled valve bypasses the solar collector. If the fluid temperature is higher than the bottom temperature of the domestic hot water tank the fluid is lead through the DHW tank before it reaches the PCM storage. Hourly values of the space heating demand is read from a file generated with a detailed building simulation program tsbi3 [4]. The building is a single-family low energy house with an annual space heating demand of approximately 15 kWh/m<sup>2</sup> (2000 kWh/year) corresponding to the Passive House concept.

Table 2. Data for the main components in the TRNSYS simulations

DHW tank	
Hot water tank volume	0.180 m <sup>3</sup>
Inner height	1.5 m
Number of identical layers	10
Auxiliary heat supply	1.2 kW, supplied 0.6 meter from top
Uniform insulation, U-value	0.66 W/m <sup>2</sup> K
Draw-off	50 l at 7:00, 12:00 and 18:00 (total 150 l/day)
Solar collector	
Producer	ARCON Solvarme A/S
Type	HT
Area	6 m <sup>2</sup>
Start efficiency	0.82
1 <sup>st</sup> order heat loss coefficient	2.44 W/m <sup>2</sup> K
2 <sup>nd</sup> order heat loss coefficient	0.005 W/m <sup>2</sup> K <sup>2</sup>
Incident angle modifier (tan equa.)	3.6
PCM storage	
Volume	1.5 m <sup>3</sup>
Number of sections	10
Number of internal time steps	50
U-value (uniform)	(0.001) / 0.66 W/m <sup>2</sup> K
PCM material	Sodium acetate with xanthan rubber
Heat of fusion	265 kJ/kg
Melting point	58 °C
Collector loop	
Flow	0.833 l/min/m <sup>2</sup>
Other	
Climatic data	Danish design reference year [5]
Space heating demand	Output from tsbi3 simulation of low energy house

Figure 6 shows the temperature evaluation and the status of the PCM storage for a theoretical example with almost no heat loss from the storage ( $U = 0.001 \text{ W/m}^2\text{K}$ ). The example has been chosen for illustrative purpose only.

It is clearly seen that during the late winter and early spring the storage is charged and discharged several times without fully melting of the PCM material (the temperature does not exceed the melting point of 58 °C).

When the space heating demand becomes close to zero in the late spring the storage is charged and the status becomes equal to 1 meaning that the storage is fully liquid. In the autumn the storage is discharged and the status drops from 1 to zero with only a small plateau at 58 °C.

Fig. 7 shows the same system but with a U-value for PCM storage insulation of 0.66 W/m<sup>2</sup>K. The system is not supposed to be optimised. The annual results are shown in table 3

Table 3. Results of simulation with 1.5 m<sup>3</sup> storage and values shown in table 2.

DHW tapped	DHW auxiliary	Space heating demand	Aux. space heat	Net utilized solar energy
2935 kWh	1346 kWh	2009 kWh	1727 kWh	1871 kWh

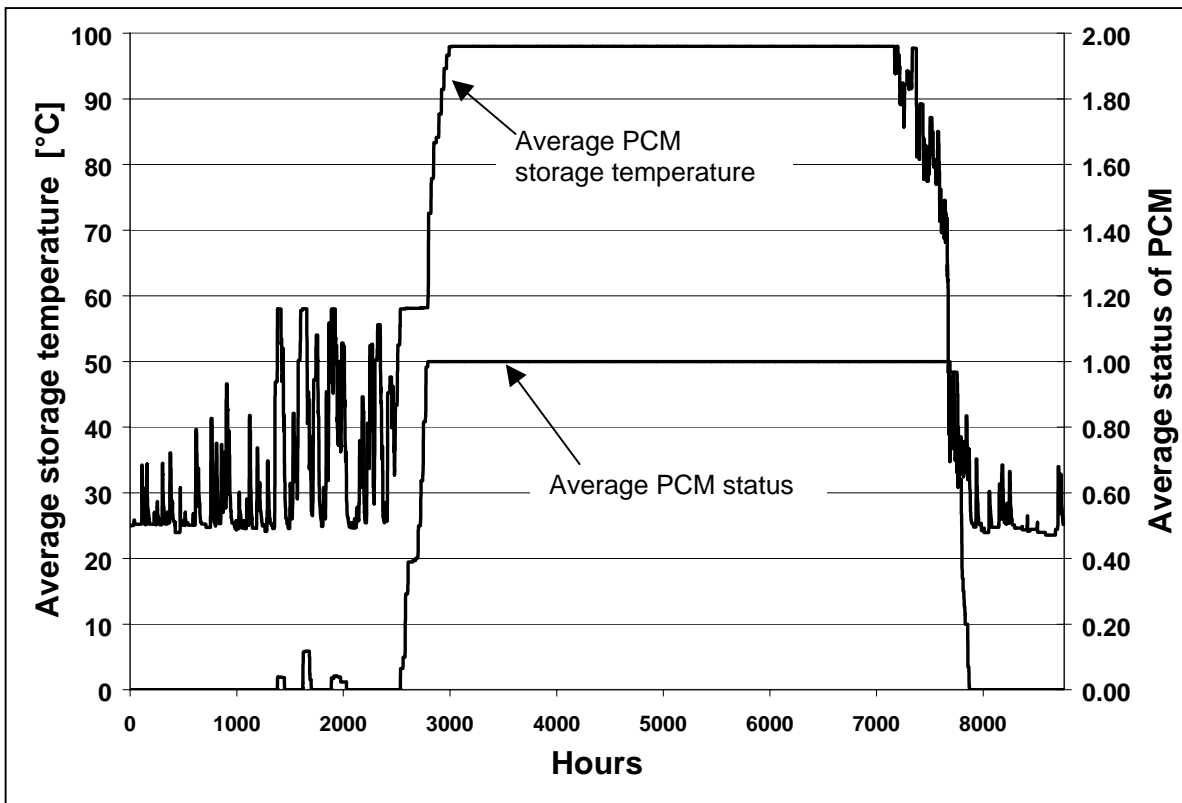


Fig. 6 Yearly distribution of average storage temperature and status for a theoretical storage with no heat loss.

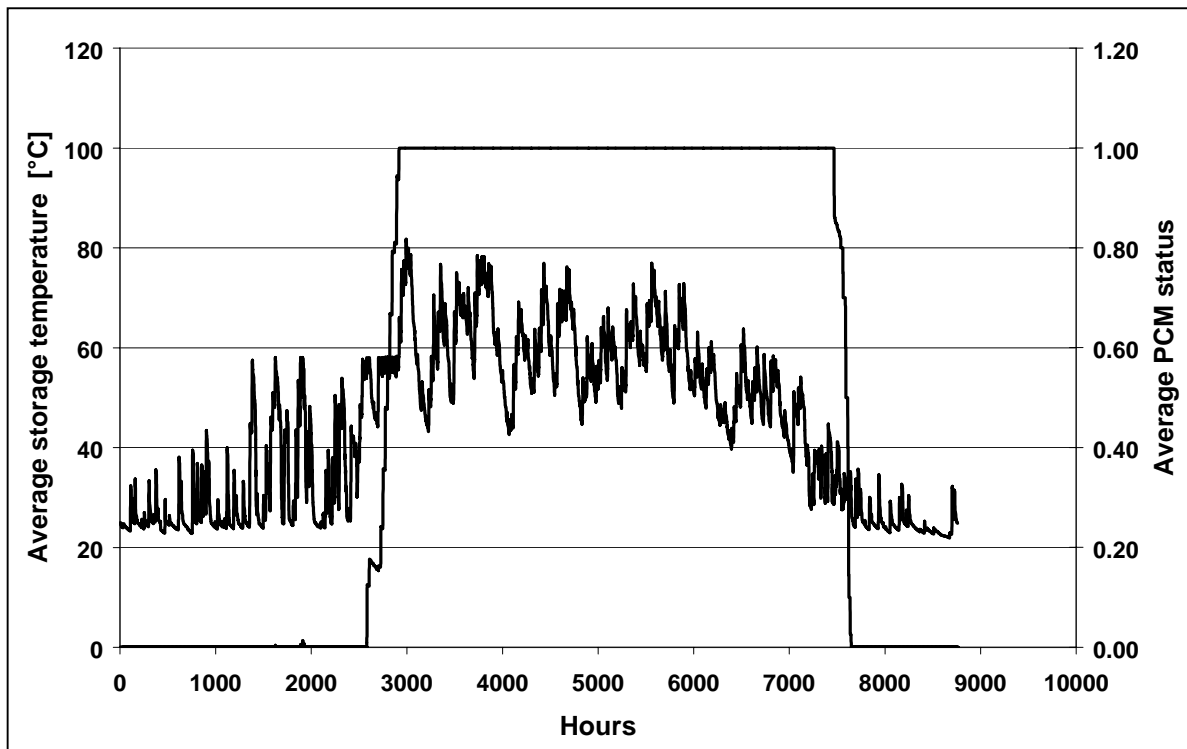


Fig. 7 Yearly distribution of average storage temperature and status for a 1.5 m<sup>3</sup> storage with a heat loss coefficient of 0.66 W/m<sup>2</sup>K.

## Conclusion

Phase Change Materials (PCM) for heat storage in combined solar systems offers the possibility of reducing the storage size compared to traditional water storages. Of special interest is the use in combination with low energy houses with low temperature heating systems. If the PCM further allows for stable super cooling the possibility exists for a storage with very low heat losses.

As part of the IEA Task 32 project “Advanced storage concepts for solar thermal systems in low energy buildings” a first draft of a TRNSYS type model of a PCM storage has been developed.

The first simulations with the model have proven the functionality of the model and reasonable overall results are obtained. On a detailed scale some irregularities are observed with respect to unexpected temperature drops (1 – 2 K) during periods with no space heating demand.

The future work will be concentrated on more detailed evaluations of the model and afterwards use of the model for detailed parametric studies in order to evaluate in detail the energetic potential of PCM storages compared to traditional water tanks.

## References

- [1] “TRNSYS 15, User Manual”. The University of Wisconsin. Madison, USA.
- [2] “Report on heat storage in a solar heating system using salt hydrates”. S. Furbo & S. Svendsen. Report No. 70, Thermal Insulation Laboratory, Technical University of Denmark, July 1977.
- [3] “Triggering crystallization in supercooled fluids. B. Sandnes. Department of Physics, University of Oslo, Norway. 2004.
- [4] “tsbi3 User Manual”. Danish Building Research Institute, 1993.
- [5] “Design Reference Year – A new Danish reference year”. J.M. Jensen & H. Lund. Report No. 281, Thermal Insulation Laboratory, Technical University of Denmark, 1995.



## **Bilag 3**

### **Investigation of heat of fusion storage for solar low energy buildings.**

Jørgen M. Schultz og Simon Furbo.  
Proceedings of ISES Solar World Congress 2005,  
Orlando, USA.



# INVESTIGATION OF HEAT OF FUSION STORAGE FOR SOLAR LOW ENERGY BUILDINGS

Jørgen M. Schultz  
Simon Furbo  
Department of Civil Engineering  
Technical University of Denmark  
DK-2800 Kgs. Lyngby  
Denmark  
e-mail: [js@byg.dtu.dk](mailto:js@byg.dtu.dk)  
e-mail: [sf@byg.dtu.dk](mailto:sf@byg.dtu.dk)

## ABSTRACT

This paper describes a theoretical investigation by means of TRNSYS simulations of a partly heat loss free phase change material (PCM) storage solution for solar heating systems. The partly heat loss free storage is obtained by controlled use of super cooling in a mixture of sodium acetate and xanthane rubber. The storage can cool down to surrounding temperature preserving the latent heat in form of the heat of fusion energy. The basis for the calculations is a super low energy house with a space heating demand of 2010 kWh/year and a domestic hot water demand of 2530 kWh/year. For storage volumes in the range of 500 – 3000 litres the heat loss free state is seldom reached and the effect of super cooling is limited. For larger volumes the heat loss free state may be reached. The benefit of using a PCM storage compared to a traditional water storage is limited with respect to energy savings for storage sizes up to 1 m<sup>3</sup>, but if the same amount of net utilised solar energy should be reached it would require a water storage that is 2 – 3 times larger.

## 1 INTRODUCTION

The time displacement between maximum solar insolation and demand is a well-known problem for solar heating systems with high coverage of domestic hot water, DHW, and space heating demand. A key issue to solve this problem is development of efficient heat storages for short-term (DHW) and long-term (space heating) storage of solar energy. This is the background for the ongoing IEA Solar, Heating and Cooling programme, Task 32: “Advanced Storage Concepts for Solar and Low Energy Buildings”. Water storages are the most widespread storage solutions and research in achievement of maximum

stratification and thereby the most efficient use of the solar energy is still improving the water storage performance.

However, in solar combi systems, systems for both DHW and space heating, the required storage size for achievement of a large solar fraction often turns out to be a problem with respect to fitting the storage into a typical house. Therefore, research on use of Phase Change Materials, PCM's, has been going on for many years as a way to increase the storage capacity for a given volume exploiting the large heat capacity related to the transition from solid to liquid state and vice versa – the heat of fusion.

Most of the research in PCM storage solutions is focused on increasing the thermal capacity of traditional water storage by adding encapsulated PCM in the storage. One of the problems encountered is the tendency of the PCM to super-cool, i.e. to cool down below the melting point without changing its state in which case the heat of fusion will not be released. This will be a major drawback for use as a substitute for a traditional water storage.

However, as part of the IEA Task 32 project, the idea of active use of stable super cooling as a measure to obtain a partly heat loss free seasonal storage is investigated. When first melted the storage will cool down to the surrounding temperature without phase change preserving the latent heat related to the phase change. In this state the storage will have no heat loss until the phase change is activated. The process is illustrated in Fig. 1 for a mixture of sodium acetate and xanthane rubber, which has proved to super-cool in a stable way. The melting point for sodium acetate is 58 °C and the heat of fusion energy is 265 kJ/kg.

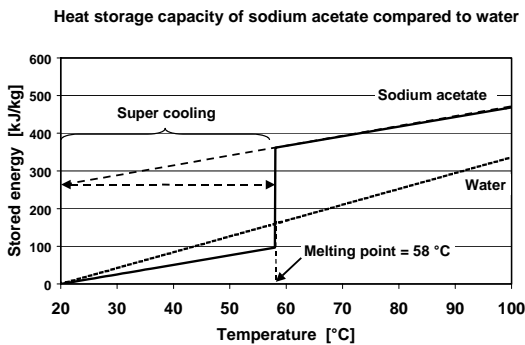


Fig. 1: Illustration of energy content of sodium acetate compared to water as well as the super cooling process.

As shown in Fig. 1 the storage capacity of sensible heat is larger for water compared to the sodium acetate, e.g. if the storage temperature is just below the melting point the stored energy in 1 kg of water is approx. 62 kJ or 64% higher than the stored energy in 1 kg of sodium acetate. So in order to benefit from the PCM the melting point should be exceeded.

The effect of the super cooling is shown in Fig. 1. When the storage cools down from a temperature above the melting point it continues to cool down as a liquid following the dotted line. When the storage temperature reaches the surrounding temperature the storage becomes heat loss free. When energy is required the super-cooled PCM is triggered to solidify and the temperature rises almost immediately to the melting point. But some of the heat of fusion energy is used to increase the temperature of the PCM from its super-cooled temperature to the melting point, which is illustrated by the horizontal dotted line in Fig. 1.

The purpose of the research is to investigate the potential of the PCM storage compared to traditional water storage. Therefore as a first step an ideal PCM storage with optimum control possibilities without regards to practical issues and economy is theoretically investigated by development of a special TRNSYS (1) type for simulation of a solar heating system with a PCM storage making use of the controlled super cooling.

This paper presents the results of the theoretical analyses leading to a proposal for an optimised PCM storage for a super low energy house in a Danish climate (56° north, approx. 3000 degree days). The ideal PCM storage is further compared to a traditional water storage solution.

## 2 SYSTEM DESCRIPTION

### 2.1 System design

The simulated solar system is shown in Fig. 2.

The system has two separate storage tanks, a 180 l hot water tank for domestic hot water and a PCM storage for space heating. The PCM storage is subdivided into a number of individual sections. The separate DHW tank is introduced in order to make full use of the super cooling, i.e. to avoid daily discharge of the PCM storage. Furthermore, the separate DHW tank also solves the problem with extraction of sufficient power during tapping of DHW.

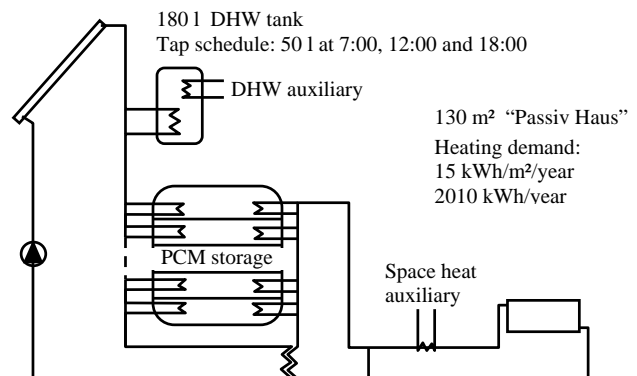


Fig. 2: Solar heating system design.

When solar energy is available the strategy is:

- If possible the DHW tank is heated until the bottom of the tank has reached 60 °C.
- In periods with a space heating demand the solar collector fluid is let through the PCM storage if the outlet temperature of the solar collector fluid from the PCM storage is sufficiently high to cover the space heating demand in the heat exchanger. Otherwise, the PCM storage is by-passed.
- In periods without space heating demand the PCM storage is heated one section at the time until all sections are melted. Thereafter the storage is heated until the maximum allowable temperature set at 95 °C is reached.

The DHW demand is 150 l/day heated from 10 °C to 55 °C distributed over 3 equal tap periods. The yearly domestic hot water demand is 2530 kWh. The auxiliary energy for the DHW is delivered by an electrical heating element in the tank.

The space heating demand is calculated on hourly basis for a super low energy house with a yearly space heating demand of 15 kWh/m<sup>2</sup> corresponding to approximately 2010 kWh/year in total. The heating system is a floor heating system with a constant return temperature of 25 °C, i.e. the required supply temperature to the heating system varies with the space-heating load.

The space heating demand is covered or preheated by solar energy in the heat exchanger if possible. If the required supply temperature to the heating system has

not been met the space heating fluid is let through the PCM storage for additional heating if possible. An electrical heater delivers auxiliary energy for the space heating if needed.

## 2.2 PCM storage design

The PCM storage is designed as a cylindrical storage with optimum volume to surface area fraction. The storage consists of a number of individual controllable horizontal sub-sections adiabatic separated from each other but with heat loss to the surroundings, Fig 3. The purpose of the sub-sections is to avoid activating the total volume of super-cooled PCM at one time, i.e. the sub-sections make it possible to match the demand in a more efficient way.

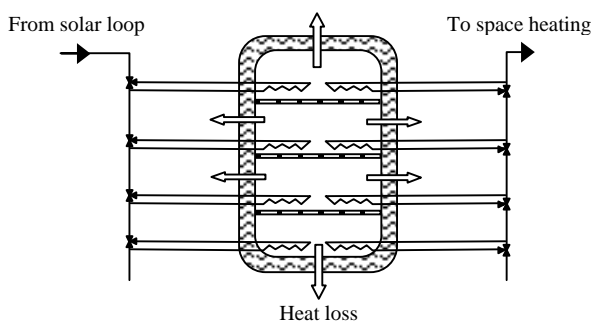


Fig. 3: PCM storage design.

The phase change material is a mixture of sodium acetate and xanthane rubber, which is characterised by stable super cooling. The melting point is 58 °C with a heat of fusion energy of 265 kJ/kg. The density is assumed to be 1301 kg/m<sup>3</sup> and the heat capacity of the solid salt hydrate crystals is 2540 J/(kg K) and 2551 J/(kg K) in the liquid phase (2).

Each sub-section contains two separate heat exchangers for charging and discharging of the section respectively as well as control valves for controlling the flow in the heat exchangers. Finally a fully controllable device for activation on demand of the solidification of the super-cooled PCM is anticipated in each sub-section as well. A heat exchange capacity rate of 1000 W/K is assumed in each section for both charging and discharging.

## 3 SYSTEM OPTIMISATION

### 3.1 PCM storage volume and sub-sectioning

The influence of the PCM storage volume and the effect of sub-sectioning have been investigated by means of TRNSYS simulations.

The collector is a high efficient flat plate collector (start efficiency 0.82, heat loss coefficient 2.45 W/m<sup>2</sup>K, incidence angle modifier 3.6 (tangent relation)). For this investigation the area is fixed at 6 m<sup>2</sup> and the collector

slope is 55°. The calculated net utilised solar energy for several combinations of total PCM storage volume and sub-section volume is shown in Fig. 4. It is noticeable that increasing the storage size above 500 litres without sub-sectioning only leads to a small increase in net utilised solar energy. However, dividing the storage into several sub-sections increases the system performance and as expected the higher number of sections the higher system performance. However, the difference in net utilised solar energy between a 500 litres and 3000 litres storage is in the range of approx. 200 kWh/year corresponding to 10% increase for a storage increase of 600%.

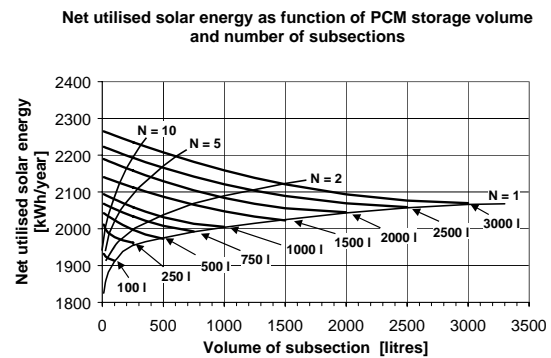


Fig. 4: Net utilised solar energy [kWh/year] as function of PCM storage size and number of subsections, N.

The reason for the relatively small effect of increasing the storage size can be explained by Fig. 5, which shows the space heating demand and the average storage temperature for a 1 m<sup>3</sup> storage. The storage is fully charged during the summer but a large part of the stored sensible heat is lost before start of the heating season mid of October. The average storage temperature is approx. 40 °C when the heating season starts. The latent heat in form of heat of fusion is still available and solidification is activated in the first section mid of November. All sections are solidified end of November.

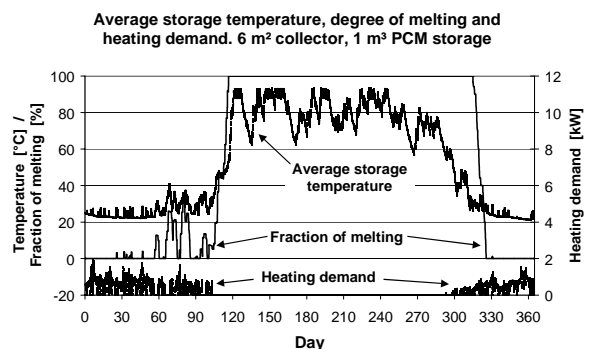


Fig. 5: Plot of the yearly distribution of average storage temperature, the fraction of melted PCM and the space heating demand.

Fig. 5 also shows that no significant charging of the storage takes place before beginning of March. So most of the space heating savings from mid of October to beginning of March is related to the energy content of the storage when the heating season starts. As an example a 1 m<sup>3</sup> PCM storage in liquid state at 60 °C has a usable sensible energy content of 23 kWh and a latent energy content of 75 kWh if the required supply temperature to the floor heating is 35 °C. All in all an energy content of approx. 100 kWh. For a 3 m<sup>3</sup> storage the equivalent energy content would be approx. 3 times larger, i.e. 300 kWh leading to an increased energy saving of 200 kWh/year.

The results do not give a clear idea of the optimum PCM storage solution. For instance 1m<sup>3</sup> storage with 5 subsections results in the same thermal performance as 3m<sup>3</sup> storage without sub-sectioning. An optimisation has to be based on an economic evaluation, which is outside the scope of this investigation.

Therefore a 1 m<sup>3</sup> PCM storage with 10 subsections is chosen for the following analyses based on an assumption that 1 m<sup>3</sup> would be a reasonable size with respect to space allocation in a typical house.

### 3.2 Collector area and collector slope

Above, the storage volume was shown only to have a limited influence on the energy savings due to large periods with a low amount of solar radiation. This points towards increasing the collector area in order to collect as much solar energy as possible when the sun occasional shines during the winter months. Putting focus on increased solar energy utilisation in the winter months should also involve an optimisation of the collector slope.

Fig. 6 shows the results of a parametric study of the influence of collector area and collector slope on the annual net utilised solar energy for the solar heating system shown in Fig. 2.

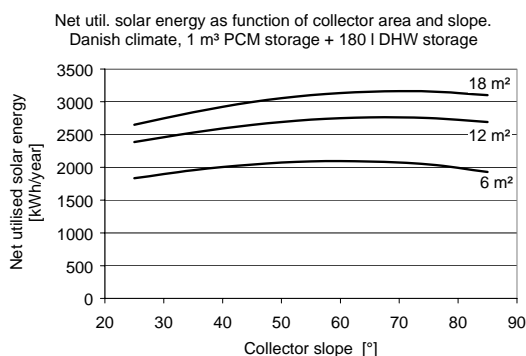


Fig. 6: Net utilised solar energy as function of collector area and collector slope. 1 m<sup>3</sup> PCM storage volume.

The curves in Fig. 6 shows that an increase of collector area from 6 m<sup>2</sup> to 12 m<sup>2</sup> increases the net utilised solar energy with approx. 700 kWh/year. a further collector area increase to 18 m<sup>2</sup> increases the net utilised solar energy with approx. 1100 kWh/year compared to the 6 m<sup>2</sup> solution. Fig. 6 also shows that the optimum collector slope changes towards a more vertical position when the collector area is increased. The optimum slope in Denmark is 55° for the 6 m<sup>2</sup> collector, 65° for the 12 m<sup>2</sup> collector and 75° for the 18 m<sup>2</sup> collector. Based on the analyses of collector area and PCM storage volume the system with 12 m<sup>2</sup> collector area and 1 m<sup>3</sup> PCM storage is chosen as the most promising design.

Table 1 shows the annual coverage of DHW and space heating for the solar heating system with 12 m<sup>2</sup> collector area, 180 litres DHW water tank and 1 m<sup>3</sup> PCM storage with sodium acetate.

**TABLE 1: ANNUAL DHW AND SPACE HEATING DEMAND COVERED BY SOLAR ENERGY**

	DHW	Space heating	Total
	kWh/year	kWh/year	kWh/year
Demand	2530	2010	4540
Auxiliary	650	1130	1780
Solar fraction	1880 (74%)	880 (44%)	2760 (61%)

### 3.3 Effect of super cooling

The effect of active use of super cooling as a measure to increase the annual performance of the solar heating system with PCM storage through minimising the storage heat losses has been investigated. The results of a simulation with and without super cooling are shown in Fig. 7

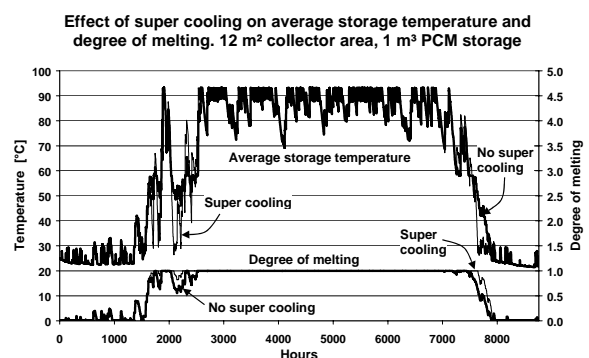


Fig. 7: Illustration of the effect of super cooling vs. no super cooling for 1 m<sup>3</sup> PCM storage.

As shown in Fig. 7 very limited differences are observed mainly around mid of October (~ hour 7500) where the average storage temperature for a short period is lower in case of super cooling than without. A

lower storage temperature results in lower heat losses. However, the calculated difference in net utilised solar energy only amounts to approximately 10 kWh/year in favour of the storage with super cooling.

The small effect is due to the fact, that the temperature in the melted storage never reaches a temperature close to the surroundings, i.e. the idea of a partly heat loss free storage is seldom realised. This would require a much larger storage in which most of the volume does not need to be solidified right in the beginning of the heating season.

### 3.4 Charge control strategy

Two different charge control strategies have been considered: 1) Maximum cooling of the solar fluid, i.e. the coldest section of the storage is heated and 2) maximum melting, i.e. if possible one section at the time is heated until fully melted. The first option results in the lowest return temperature to the solar collector, while the second option makes maximum use of the super cooling because when a section is melted it could cool down in the liquid phase resulting in lower heat losses. As for the super cooling / no super cooling case the difference for the 1 m<sup>3</sup> storage between the two charge strategies is almost negligible. However, this should be expected, as the benefit of the super cooling is almost not exploited.

### 3.5 PCM melting temperature

The melting temperature of sodium acetate is 58 °C, which is relatively high compared to the required supply temperature to the floor heating system in the super low energy house. Therefore, it might be a better solution to use a phase change material with a lower melting temperature. Analyses have been carried out for a imaginary phase change material with the same thermal characteristics as for sodium acetate except for the melting temperature, which is varied. The results are shown in Fig. 8.

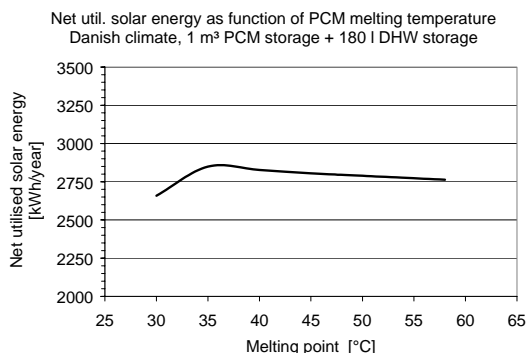


Fig. 8: Illustration of the influence of PCM melting point on the net utilised solar energy. Thermal properties are equal to that of sodium acetate except for the melting temperature.

Fig. 8 shows that the optimum melting temperature for the phase change storage is as close as possible to the required supply temperature in the heating system. In this case a melting temperature of approx. 35 °C corresponding to the maximum required supply temperature for the space heating results in maximum net utilised solar energy – an increase of approx. 100 kWh/year corresponding to an increase of 4% in net utilised solar energy.

## 4 PCM / WATER STORAGE COMPARISON

The developed model used for simulation of the PCM storage has also been used for simulation of the water storage. The sectioning feature of the model makes it possible to simulate stratified water storage with good approximation and using the same model for both types of storage material excludes differences caused by model differences. The result of the analysis is shown in Fig. 9

The absolute difference in the net utilised solar energy between the two systems for a fixed storage volume is in the range of 80 kWh/year for storage volumes below 1 m<sup>3</sup>. For larger storage volume the difference increases as the yield of the PCM storage continues to increase, while the benefit of increasing the water storage volume becomes insignificant.

The reason is the high thermal storage capacity of the PCM at 58 °C due to the heat of fusion. Increasing the PCM storage volume means that a larger part of the storage is just heated until melting, i.e. the storage temperature will be close to the melting temperature. If the same amount of energy should be stored in the water storage the mean storage temperature becomes significant higher and by then also a significant higher heat loss. The difference between the two curves in Fig. 9 is in fact a measure of the difference in storage heat loss.

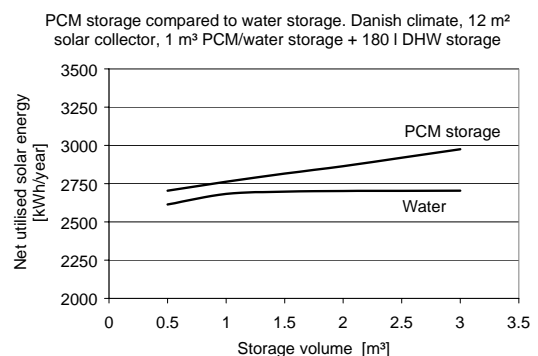


Fig. 9: Comparison of the net utilised solar energy for a system with PCM storage and a system with water storage.

## 5 DISCUSSION

The basis for the analyses presented in the previous sections is a super low energy building located in Denmark with a very low space heating demand concentrated in the late autumn and winter months where the amount of solar radiation is very limited. It has also been anticipated that the storage size should fit into a typical single-family house.

The results of the analyses show that it is impossible to cover most of the space heating demand by a storage volume in the range of 1 – 2 m<sup>3</sup> as the storage due to the climatic conditions should be able to deliver almost the total space heating demand from the energy stored during the summer.

The energy content of a 1 m<sup>3</sup> PCM storage is approx. 100 kWh so in order to cover the total space heating demand of 2000 kWh a 20 m<sup>3</sup> storage would be required.

Limiting the storage volume to 1- 2 m<sup>3</sup> makes the collector area a more important parameter than the storage volume. A large collector area will be able to collect a large amount of energy on a short time, i.e. the limited days during winter with high solar insolation. In this context the storage volume should “just” be able to store the solar energy acquired on a typical sunny winter day.

The initial idea of creating a partly heat loss free storage has not been realised. The reason is that a storage with a volume of 1- 2 m<sup>3</sup> never experience a period when fully charged where the storage temperature due to heat loss equals the temperature of the surroundings. However, for a very large storage of e.g. 20 m<sup>3</sup> subdivided into a large number of individual sections the partly heat loss free storage may be realised by active use of super cooling.

Compared to traditional water storage the benefit of PCM storage is relatively small with respect to energy saving for storage volumes up to 1 m<sup>3</sup>, but if the same amount of net utilised solar energy should be reached with the two types of storages the water storage volume need to be 2 – 3 times larger than the PCM storage. For larger volumes it will not be possible for a water storage to match the performance of a PCM storage due to differences in the storage heat loss.

## 6 CONCLUSIONS

An idea of making a partly heat loss free phase change material (PCM) storage with controlled use of super cooling has been investigated theoretically in a solar heating system for domestic hot water and space heating. The space heating demand is approx. 2010 kWh/year corresponding to a super low energy house.

A mixture of sodium acetate and xanthane rubber, which super cools in a stable way, has been used for the investigations. The super cooling makes it possible to cool down the storage to surrounding temperature preserving the latent heat. In this state the storage is heat loss free.

The storage is divided into a number of individual sections in order only to activate the solidification in a small part of the storage at the time. The analyses show that an increase in number of subsections for a fixed volume increases the net utilised solar energy with 5 – 10% for storage volumes in the range of 500 – 3000 litres.

Increasing the solar collector area from 6 to 12 m<sup>2</sup> increases the net utilised solar energy with approx. 30 % for a fixed PCM storage volume of 1000 litres. The large effect compared to increasing the storage volume is due to the very low space heating demand that occurs only in wintertime with sparse solar insolation. In this case acquisition of a large amount of solar energy in short time is more important than the capability of the storage to store energy for longer periods.

The effect of the super cooling is very limited for the storage volumes considered (500 –3000 litres) as the storage seldom reaches the heat loss free state. If most of the space heating consumption should be covered by solar energy a storage volume of approx. 20 m<sup>3</sup> would be required for the low energy house. In this case the partly heat loss free storage would probably be a reality.

Parametric studies of the PCM melting temperature show that the optimum melting temperature is equal to the maximum supply temperature to the heating system. The benefit of using a PCM storage compared to a traditional water storage is limited with respect to absolute annual energy savings for storage sizes up to 1 m<sup>3</sup>, but if the same amount of net utilised solar energy should be reached it would require a water storage that is 2 – 3 times larger. For larger storage volumes water storages will not be able to match the PCM storage.

## 7 ACKNOWLEDGEMENTS

The project is financed by the Danish Energy Authority.

## 8 REFERENCES

1. TRNSYS 15, ver. 3.0.0.20
2. S. Furbo & S. Svendsen. Report on heat storage in a solar heating system using salt hydrates. Report no. 70, Thermal Insulation Laboratory, Technical University of Denmark, 1977.

## **Bilag 4**

### **Theoretical and Experimental investigations of Inlet stratifiers for Solar Storage Tanks.**

Louise Jivan Shah, Elsa Andersen og Simon Furbo.  
Applied Thermal Engineering 25 (2005). pp 2086–2099





# Theoretical and experimental investigations of inlet stratifiers for solar storage tanks

Louise Jivan Shah <sup>\*</sup>, Elsa Andersen, Simon Furbo

*Department of Civil Engineering, Technical University of Denmark, Building 118, DK-2800 Kgs. Lyngby, Denmark*

Received 6 September 2004; accepted 24 January 2005

Available online 22 March 2005

---

## Abstract

A rigid stratifier is investigated theoretically with Computational Fluid Dynamics and experimentally with Particle Image Velocimetry and temperature measurements. The stratifier consists of a main tube with three circular openings. The stratifier is mounted inside a 144 l water tank.

During a tank charge test, the investigations show that cold tank water is sucked into the stratifier through the lowest opening. The mixed fluid enters the tank through the top opening.

To illustrate the influence of mounting flaps working as “non-return valves” at the stratifier openings, the experiment is repeated with the stratifier with flaps. The results show that the “non-return valves” reduce the unwanted flows into the lowest opening.

To quantify how well the stratifier with the flaps works for other flow rates more tank charge tests are carried out. Based on a stratifier efficiency it is found that the stratifier is most efficient for flow rates between 5 l/min and 8 l/min.

© 2005 Elsevier Ltd. All rights reserved.

*Keywords:* Thermal stratification; Solar storage; Computational Fluid Dynamics; Particle Image Velocimetry

---

---

<sup>\*</sup> Corresponding author. Tel.: +45 45 25 18 88; fax: +45 45 93 17 55.

*E-mail address:* [ljs@byg.dtu.dk](mailto:ljs@byg.dtu.dk) (L.J. Shah).

## Nomenclature

$Q_1$	actual energy amount supplied to the tank [J]
$Q_2$	maximum possible exchanged energy amount [J]
$V$	exchanged tank volume [m <sup>3</sup> ]
$\dot{V}$	volume flow rate [m <sup>3</sup> /s]
$t$	time [s]
$T_{\text{initial}}$	initial tank temperature [°C]
$T_{\text{inlet}}$	inlet temperature [°C]
$T_{\text{outlet}}$	outlet temperature [°C]
$T_{\text{average,inlet}}$	average inlet temperature during the experiment [°C]
$c_p$	water heat capacity [J/kg K]
$\rho$	water density [kg/m <sup>3</sup> ]

## 1. Introduction

Thermal stratification in sensible energy storages plays an important role on the efficiency of the energy system of which the storage is a part of. For example in hot water tanks heated by gas burners a well stratified storage, where the cold water inlet does not disturb the thermal stratification, leads to better operation of the gas burner (less starts and stops) and thus an increased burner efficiency. Analogous, energy systems with stratified heat storages heated by biomass burners will have a higher efficiency compared to systems with non-stratified storages.

Thermal stratification in solar storage tanks has a major influence on the thermal performance of a solar heating system. In solar combisystems, which are solar heating installations providing space heating as well as domestic hot water [1], very often diffuser manifolds or stratifiers, which should promote stratification, have been adopted.

These stratifiers are used in the solar storage tanks for the return flow from the solar collector, and/or from the space heating system and/or from the return of the domestic hot water preparation. Fig. 1 shows a diagram of a solar combisystem with two stratifiers in the solar collector loop and the space heating loop respectively.

Generally, stratifiers are developed for variable inlet-temperature and flow, corresponding to the conditions in the solar collector loop and the space heating loop of a solar combisystem. The main purpose for a stratifier is to allow the incoming fluid to enter the tank at the “right” height of thermal equilibrium.

One of the first stratifier designs was suggested by van Koppen et al. [3]. A floating flexible light rubber hose was used, and by buoyancy forces the hose should reach the thermal equilibrium in the tank of the incoming fluid. Due to problems with dirt accumulated in the hose, this solution never worked in practice.

Loehrke et al. [4] investigated two types of stratifiers. One was based on a rigid perforated PVC drain pipe with a diameter of 10 cm and another was based on a flexible 10 cm diameter “sleeve” made of a polyester cloth. It was found that the performance of the flexible stratifier was superior

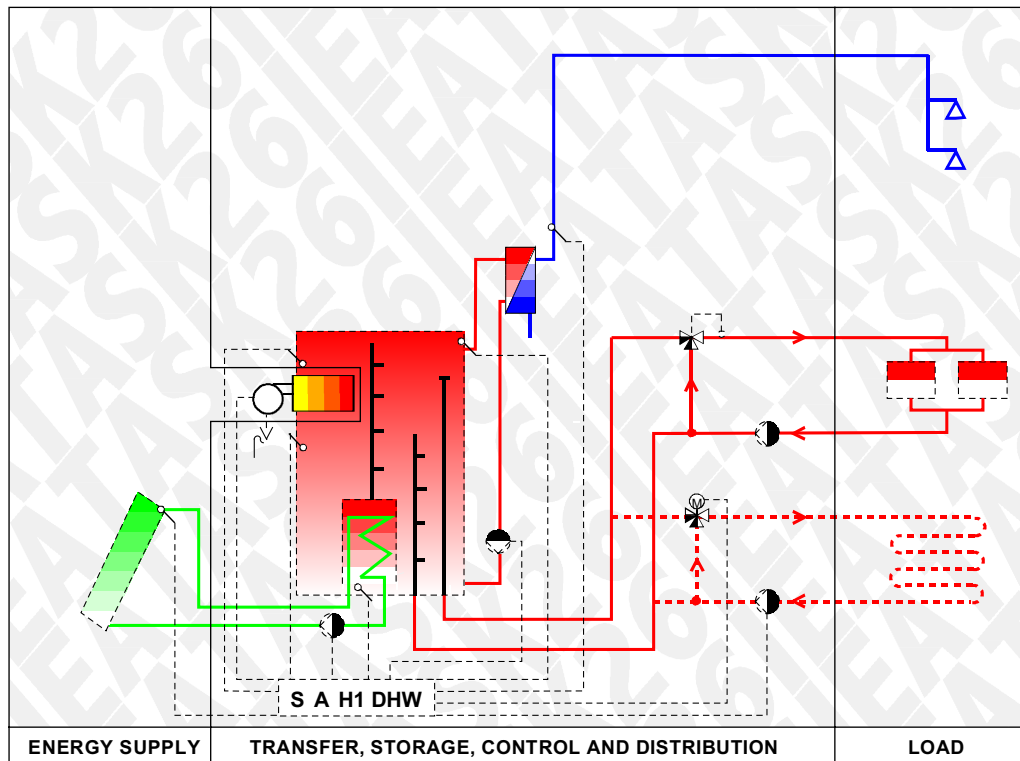


Fig. 1. A solar combisystem with two stratifiers in the solar collector loop and the space heating loop respectively (figure from [2]).

to the rigid stratifier, due to the fact that the “sleeve” diameter changed with the inlet flow rate and the thermal conditions in the tank.

Davidson and Adams [5] worked further on flexible stratifiers. Experimentally, they investigated different fabric materials for the flexible sleeve and they concluded that synthetic fabrics were superior to natural fibres and that effective manifold materials should be rib-knit which stretch easily in one direction. Based on the MIX-number [6] they also found that the flexible stratifier was 4% more effective than a rigid stratifier and 48% more effective than a traditional drop-tube inlet.

Abu-Hamdan et al. [7] investigated a highly perforated tube with a diameter of 35.6 cm and a length of 1.47 m. For variable inlet conditions they found that this configuration offered no advantages over conventional side and top inlets.

On the market today there are several rigid stratifier designs. A design based on a long tube with openings is used. One example of the use of this stratifier design is shown in Fig. 2.

Another more advanced stratifier design is shown in Fig. 3. Here, at the openings there are mounted flaps, which work as “non-return valves”. The flaps are constructed with a soft material which allows the flap to close and open depending on the temperature and pressure conditions inside and outside the pipe. The stratifier is designed by the German company Solvis GmbH, and according to the company the stratifier is suitable for flows up to 13 l/min.

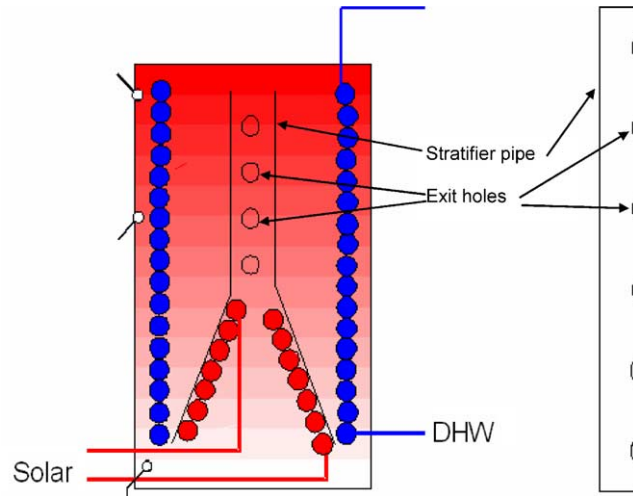


Fig. 2. Left: Stratifiers for the return flow from the solar collector inside a storage tank. The stratifier is based on a pipe with openings. Inside the stratifier the flow is natural convection driven. Right: The stratifier seen from the side.

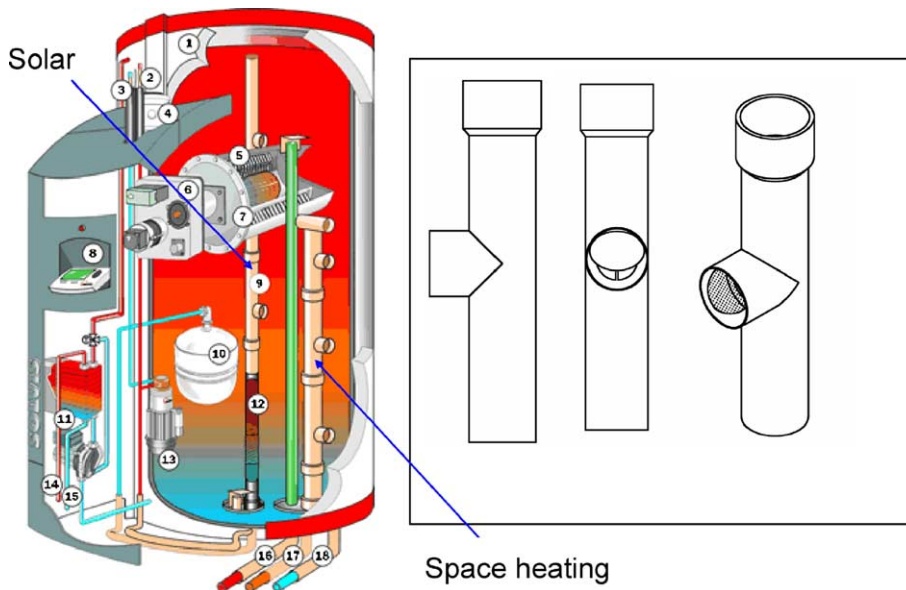


Fig. 3. Left: The SOLVIS stratifiers for the return flow from the solar collector and from the space heating system inside a storage tank. The stratifier design is based on a pipe with openings where flaps working as “non-return valves” are mounted. Right: Schematics of the stratifier.

Essert [8] experimentally investigated this stratifier and found that the stratifier was well working for flows below 10 l/min. For higher flow rates it was found that the performance also strongly depended on the thermal conditions.

Also Andersen et al. [9] experimentally investigated this stratifier design. Several tank charge tests were performed and generally, it was found that thermal stratification was well built up with the stratifier. However, they also concluded that further detailed investigations are needed, before the function of this stratification inlet pipe is fully elucidated.

The aim of the present work is to evaluate by theoretical and experimental means, how a stratifier with unobstructed openings performs. The aim is also to illustrate the influence of mounting flaps at the openings.

## 2. Theoretical investigations

A water tank with a stratifier is investigated by means of Computational Fluid Dynamics (CFD) calculations. The tank is square with side lengths of 0.4 m and a height of 0.9 m, and thus a volume of approximately 144 l.

The investigated stratifier is designed as the stratifier shown in Fig. 3, however, the flaps are removed. The distance between the bottom of the tank and the centre of the lowest opening is 0.15 m and the distances between the openings are 0.30 m. Each opening diameter is 0.06 m, the pipe is closed at the top and the fluid enters the stratifier through the bottom. The tank outlet is also placed at the tank bottom. Fig. 4 (left) shows a schematic illustration of the investigated stratifier.

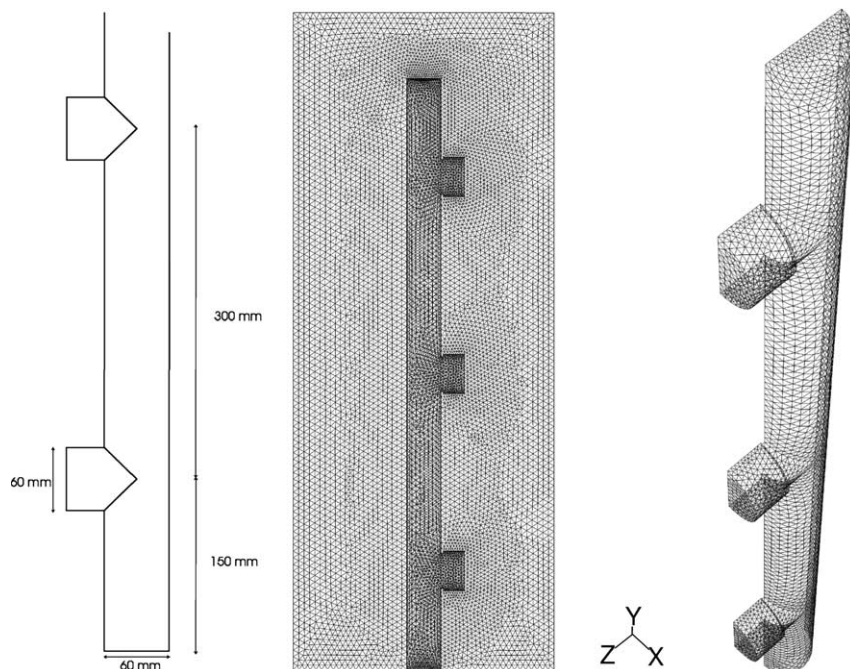


Fig. 4. Left: Measures of the stratifier. Middle: The grid distribution in the symmetry plane. Right: The wall grid of the stratifier.

A 50 min long charge test is modelled. The tank is initially cold (20 °C) and through the stratifier, the tank is charged by an inlet flow of about 2 l/min and a temperature of about 43 °C, corresponding to the test conditions of the experiments described later.

To solve the flow and energy equations, a simulation model of the flow in the tank is developed using the CFD code Fluent 6.1 [10]. A stratifier with three openings is investigated. The tank outlet is placed at the bottom corner of the tank. The tank walls are not modelled and symmetry is assumed in the centre plane of the tank. Further, the heat loss from the tank is not modelled. This has no significant influence on the results as the simulated tests are of a duration of only 50 min and as the heat loss power through the tank wall is magnitudes lower than the tank charge power. The mesh is built up of 580,149 tetrahedral cells and is thus an unstructured mesh. Fig. 4 shows the model outline, the grid distributions in the symmetry plane and the wall grid of the stratifier.

Numerical solutions are obtained for transient laminar flow with the Boussinesq assumption for the buoyancy modelling. The velocity-pressure coupling is treated by using the SIMPLE algorithm and the First Order Upwind scheme is used for the momentum and energy terms. A time step of 0.5 s is used.

Fig. 5 shows the temperature distribution in the tank centre plane after 10 min, 30 min and 50 min. The temperature profiles show how the tank water is sucked into the stratifier especially through the bottom opening. The cold tank water is mixed with the hot inlet flow and this mixed flow enters the tank through the top opening. After 50 min. there is almost no thermal stratification in the tank. The temperature difference between the top and bottom of the tank is only about 5–6 K.

The computations show that under the present operating conditions (2 l/min inlet flow) this type of stratifier actually works more as a “mixing device” than as a stratifying device.

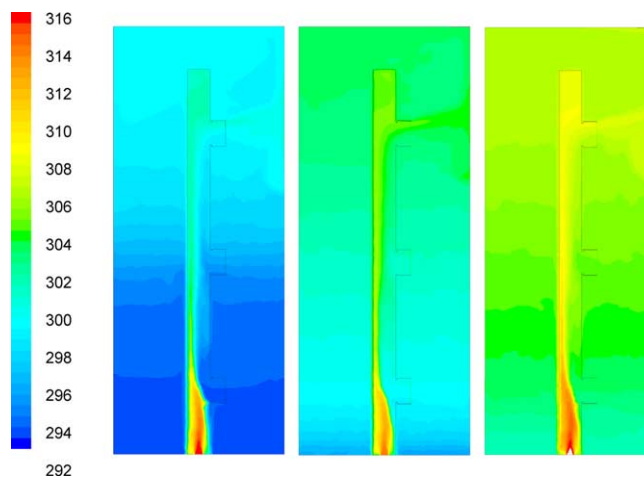


Fig. 5. Temperatures in the tank after 10 min, 30 min and 50 min. The scale at the left shows the temperature level in [K].

### 3. Experimental investigations

In order to verify the simulated results, the stratifier is experimentally investigated by means of PIV (Particle Image Velocimetry).

The experimental set-up is shown in Fig. 6. The set-up consists of a rectangular glass tank with side lengths of  $400 \times 400 \times 900 \text{ mm}^3$ , a heating and a cooling unit, and standard PIV equipment (Dantec Dynamics). The PIV equipment consists of a laser, a camera and a processing system for analysing the pictures taken by the camera. More details about the PIV equipment and the heating/cooling unit are given in [9].

With the PIV equipment the two-dimensional flow field near each opening is visualized. The interrogation area near each opening has the size  $0.127 \times 0.159 \text{ m}^2$  as illustrated in Fig. 7. Fig. 8 shows photos of the stratifier.

In addition to the PIV measurements, also temperature measurements are carried out. The inlet temperature, the outlet temperature and five temperatures inside the tank are measured. The temperature sensors inside the tank are respectively placed at 145 mm, 345 mm, 545 mm, 705 mm and 865 mm from the bottom of the tank.

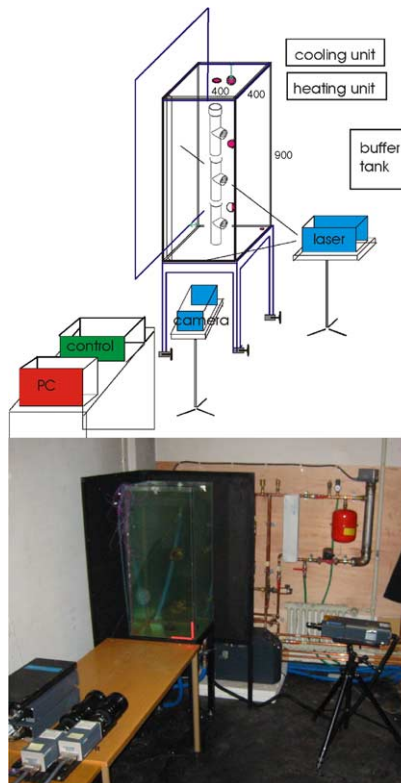


Fig. 6. Experimental set-up (figure from [8]).

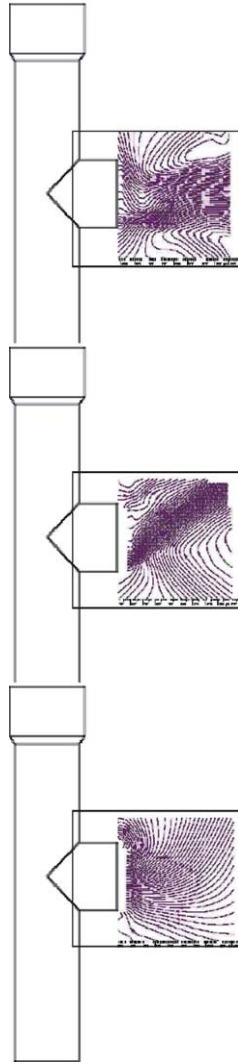


Fig. 7. Illustration of the interrogation areas (figure from [8]).

A 47 min. long charge experiment is carried out. As in the previous computations, the tank is initially cold (20 °C) and through the stratifier the tank is charged by an inlet flow of about 2 l/min and a temperature of about 43 °C.

Fig. 9 shows tank inlet- and outlet temperatures, the flow rate and the temperatures in the tank. It can be seen that the tank outlet temperature rises after only 25 min, which is after only a 50 l draw-off. This shows that the thermal stratification is not build up in a good way. If the thermal stratification was build up in an ideal way the bottom outlet temperature should rise after approximately 60 min. as the tank volume below the top opening is approximately 120 l and the flow rate is about 2 l/min.

As an example, Fig. 10 shows calculated and measured velocity vectors near the openings after 40 min. The main flow stream in both the experiments and the calculations enters the tank

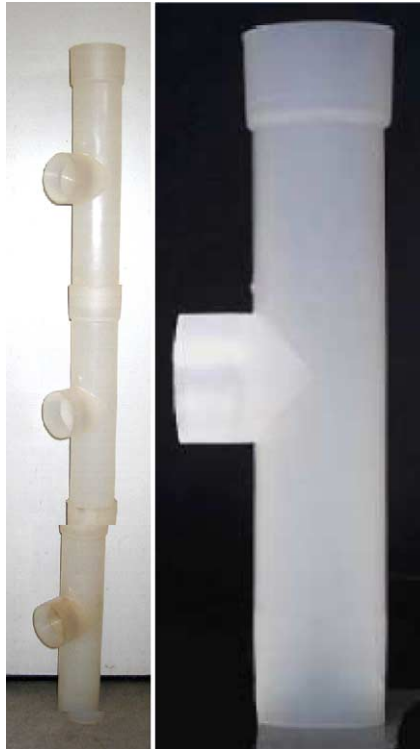


Fig. 8. Photos of one stratification inlet pipe (right) and the stratifier made of three compound inlet pipes.

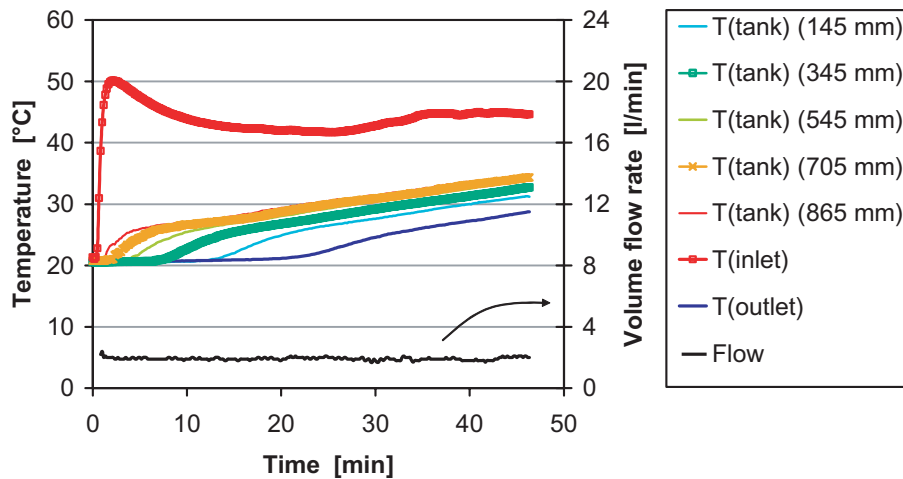


Fig. 9. The test conditions and the temperatures in the tank during the experiment.

through the top opening of the stratifier. At the middle outlet there is a difference between the measured and calculated flow patterns as the measurements show a small flow entering the bottom of the opening and a significant flow stream leaving at the very top of this opening. The rea-

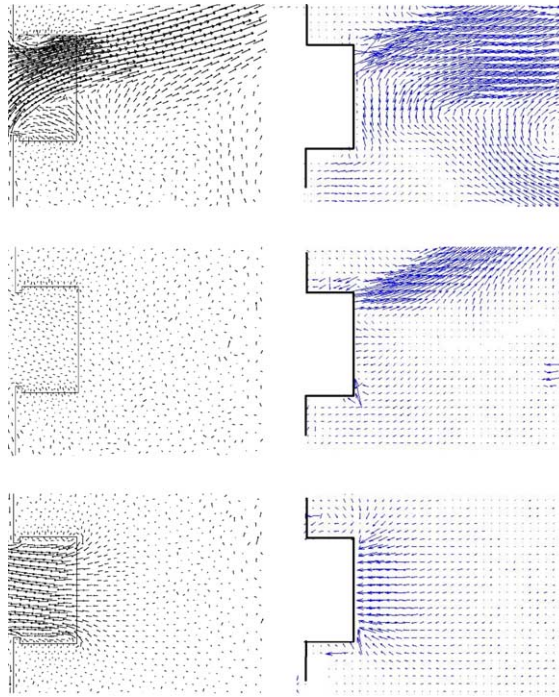


Fig. 10. Calculated (left) and measured (right) velocity vectors. Calculated and measured velocity magnitude: 0–0.06 m/s.

son for the difference is most likely that the numerical grid is too coarse to solve this complicated flow. Another reason could be that the modelled and the actual stratifier geometry is not completely identical as the stratifier is modelled as a thin non-conducting shell instead of a 3 mm thick wall. However, both in the calculations and in the measurements, a significant flow through the bottom opening into the main stratifier pipe is present.

To illustrate the influence of placing the flaps at the openings, the experiment was repeated now with the stratifier with the flaps. The flaps are made of a soft rubber material and they should work as “non-return valves”. Each flap is mounted on a small hook in the top of each opening. This allows the flap to open when there is a flow going out and to close when the flow inside the main tube is rising to an upper opening.

Fig. 11 shows tank inlet- and outlet temperatures, the flow rate and the temperatures in the tank during this experiment. Now it can be seen that the bottom outlet temperature hardly rises during the test. This means that the thermal stratification is build up in a better way with the stratifier with “non-return valves” compared to the stratifier without “non-return valves”.

The influence of the “non-return valves” is further illustrated in Fig. 12. Here, the measured velocity vectors near the openings after 40 min. in the experiment for the stratifiers without and with the “non-return valves” are compared. Here it is quite clear that the “non-return valves” reduces the unwanted flow going into the stratifier at the lowest opening.

For the stratifier with the “non-return valves”, it can also be seen that there are some natural convection flows near the stratifier wall below and above the lower opening. Since there is less

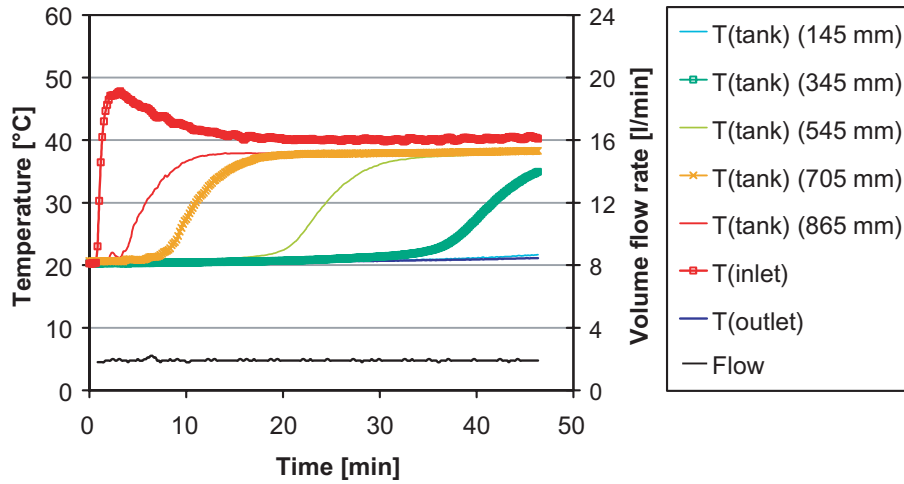


Fig. 11. The test conditions and the temperatures in the tank during the experiment with the stratifier with “non-return valves”.

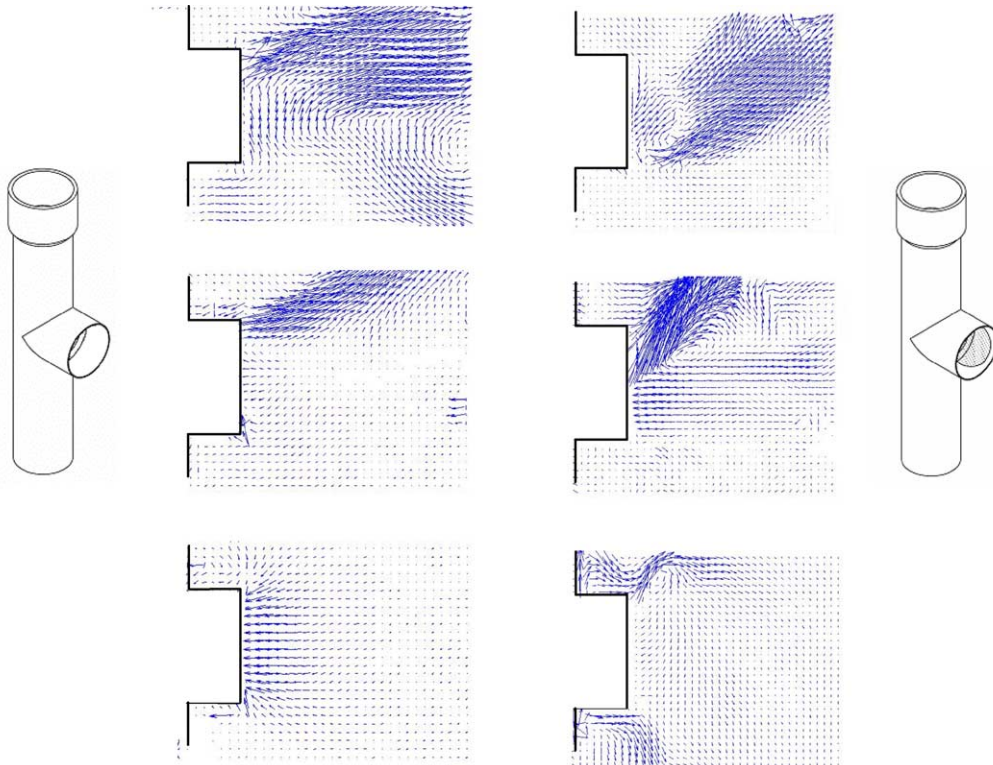


Fig. 12. Measured velocity vectors for the stratifier without the “non-return valves” (left) and with the “non-return valves” (right).

fluid being sucked into the stratifier pipe, the fluid temperature in the stratifier with “non-return valves” is higher compared to the stratifier without the “non-return valves”. Furthermore, the tank bottom temperature is colder compared to the bottom temperature in the tank without the “non-return valves”. Consequently, the temperature difference, and thus the natural convection, between the stratifier wall and the fluid in the tank are more significant for the system with “non-return valves” compared to the system without the “non-return valves”.

Fig. 12 also shows that the stratifier with the “non-return valves” is not ideally working. As the flow leaving the top opening seeks upwards, the temperature inside the stratifier must be warmer than the tank temperature in the same height. This means that the flow should only leave the top opening. From the figure, however, it is quite clear that there is also fluid streaming out of the middle opening.

The investigations clearly show that the flaps have a significant influence of how well the thermal stratification is being built up in the tank. However, the investigations also show that the stratifier with the flaps is not ideally working.

The results described above are valid for a flow rate of about 2 l/min. To quantify how well the stratifier with flaps works for other flow rates other tank charge tests have been carried out. In total 5 experiments are performed with flow rates of 2 l/min, 4 l/min, 5 l/min, 8 l/min and 10 l/min. These experiments are in detail described in [11].

By means of the measured inlet and outlet temperatures and the flow rate, the actual energy amount supplied to the tank,  $Q_1$ , is determined until one tank volume is exchanged.

Further, assuming that no mixing occurs, the maximum possible energy amount supplied to the tank,  $Q_2$ , is determined.  $Q_1$  and  $Q_2$  are described by Eqs. (1) and (2):

$$Q_1 = \int_{t_{\text{start}}}^{t_{\text{stop}}} \dot{V} \cdot \rho \cdot c_p \cdot (T_{\text{inlet}} - T_{\text{outlet}}) dt \quad [J] \quad (1)$$

$$Q_2 = V \cdot \rho \cdot c_p \cdot (T_{\text{average,inlet}} - T_{\text{initial}}) \quad [J] \quad (2)$$

The efficiency of the stratifier is defined as  $Q_1/Q_2$ . Thus, the stratifier is ideally working if  $Q_1/Q_2$  equals 1 when one tank volume has been charged. In order to take into account that the test periods do not have equal lengths, the efficiency results are corrected for the tank heat loss. That is, the calculated efficiencies are based on the measured temperatures, which are corrected to the values they would have obtained if there were no heat losses.

As a function of the volume flow rate the efficiencies are shown in Fig. 13. Here it can be seen that the stratifier efficiency is highest for flow rates between 5 l/min and 8 l/min. The reasons are as follows:

For small volume flow rates, the inlet flow rises as expected in the stratifier but the heat transfer through the stratifier wall from the hot inlet fluid to the colder tank will significantly decrease the temperature at the top opening. Consequently, the temperature at the top opening is reduced and thus the efficiency is reduced. Further, during the experiments it was noticed that the lowest flap does not close completely tight as the suction on the lower flaps is quite small due to the relatively small velocity in the stratifier. Therefore, some fluid is sucked in to the stratifier through the lowest hole. This is, however, not clearly seen in Fig. 12.

For higher flow rates, the temperature drop inside the stratifier due to heat transfer through the stratifier is less significant. Consequently, compared to the lowest flow rate, the temperature at the

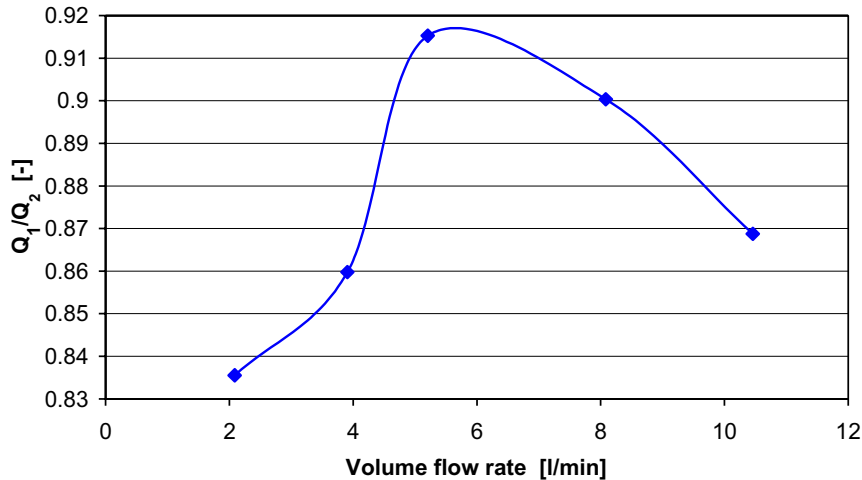


Fig. 13. The stratifier efficiency as a function of the volume flow rate.

top opening is increased and thus the efficiency is increased. Further, under these experiments it was noticed that the lowest flap is completely closed. As the velocity in the stratifier is increased the suction on the lower flaps is higher and the flaps close more tightly.

For the highest flow rate, the velocity in the stratifier is so large that, due to the momentum forces, the fluid exits not only the top opening. Therefore, the efficiency is decreased again.

#### 4. Conclusion

A rigid stratifier is investigated theoretically with Computational Fluid Dynamics and experimentally with Particle Image Velocimetry and temperature measurements. The stratifier is designed as a main tube with three circular openings. The stratifier is mounted inside a 144 l water tank.

A tank charge investigation is performed. The tank was initially cold (20 °C) and through the stratifier the tank is charged by an inlet flow of about 2 l/min and a temperature of about 43 °C.

Both the experimental and the theoretical investigations show that cold tank water is sucked into the stratifier especially through the lowest opening and the mixed fluid enters the tank through the top opening. Consequently, under the examined operating conditions this type of stratifier actually works more as a “mixing device” than as a stratifying device.

To illustrate the influence of placing “non-return valves” at the stratifier openings, the experiment is repeated with the stratifier with flaps working as “non-return valves”. Here it is clear that the “non-return valves” reduces the unwanted flows at the lowest opening.

To quantify how well the stratifier with the flaps works for other flow rates more tank charge tests are performed. In total five experiments are performed with flow rates in the interval from 2 l/min to 10 l/min.

Based on a stratifier efficiency defined as the ratio between the actual energy amount supplied to the tank and the maximum possible energy amount supplied to the tank assuming that no mixing occur, it is found that the stratifier is most efficient for flow rates between 5 l/min and 8 l/min.

As the investigated stratifiers often are used for volume flow rates much less than 5 l/min it is concluded that there still is a need for further development of these stratifier designs.

## References

- [1] IEA-SHC, Task26, 2003. Available from: <<http://www.iea-shc.org/task26/index.html>>.
- [2] W. Streicher (Ed.), 2003, Report on Solar Combisystems modelled in Task 26. A report of IEA SHC—Task 26. Solar combisystems, April 2003. Available from: <[http://www.iea-shc.org/outputs/task26/C\\_Streicher\\_Sys\\_Models.pdf](http://www.iea-shc.org/outputs/task26/C_Streicher_Sys_Models.pdf)>.
- [3] C.W.J. van Koppen, J.P.S. Thomas, W.B. Veltkamp, The actual benefits of thermally stratified storage in a small and medium size solar system, in: Proceedings ISES Biennial Meeting, vol. 2, Atlanta, 1979, pp. 576–580.
- [4] R.I. Loehrke, J.C. Holtzer, H.N. Gari, M.K. Sharp, Stratification enhancement in liquid thermal storage tanks, *Journal of Energy* 3 (3) (1979) 129–130.
- [5] J.H. Davidson, D.A. Adams, Fabric stratification manifolds for solar water heating, *Journal of Solar Energy Engineering* 130 (1994) 130–136.
- [6] J.H. Davidson, D.A. Adams, J.A. Miller, A coefficient to characterize mixing in solar water storage tanks, *Journal of Solar Energy Engineering* 116 (1994) 94–99.
- [7] M.G. Abu-Hamdan, Y.H. Zurigat, A.J. Ghajar, An experimental study of a stratified thermal storage under variable inlet temperature of different inlet designs, *International Journal of Heat and Mass Transfer* 35 (8) (1992) 1927–1934.
- [8] H. Essert, Aufbau und Inbetriebnahme eines Speicherversuchsstandes, Diploma Thesis, Graz University, Austria, 1995.
- [9] E. Andersen, U. Jordan, L.J. Shah, S. Furbo, Investigations of the Solvis stratification inlet pipe for solar tanks, in: Proceedings, EuroSun2004, vol. 1, Freiburg, Germany, 2004, pp. 76–85. ISBN. 3-9809656-1-9.
- [10] Fluent 6.1 User's Guide, Fluent Inc., Centerra Resource Park 10 Cavendish Court Lebanon, NH 03766, 2003.
- [11] L.J. Shah, Statifikationsindløbsrør. Report SR-02-23. Department of Civil Engineering, Technical University of Denmark, 2002. ISSN 1393-402x. (in Danish).

## **Bilag 5**

### **Investigations of the SOLVIS stratification inlet pipe for solar storage tanks.**

Elsa Andersen, Ulrike Jordan, Louise Jivan Shah og Simon Furbo.  
Proceedings of EuroSun 2004 Congress,  
Freiburg, Tyskland.



# INVESTIGATIONS OF THE SOLVIS STRATIFICATION INLET PIPE FOR SOLAR TANKS

E. ANDERSEN, U. JORDAN, L.J. SHAH, S. FURBO  
Department of Civil Engineering, Technical University of Denmark  
Building 118, DK-2800 Kgs. Lyngby, Denmark  
Tel.: +45 4525 1901, Fax: +45 4593 1755, ean@byg.dtu.dk, uj@byg.dtu.dk,  
ljs@byg.dtu.dk, sf@byg.dtu.dk

## Introduction

Since the 1960'ties the influence of the thermal stratification in hot water tanks on the thermal performance of solar heating systems has been studied intensively. It was found, that the thermal performance of a solar heating system is increasing for increasing thermal stratification in the hot water tank.

The temperature of the storage water heated by the solar collector loop usually varies strongly during the day. In order to reach a good thermal stratification in the tank, different types of pipes, plates, diffusers and other devices have been investigated in the past (e.g. Loehrke, 1979). The aim pursued was to transport the heated water into the tank level of corresponding temperature.

Flexible stratification pipes (manifolds) have been further developed for example by (Gari et al., 1982). Furthermore, a wide variety of non flexible tubes with either open holes and perforated vertical plates inside the pipes (Davidson, 1992) or openings in form of balls (e.g. Leibfried, 2000) or flaps (e.g. described in Krause, 2001) have entered the market during the recent years.

In this paper an investigation of a stratification pipe with openings covered with flaps according to (Krause, 2001) is presented. The flaps are constructed with a soft material which allows the flap to close and open depending on the temperature and pressure differences inside and outside the pipe. Figure 1 shows schematic

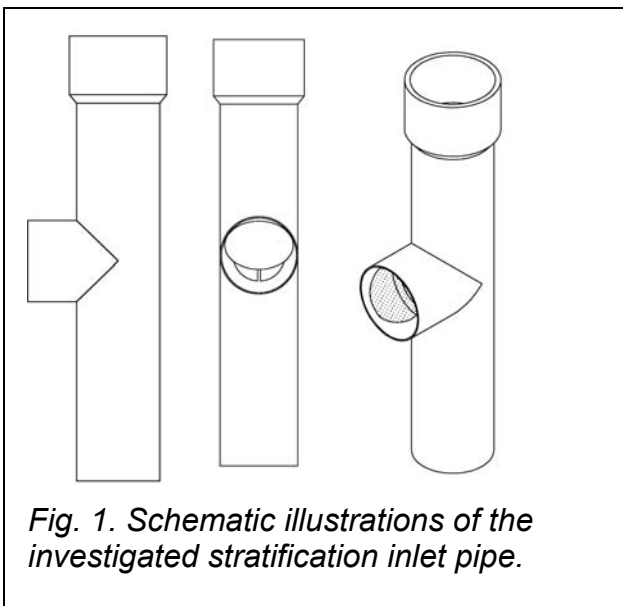


*Fig. 1. Schematic illustrations of the investigated stratification inlet pipe.*

illustrations of the pipe. The total height of the pipe is 328 mm, the outer diameter 60 mm, and the flaps are located with a distance of 292 mm in vertical direction (distance between the centre of each opening).

Preliminary laboratory tests by (Shah, 2002) with the same stratification pipe containing 5 openings showed that thermal stratification was well built up for a volume flow rate smaller than 8 l/min and larger than 4 l/min, regardless of the inlet temperature, the temperature level in the tank, and the thermal stratification in the tank. For volume flow rates larger than 8 l/min, however, the number of open flaps increased, so that

water entered the tank at different levels instantaneously. For volume flow rates smaller than 4 l/min laboratory tests indicated that cold water could be sucked in through an opening in a low level due to low pressure differences. The cold water that entered the pipe through these openings from the bottom of the store mixed with the heated water that flew through the pipe and thereby induced mixing in the tank during charging.

More detailed investigations of the flow structure close to the flaps of the stratification pipe are presented in the following for one set of operating conditions. Temperature measurements were carried out and an optical method called Particle Image Velocimetry (PIV) was used to visualize the flow around the flaps.

## Experiments

### Experimental Set-up

The experimental set-up is shown in Fig. 2. The set-up consists of a rectangular glass tank with side lengths of 400 x 400 x 900 mm<sup>3</sup>, a heating and a cooling unit, and standard PIV equipment (Dantec Dynamics). The PIV equipment consists of a laser, a camera and a processing system for analysing the pictures taken by the camera. Information about the PIV equipment is given in Table 1.

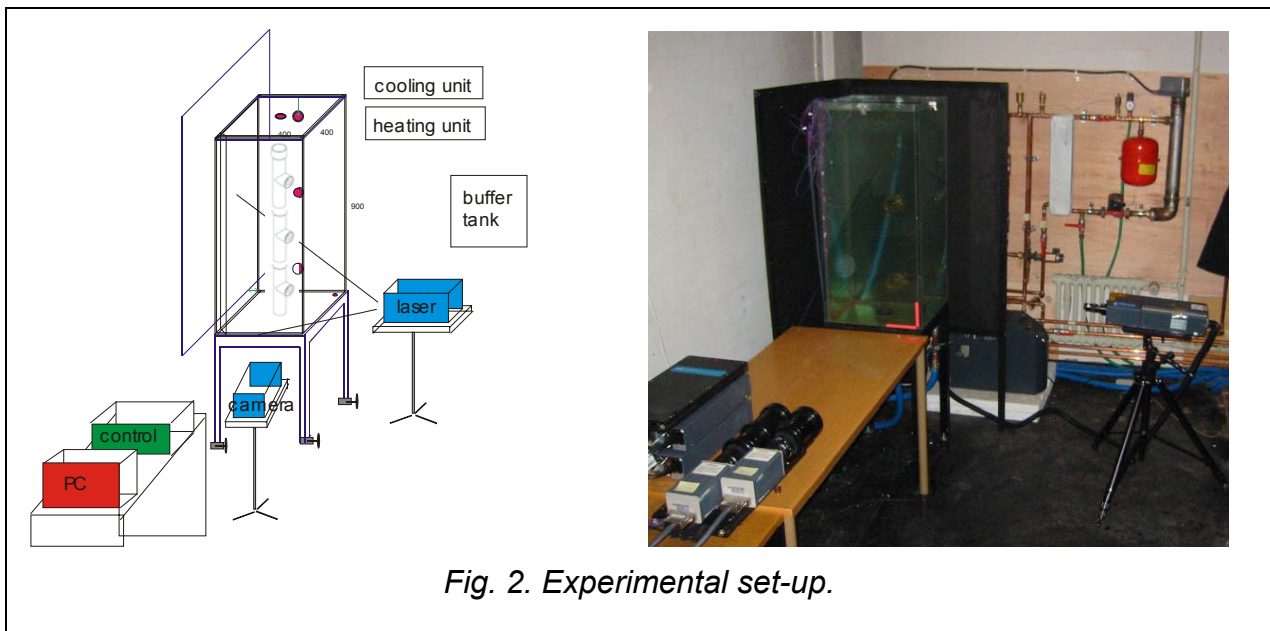


Fig. 2. Experimental set-up.

Table 1. PIV equipment.

<b>laser</b>	type	Nd:YAG, NewWave Solo (Neodym-Yttrium-Aluminium-Granat)
	energy/pulses	100 mJ/pulse
	wavelength	532 nm (frequency doubled)
<b>CCD camera</b>	type	HiSense 12 bit
	resolution	1280 x 1024 pixel (64 x 64 pixel interrogation area)
<b>particles</b>		Polyamid, 5µm (PSP-5)
<b>software</b>		Flowmanager, Dantec Dynamics

The camera is placed perpendicular to the laser that illuminates a thin slide in the flow. The inlet consisting of three compound stratification inlet pipes placed in the centre of the tank. The inlet pipe is closed at the top. The outlet is placed in the bottom of the tank in the corner behind the inlet pipe. The temperature is measured in the middle of the pipe below each inlet and in 13 uniformly distributed levels in the tank. Also the in- and outlet temperatures are measured as well as the volume flow rate. The temperatures are measured with thermocouples type TT with an accuracy of 0.5 K. The volume flow rate is measured with an electro magnetic inductive flow meter, type HGQ1 from Brunata HG a/s. The flow meter has an accuracy of about  $\pm 1$  %.

### **Particle Image Velocimetry (PIV)**

Different visualisation methods have been used in the past to gather information on the flow inside hot water tanks. Some of these methods, for example applying dyes, could only provide limited information on flow patterns. In the recent years more advanced methods have been developed. One of these methods is a non-intrusive optical method called Particle Tracking Velocimetry (PTV) to measure 2 or 3 dimensional velocity fields in a fluid. Particles are added to the investigated stream and tracked one by one. The method was used by (Shah, 1999, 2001) to investigate the flow pattern in the mantle gap of a mantle tank.

A similar optical method is called Particle Image Velocimetry (PIV). As for PTV, small tracer particles are added into the fluid and illuminated by a laser sheet. The scattered images of the particles are recorded with a camera, based on electronic solid-state images (charge couples device, CCD camera). The time delay between two laser pulses needs to be adapted to the mean velocity of the flow and the magnification at imaging. It is assumed that the tracer particles move with the local flow velocity between two illuminations.

For absorbing particles, light is mostly scattered directly by the particles and it is additionally scattered by diffraction around the edges of the particles.

To evaluate PIV recordings, the area of the laser sheet is divided into small sub-areas, called interrogation areas, with a typical size of 64 x 64 pixels.

Assuming a homogeneous flow within the interrogation area, the particle distribution of two succeeding records is identified with statistical methods (cross correlations). A local displacement vector is evaluated for each interrogation area. A velocity vector map is then calculated by taking into account the time delay between the two recordings and the magnification of imaging.

With this method, mean velocity vectors are calculated for areas containing groups of several particles. The method was used for example by (Knudsen et al., 2003) to investigate the flow pattern in the mantle of a mantle tank and the natural flow pattern in the inner tank of the mantle tank caused by heat transferred from the mantle to the tank. The method was also used by (Jordan et al., 2004) to investigate mixing in small Danish marketed hot water tanks during draw-offs with different inlet devices.

The accuracy of the measurements is influenced by the inadequacy of the statistical method and the measurement uncertainty induced by background noise of the CCD recording, particle diffraction patterns, lens aberrations, the density gap between particles and fluid, the number of particles within the volume of interest, etc. (Raffel et al., 1998).

### Example temperature measurements

Temperature measurements, carried out during two charging procedures of a storage tank are shown in Figure 3. In both experiments, a volume flow rate in the pipe of about 2 l/min was applied, as well as initial tank temperatures of about 20°C and inlet temperatures of about 40°C. During the measurement the initial temperature reaches its set value of 40°C faster in the measurements shown at the left compared to that shown on the right side. The reason for this was, that the heating unit was much warmer prior to the beginning of the experiment shown at the left side.

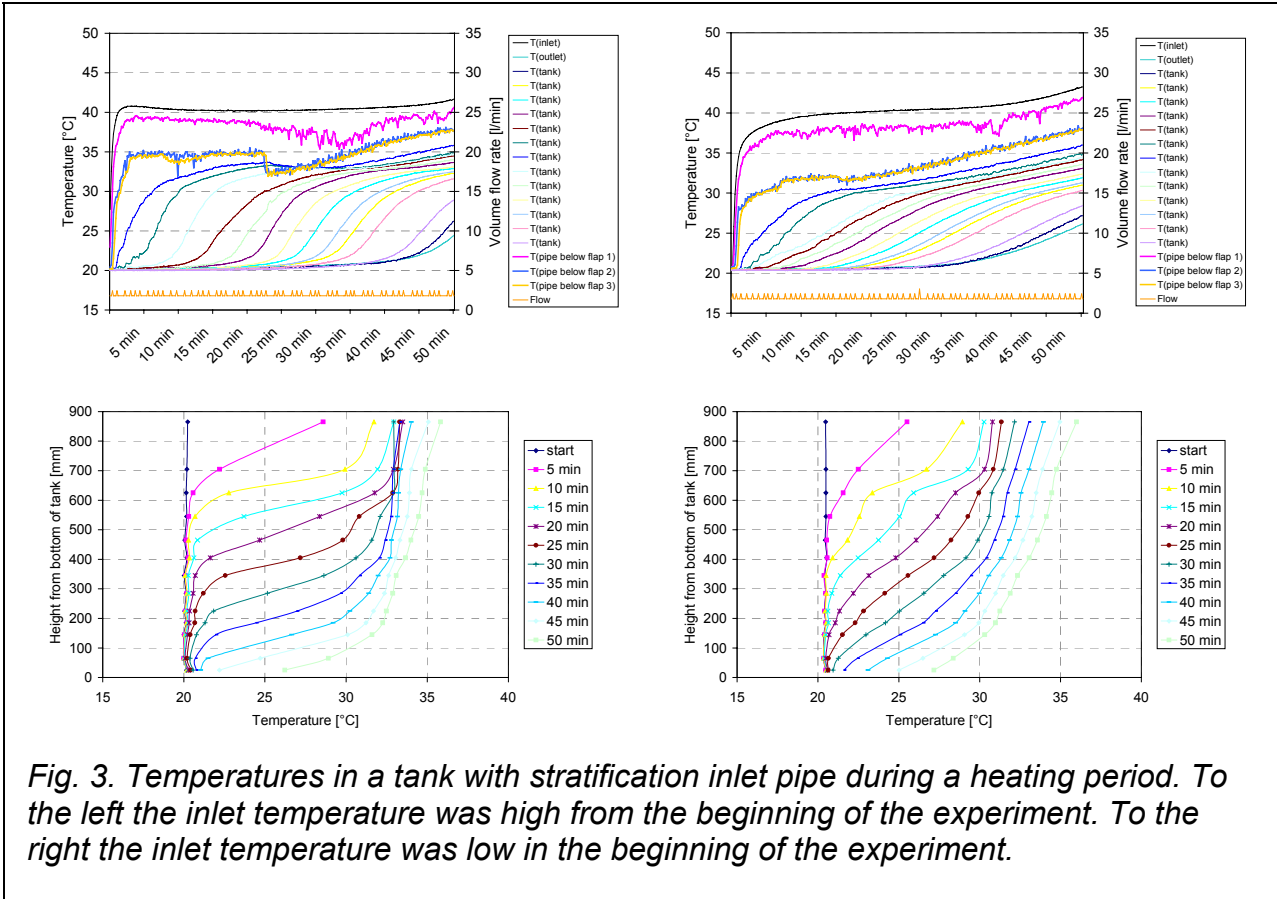


*Fig. 3. Temperatures in a tank with stratification inlet pipe during a heating period. To the left the inlet temperature was high from the beginning of the experiment. To the right the inlet temperature was low in the beginning of the experiment.*

The value of 2 l/min is a typical volume flow rate that develops if a heat exchanger is placed at the bottom of the tank below the stratification pipe and the flow inside the pipe is driven thermosyphonally.

The curves in the figures show the inlet temperature into the store (top curve), the temperatures just below the lower, the middle and the upper pipe opening and the storage temperatures, respectively (from top to bottom). After a duration of 50 min, the temperature in the bottom of the store is about 27°C, and at the top of the tank, about 36°C. The temperature below the lower flap is slightly below the inlet temperature during the entire measurements, whereas the temperatures are much lower at the two higher positions in the pipe in both measurements. This temperature drop is caused by the mixing of cold water sucked through the lower opening with the up-streaming warm water (dominating effect) and by heat losses in the pipe.

During the first about 25 min the difference between the inlet temperature and the temperatures in the upper parts of the pipe is distinctly larger for the measurement with the

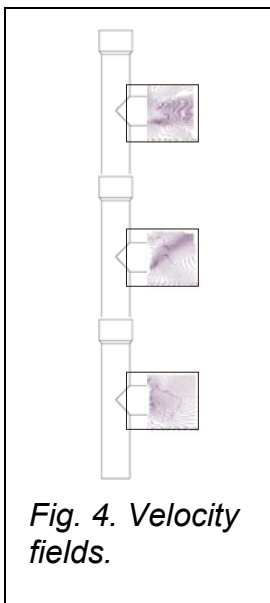
more gradually increasing inlet temperature compared to the corresponding temperatures for the more rapid inlet temperature rising. This means, that more cold water is sucked into the pipe for more gradually increasing inlet temperature.

Although the inlet temperatures are the same during the time interval between 20 minutes and 25 minutes, the values of the mixed temperatures in the pipe differ by about 3 K during this time period. This effect is mainly caused by the inertia of flow through the lower flap into the pipe, i.e. that the flow that occurred during the first 20 minutes is continuing to a certain degree. Thus, the current flow does not only depend on current reference conditions, but also on flow patterns, which occurred previously.

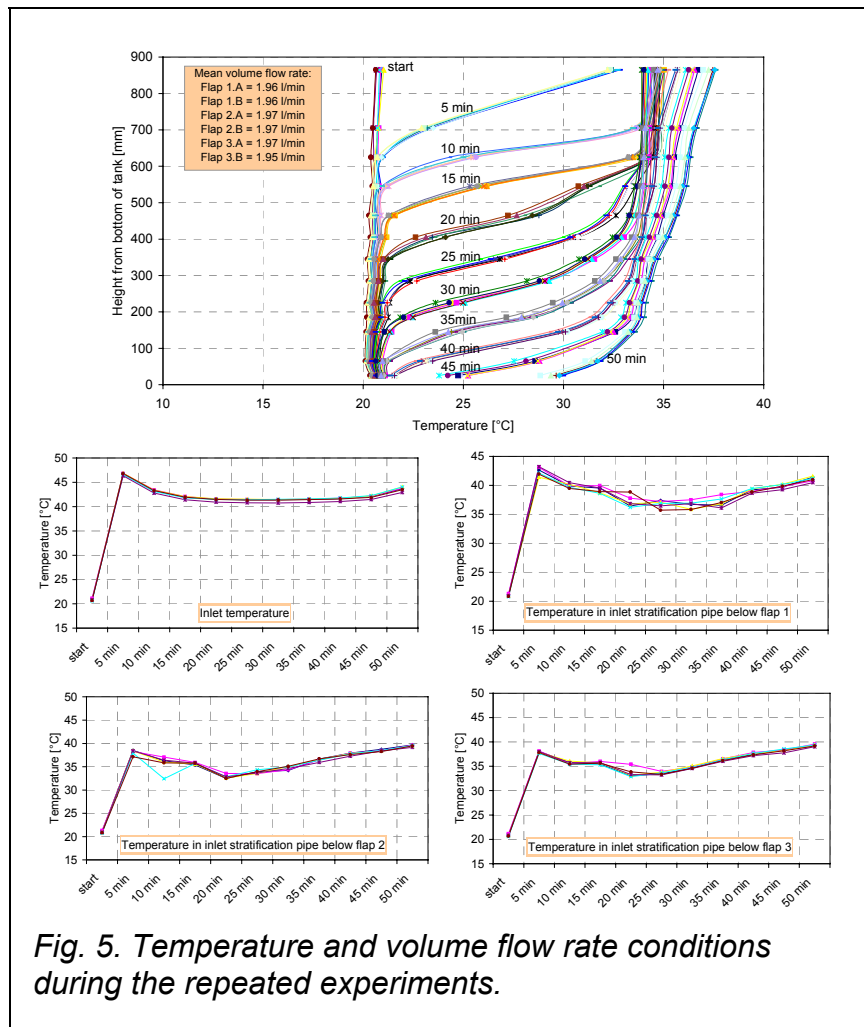
The deviations of the thermal stratification in the two experiments are relatively large during the entire period.

### Measurements

Recordings of the velocity field were taken in a frame of  $0.127 \times 0.159 \text{ m}^2$  at each inlet as shown in Fig. 4. The duration between two succeeding illuminations of the particle field varied between 8 and 100 ms depending on the flow around the inlets. The time delay between succeeding velocity vector recordings was about 250 ms. The volume flow rate was about 2 l/min. The initial tank temperature was about 20 °C. The outlet flow was lead through the heating unit where an electrical heating element of 3 kW heated the water



before it was returned to the tank. The inlet temperature was then about 40 °C. Before the circulation pump was turned on the heating unit was heated to about 60 °C. In this way the test conditions were



similar to the behaviour of a low-flow solar collector when the pump starts to circulate the flow. The laser was focused to the centre and to the position 20 mm from the centre of each of the three inlets and exactly the same experiment was repeated for each of the 6 laser positions. The duration of the experiments was 50 minutes. The flaps are referred to as flap 1, flap 2 and flap 3 counted from the bottom of the tank. Figure 5 shows the tank temperatures, the inlet temperature and the temperatures in the pipe of each experiment with a time interval of 5 minutes. From the figure it can be seen that the test conditions were practically the same in the experiments. Also the figure shows that the thermal stratification is build up in a good way.

### **Flow pattern around the stratification inlet pipe**

Figure 6 shows the velocity vector maps and the corresponding streamlines to the vector maps 5, 15 and 25 minutes after the heating is started. The velocity vector maps are calculated as mean values from 20 instantaneous velocity recordings by adaptive cross correlations and finally range validation procedure was applied. After 5 minutes the inlet takes place from flap 3. The downward stream due to the position of the outlet at the bottom of the tank passes flap 2, while some water is sucked in through flap 1. After 15 minutes the inlet takes place from flap 3 and flap 2 and cold water is still sucked in through flap 1. From this time and throughout the experiment that lasts for 50 minutes the inlet takes place from flap 3 and flap 2 while cold water is sucked in through flap 1.

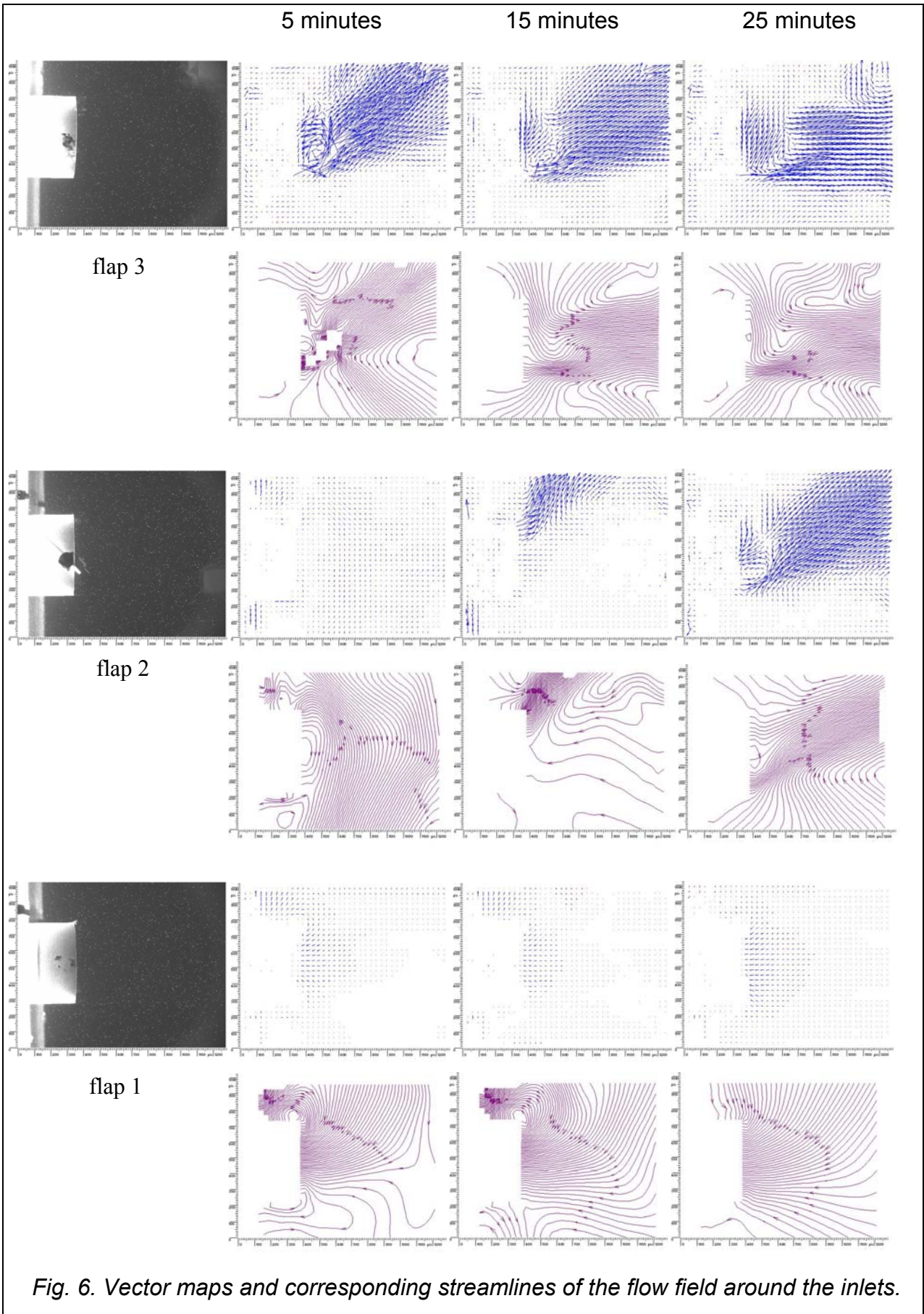
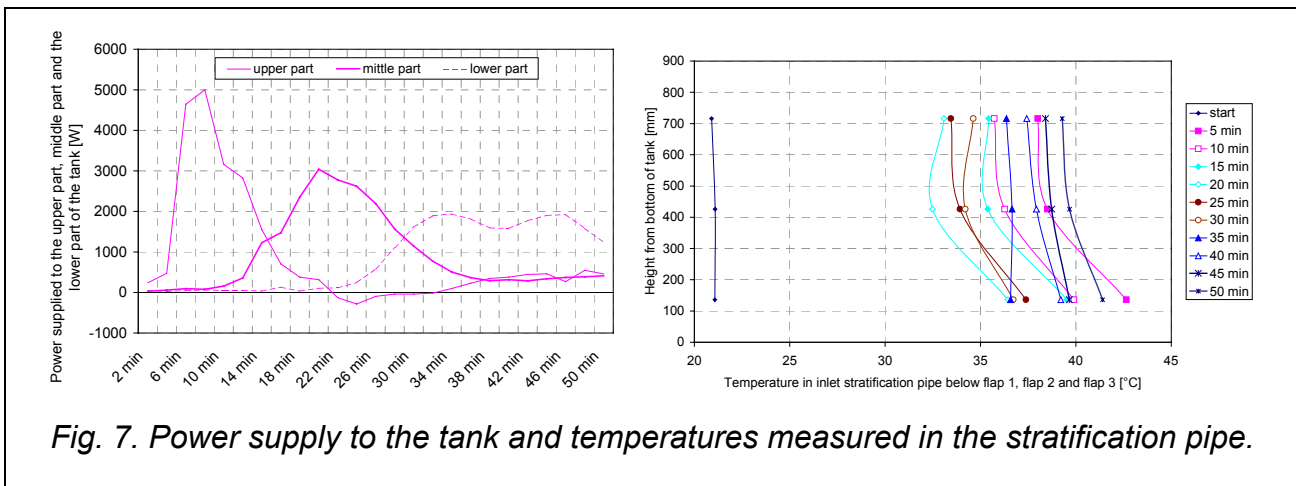


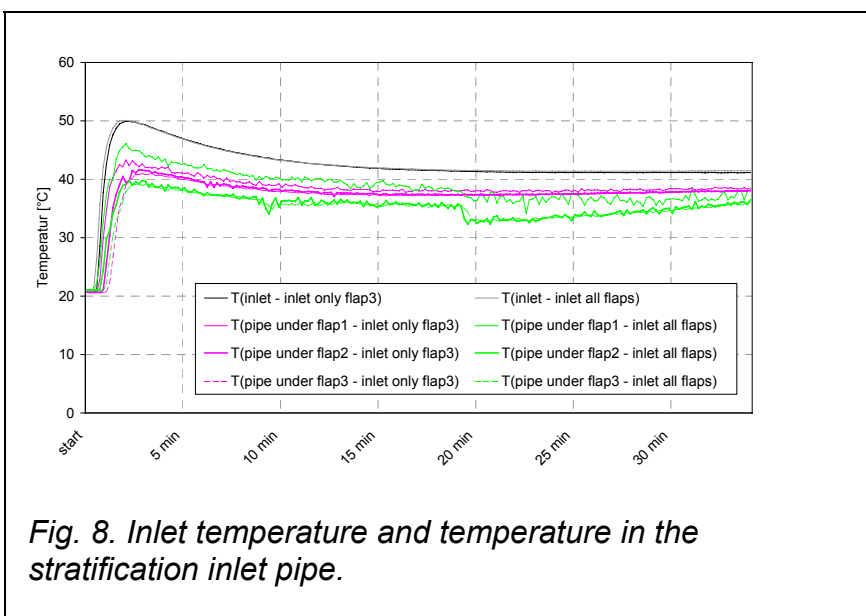
Fig. 6. Vector maps and corresponding streamlines of the flow field around the inlets.

## Analysis of the measurements

The tank is divided into three parts, where the upper part, middle part and lower part correspond to flow through from flap 3, flap 2 and flap 1 respectively. The power supply to each part of the tank and the temperatures measured in the stratification inlet pipe is shown in Fig. 7. The inlet temperature is shown in Fig. 5. The power supply to each part of the tank is a result of the water flowing through the inlet, the downward flow in the tank, the tank heat loss and the downward thermal conduction. From the figure it can be seen that the power supply to the upper part, flow through flap 3, is high in the first 10 minutes after which flap 2 opens and the power supply in the middle part of the tank is then highest. Through the whole experiment water is sucked in through flap 1 and the power supply to the lower part of the tank is first of all caused by the downward flow in the tank towards the outlet at the bottom of the tank. The temperature in the inlet pipe is higher at the bottom of the pipe than in the middle and the top of the pipe and only slightly higher in the middle than in the top. This also indicates that cold water enters the lower inlet.



An additional experiment was conducted in order to verify that water was sucked in through flap 1. The test conditions were the same as in the previous experiments but flow through the middle and lower inlets, flap 1 and 2 were physically prevented. The flow was only allowed through the upper opening, flap 3. The inlet temperature and the temperatures in the pipe with and without flap 1 and flap 2 closed is shown in Fig. 8. From the figure it is obvious that the temperature was practically the same in the whole pipe when flow through flap 1 and flap 2 was physically prevented.



In contrary, two temperature levels were measured throughout the whole experiment when all three flaps were in operation.

The power supply to the tank and the temperatures in the inlet pipe in the two experiments are shown in Fig. 9. The figure shows that the power supply to the upper part of the tank is almost the same in both experiments while the power supply to the remaining part of the tank differs in the experiments. The most significant difference between the experiments is the power supply to the lower part of the tank after about 26 minutes. At this time only a third of the tank volume has been replaced. After 34 min, nearly the total heat supply is moved to the bottom part of the store for the case that all flaps are in operation, whereas the heat is almost moved completely to the middle storage part, if the flow through the two lower flaps is prevented. Further the figure shows that the inlet temperature from the upper and middle flaps is several degrees lower when all three flaps can move freely.

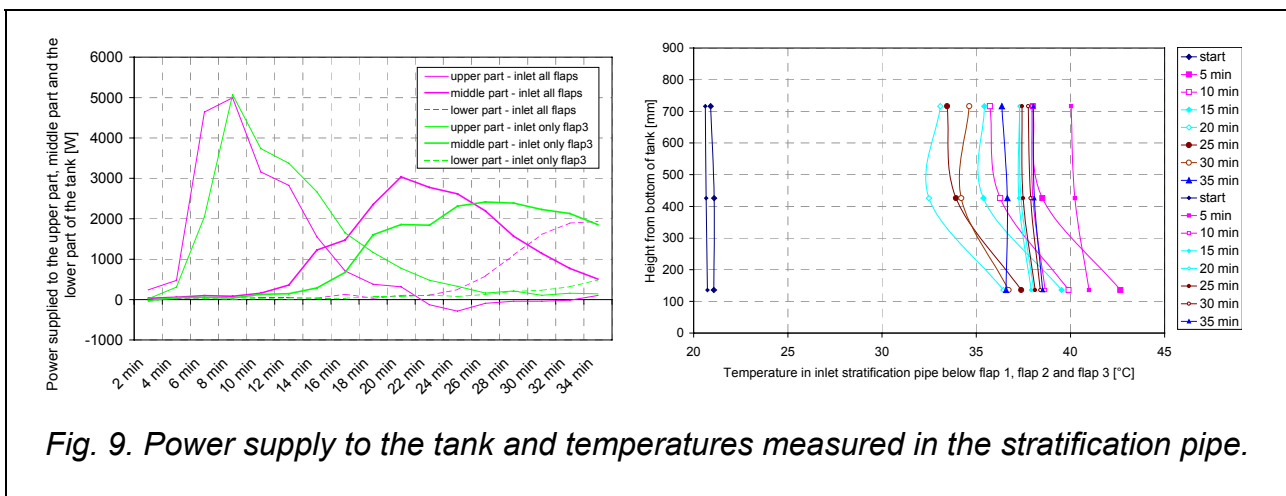


Fig. 9. Power supply to the tank and temperatures measured in the stratification pipe.

## Conclusion

A marketed stratification inlet pipe was investigated by means of Particle Image Velocimetry (PIV), a non-intrusive optical method and by temperature measurements inside and outside the inlet pipe. The pipe consisting of three compound pipes was built into the centre of a glass tank with a volume of about 140 litres. The functioning of the pipe was investigated for a typical operation condition where the tank was heated from about 20 °C to about 40 °C with a volume flow rate of about 2 l/min. The volume flow rate used in the experiment is close to a typical volume flow rate that develops from mixed (natural-forced) convection in the pipe when a compact heat exchanger is integrated below the stratification inlet device.

It was found that thermal stratification was built up in a good way with the used test conditions, but also that effects of inertia influence the flow through the stratification pipe and thereby the thermal stratification. If the inlet temperature was low compared to the tank temperature and slowly increased to the set temperature level, more cold water was sucked into the pipe from the lower flap at the beginning of the measurement.

Finally it was found that small amounts of cold water were sucked in through the flap at the bottom of the tank during the whole experiment that lasted for 50 minutes. This led to a several degrees reduced inlet temperature at the top of the tank.

Further detailed investigations are needed, before the function of the stratification inlet pipe is full elucidated.

## Reference

- Loehrke R.I., Holzer J.C., Gari H.N., Sharp M.K. (1979). Stratification enhancement in liquid thermal storage tanks. *Journal of Energy*, Vol. 3, No. 3, pp. 129-130.
- Gari H.N., Loehrke R.I. (1982). A controlled buoyant jet for enhancing stratification in a liquid storage tank. *Journal of Fluids Engineering*, Vol. 104, pp. 475-481.
- Davidson J.H., Carlson W.T., Duff W.S. (1992). Impact of component selection and operation on thermal ratings of drain-back solar water heaters. *Journal of Fluids Engineering*, Vol. 116, pp. 130-136.
- Krause Th., Kühl L. (2001). *Solares Heizen: Konzepte, Auslegung und Praxiserfahrungen*
- Shah L.J. (2002). Stratifikationsindløbsrør. Department of Civil Engineering, Technical University of Denmark, DTU.
- Shah L.J., Morrisin G.L., Behnia M. (1999). Characteristics of Vertical Mantle heat Exchangers for Solar Water Heaters. *Solar Energy*, Vol. 67, No 1-3, pp 79-91.
- Shah L.J. (2001). Heat Transfer Correlations for Vertical Mantle Heat Exchangers. *Solar Energy*, Vol. 69, No. 1-6, pp 157-171.
- Knudsen S. (2003). Analysis of the flow structure and heat transfer in a vertical mantle heat exchanger. ISES International Solar World Congress, Gothenburg, Sweden, CD-ROM P6 55
- Jordan U., Furbo S. (2004). Impact of inlet devices on the thermal stratification of a storage tank. EuroSun European Solar Energy Conference, Freiburg, Germany. Paper.
- Raffel M., Willert C., Kompenhans J. (1998). *Particle Image Velocimetry. A Practical Guide*. Springer Berlin. ISBN 3-540-63683-8.

## **Bilag 6**

### **Investigations of solar combi systems.**

Elsa Andersen og Simon Furbo.  
Proceedings of ISES Solar World Congress 2005,  
Orlando, USA.



# INVESTIGATIONS OF SOLAR COMBI SYSTEMS

Elsa Andersen and Simon Furbo  
Department of Civil Engineering  
Technical University of Denmark  
DK-2800 Kgs. Lyngby  
Denmark  
E-mail: [ean@byg.dtu.dk](mailto:ean@byg.dtu.dk)

## ABSTRACT

A large variety of solar combi systems are on the market today. The best performing systems are highly advanced energy systems with thermal stratification manifolds, an efficient boiler and only one control system, which controls both the boiler and the solar collector loop (Weiss et al., 2003). However, it is still too early to draw conclusions on the design of solar combi systems. Among others, the following questions need to be answered: Is an external domestic hot water preparation more desirable than an internal domestic hot water preparation? Is a stratification manifold always more desirable than a fixed inlet position?

This paper presents experimental investigations of an advanced solar combi system with thermal stratification manifold inlets both in the solar collector loop and in the space heating system and with an external domestic hot water preparation.

Theoretical investigations are carried out for different solar combi system types by means of the simulation program Trnsys (Klein et al., 1996) and the multiport store model (Drück, 2000) with input to the models determined by the experiments. The work is carried out within the Solar Heating and Cooling Programme of the International Energy Agency (IEA SHC), Task 32.

## 1 INTRODUCTION

In the period 1998-2002 the IEA SHC, Task 26 evaluated 21 solar combi systems (SCS's) which were on the European market. The evaluation comprised both the system costs and the thermal performance. It was found that most of the systems for one family house had solar collectors of 10 m<sup>2</sup>- 30 m<sup>2</sup> with 0.3 m<sup>3</sup>- 3 m<sup>3</sup> tank volumes and that the best systems, regarding the performance/costs ratio, were the most advanced systems with thermal stratification manifolds, an efficient boiler and only one control system, which

controls both the boiler and the solar collector loop (Weiss et al., 2003).

Further analysis of the task 26 systems was carried out by (Streicher et al., 2005). Among others it was found that the boiler efficiency is extremely important regarding a high thermal performance.

(Lorenz, 2001) investigated a number of different tanks for Swedish SCS's experimentally and made a theoretical investigation on the optimum position of different components and the impact by operating the space heating (SH) system as a high temperature system, a low temperature system or a low flow system. Among others, he found that the thermal performance could be improved with a low temperature SH system with stratification manifold in the heat storage for the return water.

(Jordan, 2002) investigated the impact of stratification manifolds in the solar collector loop for SCS's with a solar fraction of about 25 %. She found that the thermal performance increased by 1 – 2 % by using a stratification manifold instead of a fixed inlet.

An investigation on Danish SCS's installed in practice showed that the thermal performance in practice was as theoretically expected and that the heat demand, especially the summer demand was much more important regarding a high thermal performance than the system design (Andersen et al., 2003).

## 2 EXPERIMENTAL INVESTIGATIONS

A highly advanced SCS is tested in a laboratory test facility. The SCS has thermal stratification manifolds for transferring solar heat to the tank and for the space heating return water, external domestic hot water (DHW) preparation and the auxiliary energy system is an internal gas boiler. Figure 1 shows a schematic illustration of the experimentally investigated SCS. The figure also shows where temperature sensors are mounted.

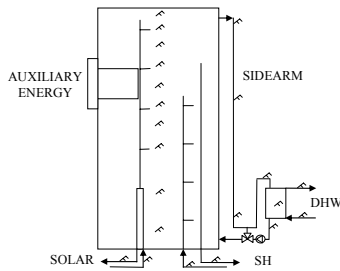


Fig. 1: Schematics of tested SCS.

### 2.1 Test results

The sidearm is made of a 22/20 mm copper pipe. The sidearm is incorporated in the tank insulation while the DHW heat exchanger is separately insulated. The heat loss coefficient for the sidearm exclusive the DHW heat exchanger and the DHW heat exchanger is measured to 0.39 W/K and 0.37 W/K respectively.

Also the measurements show that thermosyphoning takes place in the sidearm whenever the driving force equals the pressure loss by circulation in the sidearm. In order to reduce the heat loss caused by thermosyphoning in the sidearm to a minimum, it is important to insulate the sidearm well, avoid oversized pipes, and place the DHW heat exchanger low.

However, it is not possible to avoid thermosyphoning without a valve built into the sidearm. The results show, that SCS's with external DHW preparation have a large heat loss through the sidearm, even in periods without DHW consumption.

## 3 THEORETICAL INVESTIGATIONS

A number of SCS types are investigated theoretically. Figure 2 shows schematically illustration of the investigated SCS types. The investigation is based on three basically different system models, one model is designed as the tested SCS shown in Fig. 1, one model is based on a DHW tank with an internal heat exchanger spiral for the SH system and one model is based on a tank in tank storage. The base system models are referred to as model 1, 2 and 3 respectively. Further the variations in the base models are numbered successively, see Fig. 2.

The investigation is based on inputs to the models determined by the experiments. The SCS's have solar fractions between 4 % and 15 % depending on SCS type and the DHW and SH consumption.

### 3.1 Assumptions for the calculations

The SCS's are designed as described in Table 1. The Danish Design Reference Year, DRY is used as weather data (Skertveit et al., 1994). The daily hot water consumption is 50 l, 100 l, 160 l, 200 l, 250 l and 300 l. Hot water is heated from 10°C to 50°C. Hot water is

tapped at 7 am, noon and 7 pm with a volume flow rate of less than 2 l/min.

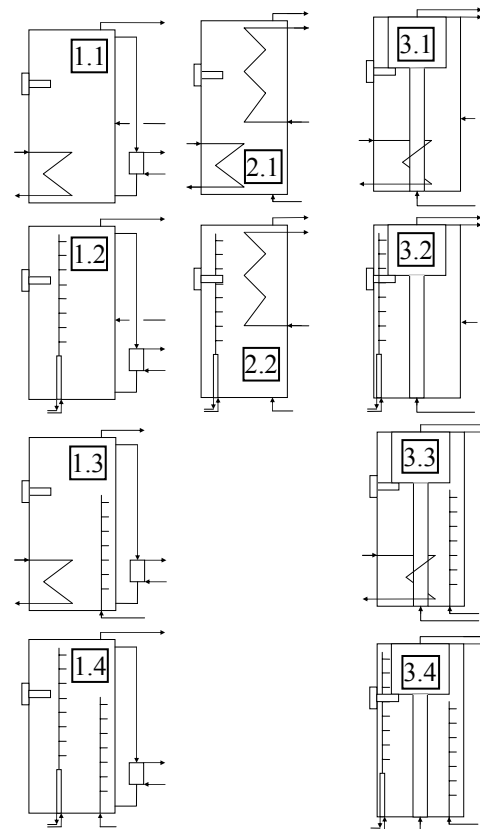


Fig. 2: Schematics of the three base models 1 (left), 2 (middle) and 3 (right) and the successively numbered variations of the base models.

The auxiliary heated part of the 460 l heat storage is 184 l. The set point temperature of the auxiliary volume is 50.5°C, 57°C, 60°C, 65°C, 70°C except for model 1 where the lowest set point temperature required in order to be able to tap hot water at a temperature of 50°C at the external DHW heat exchanger is determined by the volume flow rate during tapping and the heat transfer capacity rate of the DHW heat exchanger according to Fig. 3.

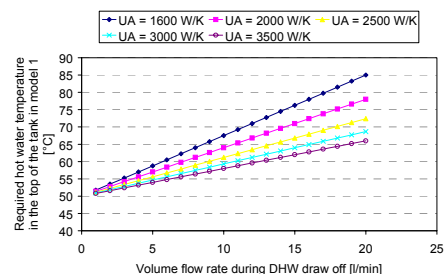


Fig. 3: Required hot water temperature in the top of the tank in model 1 with external DHW heat exchanger as a function of the volume flow rate and the heat transfer capacity rate of the DHW heat exchanger.

The figure is based on calculations with the assumption that the volume flow rate is the same on both sides of the DHW heat exchanger. From the figure it can be seen that a draw off with a volume flow rate of 10 l/min requires that the auxiliary volume is heated to 57°C–67°C depending on the heat transfer capacity rate of the DHW heat exchanger. Consequently, the calculations with model 1 are carried out with the auxiliary volume heated to 57°C, 60°C, 65°C and 70°C.

The temperature in the top of the heat storage of a SCS is determined by the set point temperature of the auxiliary energy supply system and the temperature supplied from the solar collector during sunny hours. The return temperature, Eq. (1) and the volume flow rate, Eq. (2) in the SH system is calculated based on the temperature of the water in the top of the tank, the required power for the SH system and the heat distribution system. In this way it is always possible to meet the SH demand.

The assumed SH demand is 14900 kWh/year. In Fig. 4 the required power for the SH system used in the calculations is shown.

$$T_R = \left( \frac{-\left(\frac{1}{2} \cdot T_{Fd} + \frac{1}{2} \cdot T_{Rd} - T_{Room}\right)}{P_{Load} / P_{Rad}} \right)^{0.769} + T_F \quad (1)$$

$$\dot{m}_{SH} = \frac{P_{Load}}{c_p \cdot (T_F - T_R)} \quad (2)$$

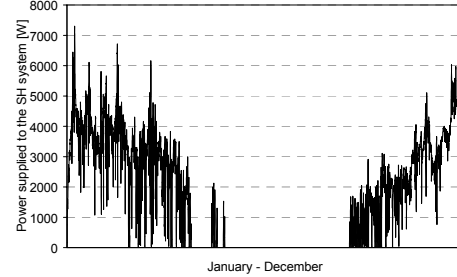


Fig. 4: Power for the SH system used in the calculations.

Table 1: Data for the SCS used in the calculations.

<b>Solar collector</b>	
Solar collector area	9 m <sup>2</sup>
Start efficiency, $\eta_0$	0.756
Heat loss coefficients, $a_1 / a_2$	4.37 W/m <sup>2</sup> /K / 0.01 W/m <sup>2</sup> /K <sup>2</sup>
Efficiency for small incidence angles, $\eta$	$\eta_0 - a_1 \cdot (T_m - T_a)/E - a_2 \cdot (T_m - T_a)^2/E$
Incidence angle modifier for beam radiation, $k_0$	$1 - \tan^{4.2}(\theta/2)$
Tilt / Orientation	45° / South
<b>Solar collector loop</b>	
Outer/inner pipe diameter	12/10 mm
Length of pipe from/to solar collector to/from storage, outdoor	10 m
Heat loss coefficient of pipe	45 kJ/h/m <sup>2</sup> /K
Solar collector fluid	40% (weight) propylene glycol/water mixture
Mass flow rate in solar collector loop, high / low, $\dot{m}_{solar}$	48 kg/h/m <sup>2</sup> / 24 kg/h/m <sup>2</sup>
Power of circulation pump	100 kJ/h
<b>Tank</b>	
Storage volume / auxiliary volume	460 l (135 l DHW tank) / 184 l
Height/diameter	1.490/0.662 m
Heat loss coefficient, tank / sidearm / DHW heat exchanger	8.42 kJ/h/K / 1.40 kJ/h/K / 1.33 kJ/h/K
Heat transfer coefficient, stratifier in solar collector loop, UA	700 kJ/h/K
Coefficient, b1, b2 and b3	0.4404, 0.3836 and 0.4943
Heat transfer coefficient, stratifier in solar collector loop.	$UA \cdot \dot{m}_{solar}^{b1} \cdot (T_{in} - T_{tank})^{b2} \cdot ((T_{in} + T_{tank})/2)^{b3}$
UA is calculated for each layer in the tank model occupied by the heat exchanger (Drück, 2000)	
Heat transfer coefficient of: spiral in solar collector loop / spiral in SH system / tank in tank heat transfer	180 kJ/h/K per m <sup>2</sup> / 2700 kJ/h/K / 1000 kJ/h/K
Efficiency of auxiliary energy supply system	100%
Relative in-/outlet height of DHW	0 / 1
Relative in-/outlet height of SH system (fixed inlet)	0.34 / 0.98
Relative in-/outlet height of spiral in solar collector loop	0.305 / 0.06
<b>Control system</b>	
Differential thermostat control with one sensor in the solar collector and one at the bottom of the tank	
Start/Stop difference	6 K/2 K

### 3.2 Theoretical results

The results are shown as the net utilized solar energy for a SCS with different domestic hot water consumption as a function of the set point temperature of the auxiliary volume. The net utilized solar energy is defined as:

$$Q_{NET} = Q_{DHW} + Q_{SH} - Q_{AUX} \quad (3)$$

In Fig. 5-7 the calculated results of model 1, 2 and 3 are shown.

Figure 5 and Fig. 7 show the thermal performance of model 1 and 3 respectively, with a heat exchanger in the solar collector loop and a direct inlet from the SH system. Further, the figures show the thermal performance of the models when first: replacing the heat exchanger in the solar collector loop with a stratification manifold, second: replacing the direct inlet from the SH system with a stratification manifold, third: replacing both the heat exchanger spiral in the solar collector loop and the direct inlet from the SH system with stratification manifolds.

Figure 6 shows the thermal performance of model 2 with heat exchangers in both the solar collector loop and the SH loop. Further, the figure shows the thermal performance of the model when the heat exchanger in the solar collector loop is replaced with a stratification manifold.

From the figures it is obvious that the thermal performance of the models is strongly influenced by the set point temperature of the auxiliary volume. For increasing set point temperature the thermal performance is decreasing.

From Fig. 5 and Fig. 7 it can be seen that the surplus in thermal performance with a stratification manifold is highest when the set point temperature of the auxiliary volume is high. Further it can be seen that the thermal performance is only slightly increased when the heat exchanger spiral in the solar collector loop is replaced with a stratification manifold while the increase in the thermal performance is much higher when the direct inlet from the SH system is replaced by a stratification manifold. Finally it can be seen that the thermal performance is only slightly increased when both the heat exchanger spiral in the solar collector loop and the direct inlet from the SH system are replaced with stratification manifolds compared to the thermal performance when only the direct inlet from the SH loop is replaced with a stratification manifold.

From Fig. 6 it can be seen that the thermal performance is almost not affected by replacing the heat exchanger spiral in the solar collector loop with a stratification manifold.

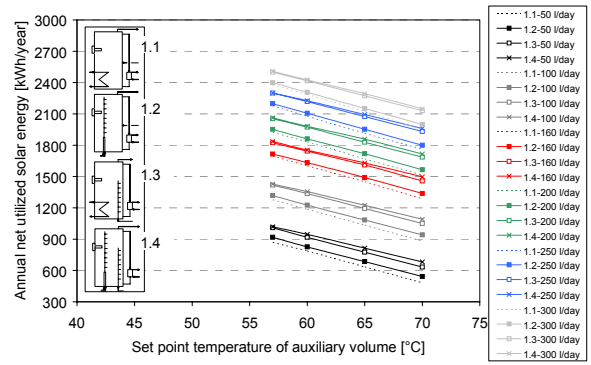


Fig. 5: The net utilized solar energy as a function of the set point temperature of the auxiliary volume for model 1.

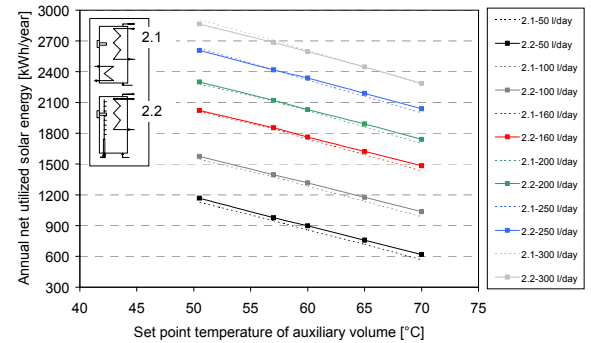


Fig. 6: The net utilized solar energy as a function of the set point temperature of the auxiliary volume for model 2.

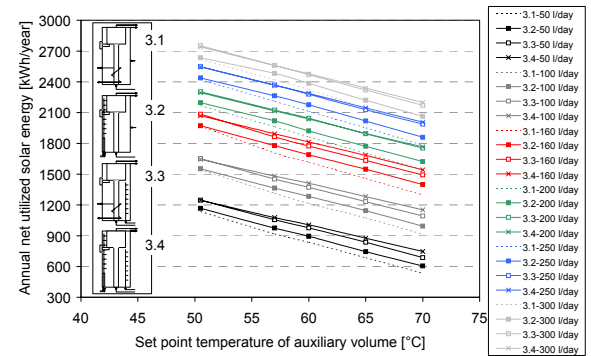


Fig. 7: The net utilized solar energy as a function of the set point temperature of the auxiliary volume for model 3.

The reason why the thermal performance is only slightly increased by introducing a stratification manifold in the solar collector loop in all of the models is most likely because the systems are oversized during the summer when only DHW is discharged from the systems. This is analyzed further by Fig. 8 that shows

the monthly net utilized solar energy for model 1.1, 1.2 and 1.3 with a DHW load of 160 l/day and a set point temperature of the auxiliary volume of 57 °C. It can be seen that the surplus in thermal performance by replacing the heat exchanger spiral in the solar collector loop with a stratification manifold is gained in the period from March to September while the surplus by replacing the direct inlet from the SH system with a stratification manifold is gained in the period from September to May. Further, the number of times the tank volume is circulated when the SH system is in operation is very high compared to the number of times the tank volume is circulated when the solar collector loop is in operation and thus it is more important to avoid mixing from circulating SH water.

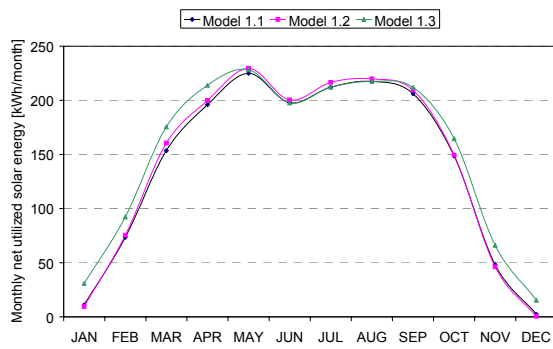


Fig. 8: Monthly net utilized solar energy for model 1.1, 1.2 and 1.3.

In fig 9-12 a comparison between model 1, 2 and 3 is facilitated.

Figure 9 shows the thermal performance of model 1.1, 2.1 and 3.1 with heat exchanger spiral in the solar collector loop and Fig. 10 shows the thermal performance of model 1.2, 2.2 and 3.2 where the heat exchanger spiral in the solar collector loop is replaced by a stratification manifold.

Figure 11 shows the thermal performance of model 1.3 and 3.3 where the direct inlet from the SH system is replaced with a stratification manifold and Fig. 12 shows the thermal performance of model 1.4 and 3.4 where both the direct inlet from the SH system and the heat exchanger spiral in the solar collector loop are replaced by stratification manifolds.

From Fig. 9 and Fig. 10 it can be seen that model 3 has always a higher thermal performance than model 1 and that model 2 has the highest thermal performance. Further it can be seen that the surplus in thermal performance for model 2 compared to model 1 and model 3 increases with increasing DHW consumption.

From Fig. 11 and Fig. 12 it can be seen that the thermal performance is always higher for model 3 than for model 1.

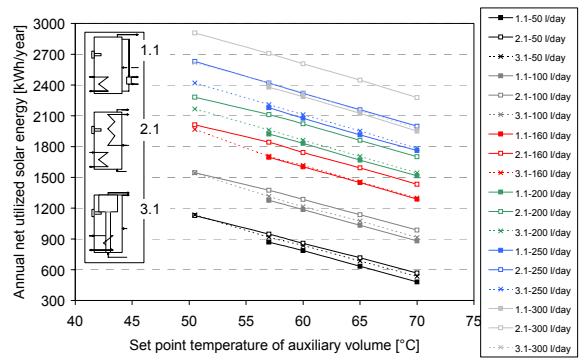


Fig. 9: The net utilized solar energy as a function of the set point temperature of the auxiliary volume for model 1.1, model 2.1 and model 3.1.

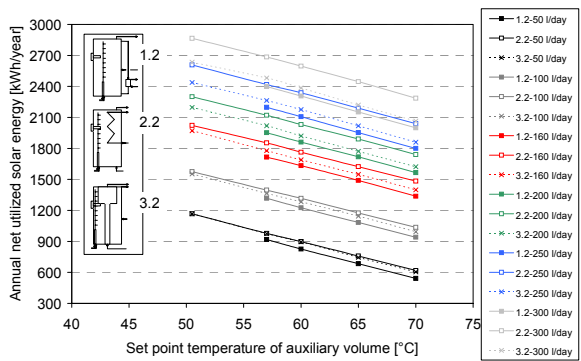


Fig. 10: The net utilized solar energy as a function of the set point temperature of the auxiliary volume for model 1.2, model 2.2 and model 3.2.

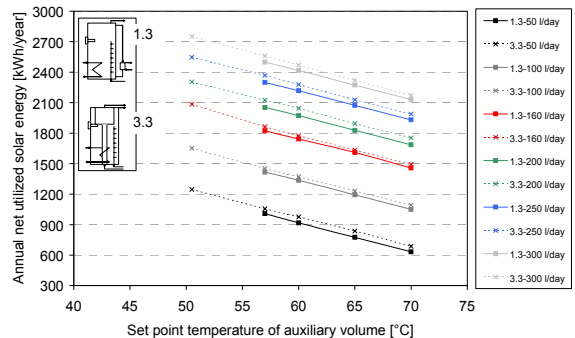


Fig. 11: The net utilized solar energy as a function of the set point temperature of the auxiliary volume for model 1.3 and model 3.3.

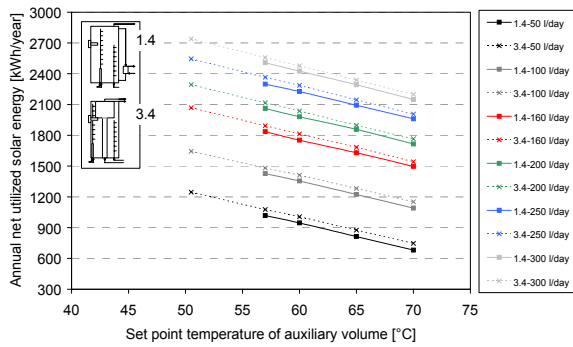


Fig. 12: The net utilized solar energy as a function of the set point temperature of the auxiliary volume for model 1.4 and model 3.4.

The reason why model 2 is performing best is most likely because the tank is a DHW tank where the incoming cold water is directly utilized to cool the lower part of the tank. In model 1 the water returning from the DHW heat exchanger to the tank is somewhat warmer than the cold water temperature. In model 3 the incoming cold water reaches a higher level in the heat storage after a DHW draw off. The reason why model 3 is performing better than model 1 is most likely due to the higher tank heat loss coefficient of model 1 since the heat loss coefficients of the sidearm and the external DHW heat exchanger are added to the tank heat loss coefficient. Finally, the set point temperature of the auxiliary volume in model 1 must be about 10 - 15 K higher than the required hot water temperature to meet the hot water demand. The set point temperature in model 2 and model 3 only needs to be slightly higher than the required hot water temperature to meet the same demand.

#### 4 CONCLUSIONS

An advanced SCS system is experimentally investigated. The system has a sidearm with a heat exchanger for DHW preparation, an integrated boiler and stratification manifolds both in the solar collector loop and for the return water from the SH system. The investigation showed that it is not possible to avoid thermosyphoning in the sidearm in periods without DHW demand without a valve built into the sidearm. In order to reduce the heat loss caused by thermosyphoning as much as possible, the sidearm must be well insulated, oversized pipes must be avoided and the DHW heat exchanger must be placed low.

Three different SCS types were investigated theoretically. The first type corresponds to the experimentally investigated system, the second type is based on a DHW tank with discharge for the SH system through a heat exchanger spiral. The third type has a tank in tank heat storage.

It was found that for SCS's with a solar fraction from 4 %- 15% and low DHW consumption the best performing SCS was the third system type with a tank in tank heat storage and for high DHW consumption the best performing system type was the second system with a heat exchanger spiral for the SH system.

Further, it was found that stratification manifolds improve the thermal performance but most when the stratification manifold is used to lead the return water from the SH system into the tank.

#### 5 NOMENCLATURE

$E$	=	Total solar irradiance on collector ( $\text{W}/\text{m}^2$ )
$T_{Fd}, T_{Rd}$	=	Design flow and return temperature to SH system ( $^{\circ}\text{C}$ )
$T_F, T_R$	=	Flow and return temperature to SH system ( $^{\circ}\text{C}$ )
$T_{Room}$	=	Room temperature ( $^{\circ}\text{C}$ )
$P_{Load}$	=	Heat load for SH system ( $\text{kJ}/\text{h}$ )
$P_{Rad}$	=	Heat load of radiator ( $\text{kJ}/\text{h}$ )
$c_p$	=	Specific heat capacity ( $\text{kJ}/\text{kg}/\text{K}$ )
$\dot{m}_{SH}$	=	Mass flow rate in the SH system ( $\text{kg}/\text{hr}$ )
$Q_{AUX}$	=	Auxiliary energy consumption (J)
$Q_{DHW}$	=	DHW load (J)
$Q_{NET}$	=	Net utilized solar energy (J)
$Q_{SH}$	=	SH load (J)

#### 6 REFERENCES

- (1) Andersen A., Shah L. J., and Furbo S., Thermal Performance of Danish Solar Combi Systems in Practice and in Theory. Journal of Solar Energy Engineering, Vol. 126, pp 744-749, 2004.
- (2) Drück H., MULTIPORT Store – Model, Type 140 for TrnSys. Institut für Thermodynamik und Wärmetechnik. Universität Stuttgart, 2000.
- (3) Jordan U., Untersuchung eines Solarspeichers zur kombinierten Trinkwassererwärmung und Heizungsunterstützung. VDI Verlag GmbH, Düsseldorf. ISBN 3 18 313819 0, 2001.
- (4) Klein S.A et al., TRNSYS 15, User Manual. University of Wisconsin Solar Energy Laboratory, 1996.
- (5) Skertveit, A., Lund, H., and Olseth, J. A., Design Reference Year, Report no. 1194 Klima, Det Norske Institutt, 1994.
- (6) Streicher W., Heimrath R., Sensivität von Systemparametern von solaren Kombisystemen – Analyse der simulierten Systeme des IEA SHC Task 26. Thermische Solarenergie Symposium, Bad Staffelstein, 2005.
- (7) Weiss et al., Solar Heating Systems for Houses, a Design Handbook for Solar Combisystems. James & James Ltd, London. ISBN 1 902916 46 8, 2003.

## **Bilag 7**

### **Investigations of fabric stratifiers for solar tanks.**

Elsa Andersen, Simon Furbo og Jianhua Fan.  
Proceedings of ISES Solar World Congress 2005,  
Orlando, USA.



# INVESTIGATIONS OF FABRIC STRATIFIERS FOR SOLAR TANKS

Elsa Andersen, Simon Furbo and Jianhua Fan  
Department of Civil Engineering  
Technical University of Denmark  
DK-2800 Kgs. Lyngby  
Denmark  
E-mail: [ean@byg.dtu.dk](mailto:ean@byg.dtu.dk)

## ABSTRACT

The thermal performance of solar heating systems is strongly influenced by the thermal stratification in the heat storage. The higher the degree of thermal stratification is, the higher the thermal performance of the solar heating systems. Thermal stratification in water storages can be achieved in different ways. For instance, water heated by the solar collectors or water returning from the heating system can enter the water storage through stratification inlet devices in such a way that the water enters the tank in a level, where the tank temperature is the same as the temperature of the entering water.

In this paper investigations of a number of different fabric stratification pipes are presented and compared to a non flexible inlet stratifier.

Additional, detailed investigations of the flow structure close to two fabric stratification pipes are presented for one set of operating conditions by means of the optical PIV (Particle Image Velocimetry) method.

## 1 INTRODUCTION

A wide variety of rigid tubes with either open holes and perforated vertical plates inside the pipes (Loehrke, 1979, Gari and Loehrke, 1992, Davidson, 1992,) or openings in form of balls (e.g. Leibfried, 2000) or flaps (e.g. described by Krause, 2001, Shah, 2002, Andersen et al., 2004). Some of these have entered the market during the recent years. Also flexible stratification pipes (fabric manifolds) have been investigated for example by (Davidson and Adams, 1992, Loehrke, 1979, Gari and Loehrke, 1992, Yee and Lai, 2001). These investigations are carried out with flexible stratification manifolds made of one fabric layer and inlet through the top or the middle of the tank. (Davidson et al., 1994) found that fabrics with limited ability to stretch (i.e. woven fabrics) were unsuitable as stratification inlet pipes when the water enters the stratification inlet pipe through the top of the tank.

No guidelines for choosing the diameter of a fabric pipe in this type of application were found in previous studies. (Davidson et. al, 1994) investigated fabric pipes with diameters of 73 and 89 mm with a volume flow rate of 4.2 l/min. (Loehrke et al., 1979) investigated a fabric pipe with a diameter of 100 mm and a volume flow rate of 23 l/min.

In spite of promising results, fabric stratification pipes have not yet entered the market.

In this paper, stratification manifolds made of one or two fabric layers with diameters between 40 mm and 70 mm and with inlet through the bottom of the tank are investigated. The fabric stratifiers are made of Nylon, filament polyester, spun polyester and acrylic.

By leading water into the tank through a stratification pipe, good thermal stratification can be achieved in the tank. By placing the inlet at the bottom of the tank where the coldest water is situated, thermal bridges with high heat losses can be avoided, (Furbo, 1983). Good thermal stratification increases the thermal performance of solar heating systems.

The advantage of using a flexible fabric pipe as a stratification inlet pipe is that the fabric pipe can expand or contract leading to an equalization of the pressure in the pipe and in the tank in all levels of the tank. In this way the water in the tank will not be driven into the pipe by a higher pressure in the tank than in the pipe. The water in the pipe will first enter the tank when it either reaches the top of the pipe where it is forced to leave the pipe because new water is constantly feed into the pipe or when the temperature in the pipe equals the temperature in the tank leading to a slightly higher pressure in the pipe than in the tank. The pipe will expand in an attempt to equalize the pressure difference, but the expansion is limited by the expansion properties of the fabric and this leads to a flow of liquid from the pipe into the tank in the right temperature level. Because one layer of fabric is very thin, heat is constantly transferred horizontally between the fabric pipe and the tank. By designing the stratification inlet pipe of more than one fabric layer with a distance between the fabric layers the unwanted horizontal heat

transfer is reduced. The heat transferred through each fabric layer leads to an up going flow around each fabric layer. It is assumed that when the distance between the fabric layers is large enough a laminar flow can develop and a small amount of heat is transferred from the inlet stratification pipe to the tank. When the distance between the fabric layers is too narrow the flow is disturbed and becomes turbulent and a larger amount of heat is transferred from the inlet stratification pipe to the tank. On the other hand, a larger fabric pipe diameter results in a larger surface area of the pipe increasing the heat transfer between the inlet stratification pipe and the tank. Therefore detailed investigations are needed in order to determine the optimum diameters of the fabric pipes.

## 2 EXPERIMENTAL INVESTIGATIONS

### 2.1 Experimental set up

The experimental setup shown in Fig. 1 consists of a glass tank (400 x 400 x 900 mm), a heating and a cooling unit and standard PIV equipment from Dantec Dynamics. Table 1 shows data for the PIV equipment.

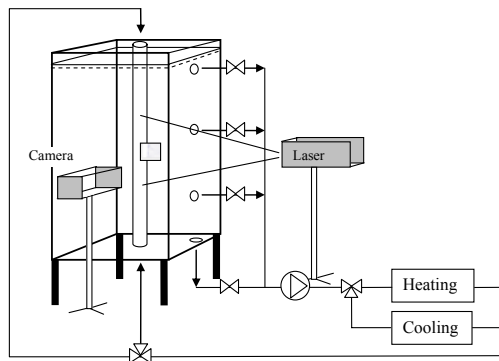


Fig. 1: Experimental setup with the glass tank, the laser and the camera.

TABLE 1: PIV EQUIPMENT.

<b>laser</b>	type	Nd:YAG, NewWave Solo (Neodym-Yttrium-Aluminium-Granat)
	energy/pulses	100 mJ/pulse
	wavelength	532 nm (frequency doubled)
<b>CCD camera</b>	type	HiSense 12 bit
	resolution	1280 x 1024 pixel (64 x 64 pixel interrogation area)
<b>particles</b>		Polyamid, 5µm (PSP-5)
<b>software</b>		Flowmanager, Dantec Dynamics

The fabric stratification pipe is mounted in the centre of the glass tank with the possibility to have a forced flow to enter the stratification pipe either from the top or the

bottom of the tank. The outlet can take place in four different levels between the top and the bottom of the tank. The thickness of the tank wall is 12 mm and the tank is not insulated. The tank temperatures are measured in 13 different levels in the tank. The temperatures are measured with copper-constantan thermocouples type TT with an accuracy of 0.5 K. The volume flow rate is measured with an electro magnetic inductive flow meter, type HGQ1 from Brunata HG a/s. The flow meter has an accuracy of about  $\pm 1\%$ .

### 2.2 Experiments

The thermal performance of the fabric stratifiers are investigated for three sets of operation conditions:

- heating tests where the tank is heated from 20°C to 40°C through one layer fabric stratification pipes with diameters of 60 mm and two layers fabric stratification pipes with diameters of 40 mm and 70 mm. The inlet to the fabric stratification pipe is through the bottom of the tank. The outlet is in the bottom of the tank.
- heating test with an initially stratified tank 50°C/20°C and an inlet temperature of 30°C through two fabric layers stratification pipe with diameters of 40 mm and 70 mm. The inlet to the fabric stratification pipe is through the bottom of the tank. The outlet is in the bottom of the tank.
- cooling test where cold water of 20°C is lead into the tank with a temperature of 50°C through two fabric layers stratification pipe with diameters of 40 mm and 70 mm. The inlet to the fabric stratification pipe is through the bottom of the tank. The outlet is in the top of the tank.

The duration of the heating and the cooling tests is 50 minutes. The duration of the stratified test is 35 minutes. The volume flow rate is 2 l/min. The investigated fabrics are listed in table 2. The fabrics are obtained from the US company Test Fabric Inc. (13). The fabrics are a mixture of knit and woven fabrics and the ability to stretch that was found important by (Davidson et al., 1994) seems not important at all in the application investigated here where the water is entering the stratification inlet pipe through the bottom of the tank. The important properties are the ability to reduce the cross sectional area by more or less collapse. Hence, the permeability and the density of the fabrics are found to be more important than the stretch abilities.

TABLE 2: INVESTIGATED FABRICS.

Fabric Style
Style 314, Texturized Nylon 6.6 Stretch Fabric, Double Knit
Style 361, Spun Nylon 6.6 DuPont Type 200 Woven Fabric (ISO 105/F03)
Style 703, Texturized Polyester, Woven
Style 769, 100% Spun Dacron Type 54 Knit (Disperse Dyeable)
Style 864, Spun Orlon Type 75 Acrylic Plain Weave
Style 867, Spun Acrilan 16 Acrylic Knit
Style 981, Creslan Acrylic Type 61

Further, the test results obtained with two fabric layers stratification pipes are compared to results of identical tests with a marketed rigid stratification pipe with three holes with “non-return” valves from Solvis GmbH & Co KG (Krause, 2001, Shah, 2002, Andersen et al., 2004).

Finally, the flow structure close to the fabric stratification pipes with one and two fabric layers, S361 are investigated during a heating test by means of the PIV method. The method is described in (Andersen et al., 2004).

Recordings of the velocity field are taken in a frame of 65.5 x 80 mm<sup>2</sup> about 450 mm from the bottom of the tank as shown in Fig. 1. The duration between two succeeding illuminations of the particle field is 100 ms. Time delay between succeeding velocity vector recordings is about 250 ms.

### 2.3 Analysis method

There are different ways to evaluate thermal stratification of thermal energy storages. (Rosen, 2001) describes how to perform an exergy analysis of a thermal energy storage. (Adams, 1993; Davidson et al., 1994) describe how to analyse a thermal energy storage with a quantitative moment of energy analysis. Both methods are suitable for comparing differently designed heat storages. The latter is used to analyse the results in this paper.

The tank is divided into  $N$  equal sized horizontal layers with the volume  $V$ . The temperature is not measured in each volume. Therefore the temperatures of the volumes are determined by linear interpolation between the measured temperatures.

In the analysis of the moment of energy,  $M$ , the energy of each layer of the tank,  $E_i = \rho_i \cdot c_i \cdot V \cdot T_i$  is weighted by the vertical distance from the bottom of the tank to the centre of each layer,  $y_i$ . The moment of energy is:

$$M = \sum_{i=1}^N y_i \cdot E_i, \quad (1)$$

A mixing number is derived based on the measured temperature profile and the corresponding ideal stratified and fully mixed temperature profiles. The mix number is:

$$MIX = \frac{M_{str} - M_{exp}}{M_{str} - M_{mix}}, \quad (2)$$

$M_{str}$ ,  $M_{exp}$  and  $M_{mix}$  are the moment of energy of a perfectly stratified tank, the experiment and a fully mixed tank respectively. The value of the mix number is between 0 and 1 where 0 corresponds to a perfectly stratified tank and 1 corresponds to a fully mixed tank. For the experiment where the tank is heated from the surrounding temperature to a higher temperature level the temperature profiles for the perfectly stratified tank and the fully mixed tank are calculated by means of the measured temperatures.

The temperature of the fully mixed tank is calculated as the measured weighted average temperature. The temperature in the perfectly stratified tank consists of a high temperature in the upper part of the tank and a low temperature in the lower part of the tank. The low temperature equals the start temperature of the tank. The lower part of the tank has a volume equal to the total water volume in the tank minus the water volume which has entered the tank during the test. Based on the measured temperatures the temperature in the upper part of the tank with a volume equal to the water volume which has entered the tank during the test is determined in such a way that the energy of the perfectly stratified tank is equal to the measured energy in the tank. For the experiment where the tank is cooled from a high temperature to a lower temperature the temperature profiles for the perfectly stratified and fully mixed tank are calculated in a similar way. In this way heat losses and the heat capacity of the tank material are accounted for. No mix number is calculated for the stratified experiment. In this case only  $M_{exp}$  is calculated with the ambient temperature as the reference temperature.

## 3 RESULTS

### 3.1 Heating tests

Fig. 2 and Fig. 3 shows the temperature stratification in the tank in different heights every 5 minutes during the heating test with stratification manifolds of one and two fabric layers, style 361.

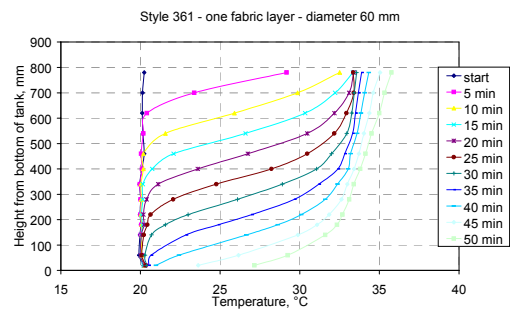


Fig. 2: Temperature profile during a heating test with fabric stratification pipes, Style 361 with one fabric layers

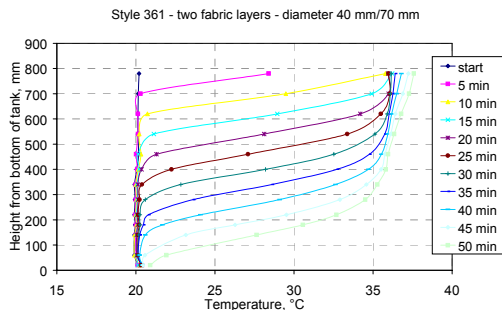


Fig. 3: Temperature profile during a heating test with fabric stratification pipes, Style 361 with two fabric layers.

From the figure it is clear that the temperature stratification profile is much more desirable when a stratification manifold of two fabric layers is used. With two layers of fabric the temperature curves are more horizontal and the temperature at the top of the tank is increased and the temperature at the bottom of the tank is decreased compared to the test with the one layer fabric stratification pipe.

Fig. 4 and Fig. 5 show the mix numbers during the heating test with one and two fabric layer stratification pipes. In Fig. 5 the mix number of the rigid pipe with three holes with “non-return” valves is also shown.

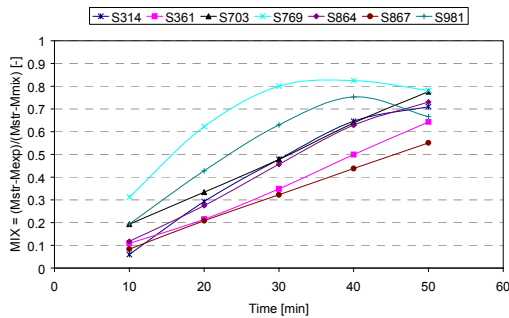


Fig. 4: Mix numbers for fabric stratification pipes of one fabric layer.

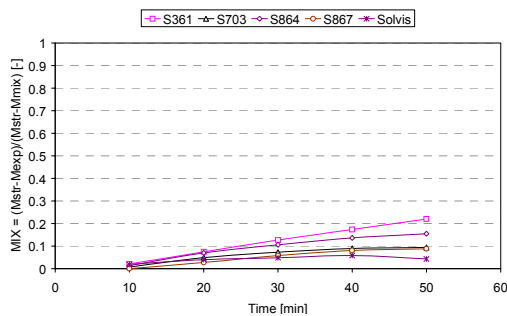


Fig. 5: Mix numbers for fabric stratification pipes of two fabric layers and the rigid pipe.

From Fig. 4 and Fig. 5 it is seen that the mix numbers are dramatically reduced by using two fabric layers with a distance between the layers instead of only one fabric

layer. The mix number increases during the experiment because the hot water enters the bottom of the tank and heat is transferred from the fabric pipe to the tank water in the lower part of the tank during the whole heating test. The mix number obtained with the rigid stratification pipe is very low and somewhat lower than the mix numbers obtained with the fabric stratification pipes. This is because the horizontal heat transfer through the wall of the rigid pipe is much lower than the horizontal heat transfer through the fabric wall.

### 3.2 Stratified heating tests

Fig. 6 shows the experimental moment of energy 1 during the stratified heating test with two fabric layer stratification pipes, S361 and the rigid pipe with holes with “non-return” valves.

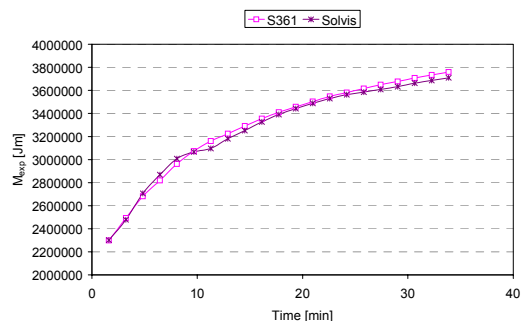


Fig. 6: Moment of energy  $M_{exp}$  of the experimental data.

From the figure it is obvious that the fabric stratification pipe with two fabric layers and the rigid pipe with holes with “non-return” valves perform almost equally under the applied test conditions. After about 10 minutes the curve from the rigid pipe switches place with the curve for the fabric pipe. In the start of the test the incoming water has entered the tank through the upper hole in the rigid pipe. After 10 minutes the inlet temperature is too low to enter the upper hole and too high to enter the middle hole. Hence, the incoming water enters both the upper and the middle hole and the temperature difference between the upper and the middle hole decreases.

### 3.3 Cooling tests

Fig. 7 shows the mix numbers during the cooling test with a two fabric layer stratification pipe, S361 and the rigid pipe with three holes with “non-return” valves.

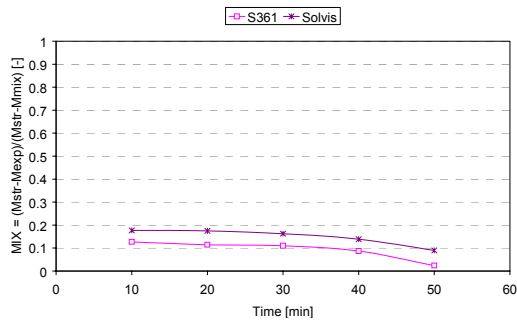


Fig. 7: Mix number for fabric stratification pipes with two fabric layers and the rigid pipe with holes with “non-return” valves.

From the figure it can be seen that the mix number is lower for the fabric stratification pipe than for the rigid pipe with holes with “non-return” valves. This is due to the fact that the incoming cold water only can leave the rigid pipe through the lowest hole whereas the incoming cold water can leave the fabric stratification pipe in any desired level.

### 3.4 PIV measurements

Fig. 8 shows the velocity vector maps and the corresponding streamlines to the vector maps 10, 20, 26 and 36 minutes after the heating is started. The velocity vector maps are calculated as mean values from 10 instantaneous velocity recordings by adaptive cross correlations and finally range validation procedure is applied. The corresponding temperature profiles are shown in Fig. 2 and Fig. 3.

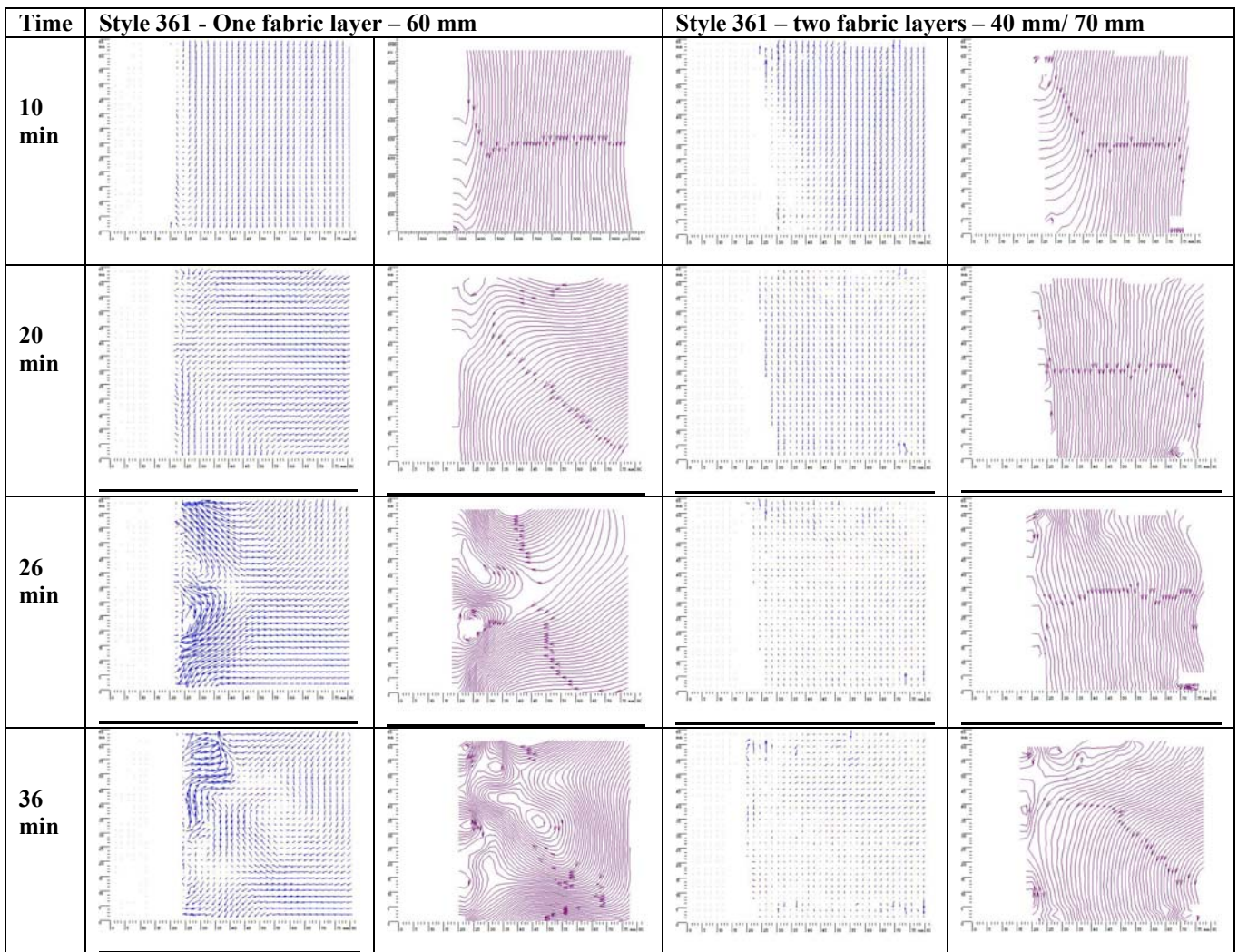


Fig. 8: Velocity vector maps and corresponding streamlines around the fabric stratification pipes with one and two fabric layers.

From the figure it can be seen that the primary movement of the tank water after 10 minutes is downward towards the outlet in the bottom of the tank. Close to the fabric stratification pipe the direction of the

water is upwards due to horizontal heat transfer through the fabric stratification pipe, especially for the one layer pipe. After 20 minutes the upward flow has stopped close to the one layer fabric pipe because thermal

stratification has been built up in the level where the pictures are taken. The thermal stratification stops the upward flow. Water is leaving the pipe just above the level of the picture. This is not the case close to the two layer fabric pipe where the picture is the same as after 10 minutes. After 26 minutes water leaves the one layer fabric pipe in the level where the picture is taken. There apparently is a mismatch temperature difference between water entering the tank and the tank water creating eddies. Close to the two layers fabric pipe no changes are observed. No temperature stratification has been build up below the level of the picture and therefore the direction of the tank water close to the two layer fabric pipe is upwards due to horizontal heat transfer through the fabric stratification pipe. For the two layer stratification pipe the water is still after 26 minutes moving downwards except very close to the pipe. After 36 minutes water starts to leave the two layer fabric pipe. At this time the temperature thermocline has reached the level of the picture. The pictures illustrate very well the advantages of using stratification fabric pipes with two fabric layers instead of one fabric layer.

#### 4 CONCLUSIONS

A number of stratifications pipes for hot water tanks made of different fabrics are investigated. The investigation comprises stratification pipes of one and two fabric layers. The performance of the fabric stratification pipes is investigated during heating, cooling and stratified heating tests. In all the tests, water enters the stratification pipe through the bottom of the tank. Further the performances of the fabric stratification pipes are compared to the performance of a marketed rigid stratification pipe with three holes with "non-return" valves.

The investigation shows that the performance of fabric stratification pipes can be improved significant by using two fabric layers with a distance of about 10 mm between each fabric layer instead of using one fabric layer.

The investigation also shows that the largest disadvantage of the fabric stratification pipes is the high horizontal heat transfer through the very thin fabric. This disadvantage is most significant when hot water enters a cold tank and flows from the bottom to the top of the fabric stratification pipe. In this particular case the rigid stratifier has an advantage because of the low horizontal heat transfer through the pipe wall.

For the cooling test the two fabric layer stratification pipe performs somewhat better than the rigid stratifier, while the two fabric layer stratification pipe and the rigid stratifier performs identical during stratified heating tests.

#### 5 NOMENCLATURE

$M$  = Moment of energy (J·m)  
 $E$  = Energy (J)

$y$  = Vertical distance (m)  
 $V$  = Volume (m<sup>3</sup>)  
 $c$  = Specific heat capacity (kJ/kg/K)  
 $\rho$  = Density (kg/m<sup>3</sup>)  
 $T$  = Temperature (K)  
 $N$  = Number of tank layers

Subscripts  
 $i$  = Tank layer  
 $str$  = Stratified  
 $exp$  = Experimental  
 $mix$  = Mixed

#### 6 REFERENCES

- (1) Adams D. E. Design of a Flexible Stratification Manifold for Solar Water Heating Systems. Master Thesis, Colorado State University, Fort Collins, CO. 1993.
- (2) Loehrke R.I., Holzer J.C., Gari H.N., Sharp M.K. Stratification enhancement in liquid thermal storage tanks. Journal of Energy, Vol. 3, No. 3, pp. 129-130, 1979.
- (3) Liebfried U. Comb tanks with internal thermosyphonically driven heat exchangers for hot water – comparison of existing systems, 2000. Proceedings Terrastock Conference, pp. 315-320.
- (4) Gari H.N., Loehrke R.I. A controlled buoyant jet for enhancing stratification in a liquid storage tank. Journal of Fluids Engineering, Vol. 104, pp. 475-481, 1982.
- (5) Davidson J.H., Adams D.A., Miller J.A. A Coefficient to Characterize Mixing in Solar Water Storage Tanks. Journal of Solar Energy Engineering, Vol. 116, pp. 94-99, 1994.
- (6) Davidson J.H., Adams D.A. Fabric Stratification Manifolds for Solar Water Heating. Journal of Solar Energy Engineering, Vol. 116, pp. 130-136, 1994.
- (7) Krause Th., Kühl L. Solares Heizen: Konzepte, Auslegung und Praxiserfahrungen, 2001.
- (8) Shah L.J. Stratifikationsindløbsrør. Department of Civil Engineering, Technical University of Denmark, DTU, 2002.
- (9) Andersen E., Jordan U., Shah L.J., Furbo S. Investigation of the Solvis Stratification Inlet Pipe for Solar Tanks. Proceedings of ISES Solar World Congress 2004, Freiburg, Germany, pp. 659-668, 2004.
- (10) Yee C. K., Lai F. C. Effects of a Porous Manifold on Thermal Stratification in a liquid Storage Tank. Solar Energy, Vol. 71, pp. 241-254, 2001.
- (11) Rosen M. A. The Exergy of Stratified Thermal Energy Storages. Solar Energy, Vol. 71, pp. 173-185, 2001.
- (12) Furbo S. Test Performance for Heat Storages for Solar Heating Systems. Int. J. Solar Energy, Vol. 1, 1983.
- (13) [www.testfabrics.com](http://www.testfabrics.com)

## **Bilag 8**

### **Performance improvement by discharge from different levels in solar storage tanks.**

Simon Furbo, Elsa Andersen, Alexander Thür, Louise Jivan Shah og Karin Dyhr Andersen.  
Solar Energy 79, pp. 431-439, 2005.



# Performance improvement by discharge from different levels in solar storage tanks

Simon Furbo \*, Elsa Andersen, Alexander Thür,  
Louise Jivan Shah, Karin Dyhr Andersen

*Department of Civil Engineering, Technical University of Denmark, Building 118, DK-2800 Kgs. Lyngby, Denmark*

Received 13 July 2004; received in revised form 12 January 2005; accepted 13 January 2005

Available online 10 March 2005

Communicated by: Associate Editor Erich Hahne

## Abstract

The thermal advantages by utilizing discharge from different levels in solar storage tanks are investigated, both for a small SDHW system and for a solar combisystem.

The investigations showed that it is possible to increase the thermal performance of both types of systems by using two draw-off levels from the solar tanks instead of one draw-off level at a fixed position.

The best position of the second draw-off level is in the middle or just above the middle of the tank. For the investigated small SDHW system with a realistic draw off hot water temperature of 40 °C and 45 °C and an auxiliary volume temperature of 50.5 °C the increase of the thermal performance by the second draw-off level is about 6%.

For the investigated solar combisystem the increase in thermal performance by using one extra draw-off level, either for the domestic hot water heat exchanger or for the heating system, is about 3%, while an improvement of about 5% is possible by using a second draw-off level both for the domestic hot water heat exchanger and for the heating system.  
© 2005 Elsevier Ltd. All rights reserved.

*Keywords:* SDHW systems; Solar combisystems; Heat storage tanks; Thermal stratification; Advanced discharge strategies

## 1. Introduction

The thermal performance of solar heating systems is strongly influenced by the thermal stratification in the heat storage tank. Investigations by [van Koppen et al. \(1979\)](#) showed that the thermal performance increases with thermal stratification in the heat storage.

Thermal stratification in solar storage tanks is normally established in two ways:

- During charge periods, where heat from the auxiliary energy supply system or from the solar collectors is transferred to the “right” level of the tank. That is, the heat from the auxiliary energy supply system is normally transferred to the top of the tank and the solar heat is transferred to the level in the storage tank, where the tank temperature is close to the temperature of the incoming fluid transferring the solar heat to the tank. [Furbo and Mikkelsen \(1987\)](#), [Shah](#)

\* Corresponding author. Tel.: +45 45 25 18 57; fax: +45 45 93 17 55.

E-mail address: [sf@byg.dtu.dk](mailto:sf@byg.dtu.dk) (S. Furbo).

and Furbo (1998) and Knudsen and Furbo (2004) showed that for small SDHW systems this is with advantage done by means of a vertical mantle heat exchanger. For large SDHW systems and for solar combisystems this is with advantage done by means of inlet stratifiers as shown by Weiss (2003), Furbo et al. (2005) and Andersen et al. (2004).

- During discharge periods where heat is discharged from a fixed level of the tank, for instance from the top of the tank for SDHW systems or from a level just above the lower level of the auxiliary volume in a storage tank for solar combisystems. Thermal stratification is best established during discharge if cold water enters the bottom of the tank in SDHW systems during draw-offs, and if the returning water from the heating system enters the tank through inlet stratifiers in solar combisystems as described by Weiss (2003).

Thermal stratification can be built up to a greater extent than normally if the solar tank is discharged from more than one level, as proposed by Furbo (1984) and Lorenz (2001). For instance, a hot water tank for SDHW systems can be equipped with two draw-off pipes, one at the very top of the tank and one at the middle of the tank. In periods where the temperature at the top of the tank is higher than the required hot water temperature, a part of the hot water can with advantage be tapped at a lower temperature through the lower draw-off pipe. In this way the volume of the cold water entering the tank during draw-off is increased, resulting in increased solar collector efficiency, decreased tank heat loss, decreased auxiliary energy supply and consequently increased thermal performance of the SDHW system.

Solar combisystems making use of two draw-off levels in the solar tanks are marketed by Jenni Energietechnik AG (2004).

This paper presents the results of theoretical as well as experimental investigations of the thermal advantage of discharge from different levels in solar storage tanks, both for SDHW systems and for solar combisystems.

## 2. Solar domestic hot water systems

### 2.1. Experiments

#### 2.1.1. System design

Two small low flow SDHW systems were tested side-by-side in a laboratory test facility for solar heating systems. With the exception of the solar tank the systems were identical.

Fig. 1 shows schematic illustrations of the two tanks. Both tanks are standard mantle tanks suitable for low

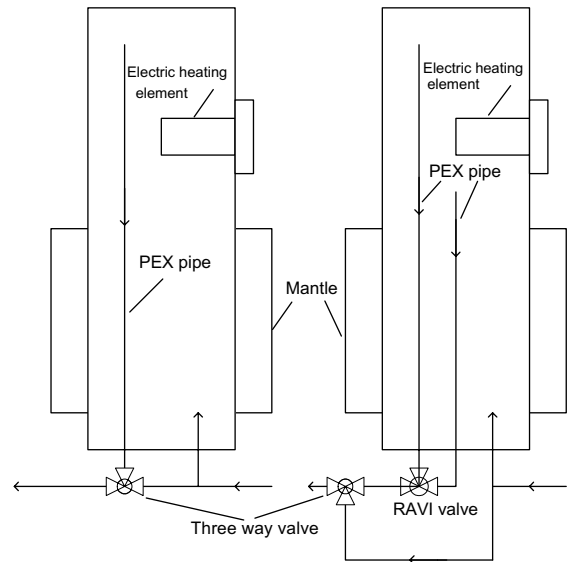


Fig. 1. Schematic illustration of the two investigated solar tanks.

flow systems. In both tanks the auxiliary energy is supplied with electric heating elements. One tank is equipped with a PEX pipe for hot water draw-off from the very top of the tank.

The other tank is equipped with two PEX pipes for hot water draw-off from the very top of the tank and from the middle of the tank.

A three way valve, type RAVI from Danfoss A/S, ensures that the temperature of the tapped water from the tank during draw-offs is equal to the required hot water temperature. If this is not possible due to high tank temperatures, the valve ensures that the difference between the tapped water temperature and the required hot water temperature is as low as possible. That is, the three way valve ensures that the right part of the hot water is tapped from the top and from the middle of the tank.

For both systems additional three way valves mixing cold water with the water from the tank ensures that the temperature of the water tapped from the systems is equal to the required hot water temperature.

The most important data of the tested systems are given in Table 1.

#### 2.1.2. Operating conditions

The electric heating elements heat up the top volume to 53 °C during all hours.

The solar irradiance on the collectors and the daily hot water consumption are the same for both systems. An energy quantity of 1.53 kWh, corresponding to 33 l of hot water heated from 10 °C to 50 °C or 36 l of hot water heated from 10 °C to 47 °C is tapped from each system three times each day: 7 am, 12 am and 7 pm.

Table 1  
Data for the two SDHW systems in the side-by-side laboratory test

Tank design	
Producer	Nilan A/S
<i>Inner tank</i>	
Hot-water tank volume, (m <sup>3</sup> )	0.175
Inner height, (m)	1.45
Inner diameter, (m)	0.394
Tank wall thickness, (m)	0.003
Auxiliary volume, (m <sup>3</sup> )	0.063
Draw-off level, (s)	1.44 m/1.44 m and 0.87 m from bottom of tank
Power of electric heating element, (W)	1200
<i>Mantle</i>	
Mantle volume, (m <sup>3</sup> )	0.0319
Mantle height, (m)	0.7
Mantle gap, (m)	0.0335
Position of mantle inlet	Top
Inside diameter of mantle inlet, (m)	0.0189
<i>Insulation</i>	
Material	Mineral wool
Insulation top, (m)	0.13
Insulation side above/below mantle, (m)	0.06
Insulation side mantle, (m)	0.06
Insulation bottom, (m)	0.0
<i>Solar collector</i>	
Producer	Arcon Solvarme A/S
Type	ST-NA
Area, (m <sup>2</sup> )	2.51
Start efficiency, (–)	0.81
1st order heat loss coefficient, (W/m <sup>2</sup> K)	3.21
2nd order heat loss coefficient, (W/m <sup>2</sup> K <sup>2</sup> )	0.013
Incident angle modifier (tangens equation)	$a = 3.6$
Heat capacity, (J/m <sup>2</sup> K)	5339
Tilt, (°)	45
Orientation	South
<i>Solar collector loop</i>	
Flow rate, (l/min)	0.5
Pipe material	Copper
Outer diameter, (m)	0.010
Inner diameter, (m)	0.008
Insulation thickness (PUR foam), (m)	0.01
Length of pipe from storage to collector, indoor, (m)	4.6
Length of pipe from storage to collector, outdoor, (m)	13.3
Length of pipe from collector to storage, indoor, (m)	5.1
Length of pipe from collector to storage, outdoor, (m)	10.0
Solar collector fluid (propylene glycol/water mixture), (%)	40
Power of circulation pump, (W)	50
<i>Control system</i>	
Producer	Danotek
Type	DTP 2200 Differential temperature controller with one temperature sensor in the top of the collector and one temperature sensor at the bottom of the mantle
Start temperature difference, (K)	10
Stop temperature difference, (K)	2

### 2.1.3. Measured results

Measured energy quantities for 6 weeks with a draw-off temperature of 50 °C are given in Table 2 and measured energy quantities for 7 weeks with a draw-off temperature of 47 °C are given in Table 3. The net utilized solar energy is the tapped energy from the solar tank minus the energy supply to the electric heating elements.

For the 6 weeks test period with a hot water draw-off temperature of 50 °C the net utilized solar energy for the solar heating system with two draw-off levels is 8 kWh higher than the net utilized solar energy for the standard system. For the 7 weeks test period with a hot water draw-off temperature of 47 °C the net utilized solar energy for the solar heating system with two draw-off levels is 18 kWh higher than the net utilized solar energy for the standard system.

The thermal performance of the systems is small, since the tests were carried out in the winter. The thermal advantage of two draw-off levels is higher for a draw-off temperature of 47 °C than for a draw-off temperature of 50 °C.

### 2.2. Calculation

#### 2.2.1. Simulation model

Calculations were carried out with the simulation model Mantlsim developed at the Technical University of Denmark by Furbo and Berg (1990), Shah and Furbo (1998), Knudsen and Furbo (2004) and Furbo and Knudsen (2004). The two tested low flow systems with the data given in Table 1 are taken into calculation. Weather data of the Danish Test Reference Year developed by Statens Byggeforskningsinstitut (1982) is used in the calculations.

The daily hot water consumption is 4.6 kWh, corresponding to 100 l water heated from 10 °C to 50 °C. Hot water is tapped with an energy quantity of 1.53 kWh three times each day: 7 am, 12 am and 7 pm. The required hot water draw-off temperature is 50 °C.

The thermal performance of the system with the two draw-off levels was calculated with one draw-off pipe at the very top of the tank and with different positions of the second draw-off level.

Table 2  
Measured thermal performance for the two tested systems with a hot water draw-off temperature of 50 °C

Period	Standard system			System with two draw-off levels		
	Tapped energy (kWh)	Auxiliary energy (kWh)	Net utilized solar energy (kWh)	Tapped energy (kWh)	Auxiliary energy (kWh)	Net utilized solar energy (kWh)
15-21/10-03	32	25	7	32	23	9
22-28/10-03	32	25	7	32	23	9
29/10-4/11-03	32	33	−1	32	32	0
5-11/11-03	32	35	−3	32	33	−1
1-7/12-03	32	35	−3	32	35	−3
17-23/12-03	32	33	−1	32	32	0
6 Weeks	192	186	6	192	178	14

Table 3  
Measured thermal performance for two tested systems with a hot water draw-off temperature of 47 °C

Period	Standard system			System with two draw-off levels		
	Tapped energy (kWh)	Auxiliary energy (kWh)	Net utilized solar energy (kWh)	Tapped energy (kWh)	Auxiliary energy (kWh)	Net utilized solar energy (kWh)
9-15/2-04	32	28	4	32	27	5
16-22/2-04	32	17	15	32	14	18
23-29/2-04	32	26	6	32	23	9
1-7/3-04	32	17	15	32	13	19
11-17/3-04	32	20	12	32	17	15
18-24/3-04	32	18	14	32	16	16
25-31/3-04	32	21	11	32	19	13
7 Weeks	224	147	77	224	129	95

2.2.2. Simulation results

Fig. 2 shows the calculated yearly net utilized solar energy of the system as a function of the relative position of the second draw-off level and as a function of the auxiliary set point temperature.

Fig. 3 shows the calculated yearly percentage increase of the net utilized solar energy by using a second draw-off pipe as functions of the relative position of the second draw-off level and the set point temperature for the auxiliary energy system. If the relative position of the second draw-off level is at the top of the tank, the system is identical to the standard system with only one draw-off level at the very top of the tank. The thermal advantage of using a second draw-off pipe is strongly influenced by the auxiliary set point temperature. The higher the set point temperature the larger the advantage. If the auxiliary set point temperature is only 0.5 K higher than the required draw-off hot water temperature, the extra thermal performance by using a second draw-off level is about 1%. If the auxiliary set point temperature is 15 K higher than the required hot

water temperature, the extra thermal performance by using a second draw-off level is about 13%. The second draw-off level is best placed in the middle of the tank.

Figs. 4 and 5 show the calculated yearly net utilized solar energy of the system and the calculated extra percentage net utilized solar energy of the system by using two draw-off levels as a function of the position of the second draw-off level for four different daily hot water consumptions: 50, 100, 160 and 180 l. Hot water is tapped by means of three daily draw-offs with the same draw-off volume: At 7 am, 12 am and 7 pm. Hot water is tapped at 45 °C at 7 am and at 7 pm, while hot water is tapped at 40 °C at 12 am. During all hours the top auxiliary volume is heated to 50.5 °C. The draw-off temperatures are realistic, since hot water is not used at the same temperature level in practice. Further, in practice the set point of the auxiliary energy supply system is often 5–10 K higher than the required hot water draw-off temperature. The figures show that the net utilized solar energy is increased by about 6% by using two draw-off levels. Again, the second draw-off level is best

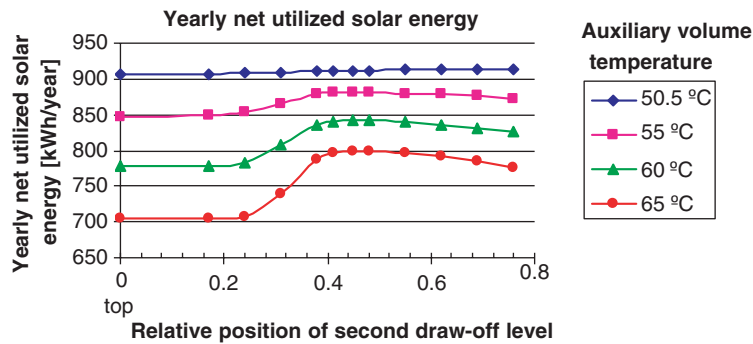


Fig. 2. Calculated net utilized solar energy of the SDHW system as functions of the position of the second draw-off level and of the auxiliary set point temperature.

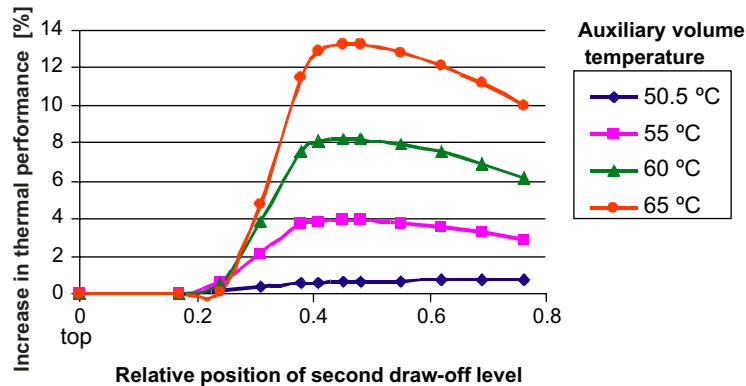


Fig. 3. Calculated increase in net utilized solar energy of the system by using two draw-off levels as functions of the position of the second draw-off level and of the auxiliary set point temperature.

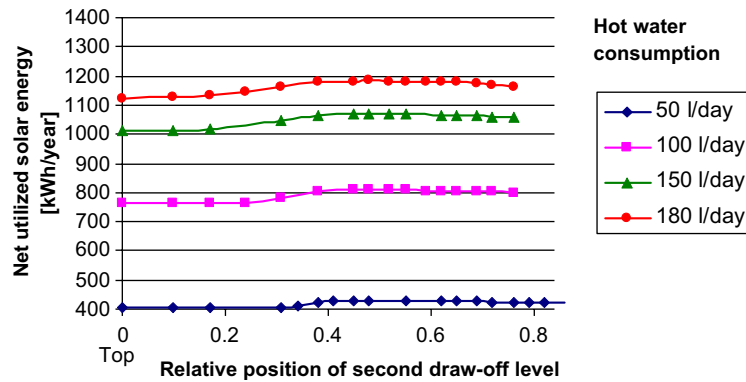


Fig. 4. Calculated yearly net utilized solar energy of the SDHW system as a function of the position of the second draw-off level for different daily hot water consumptions.

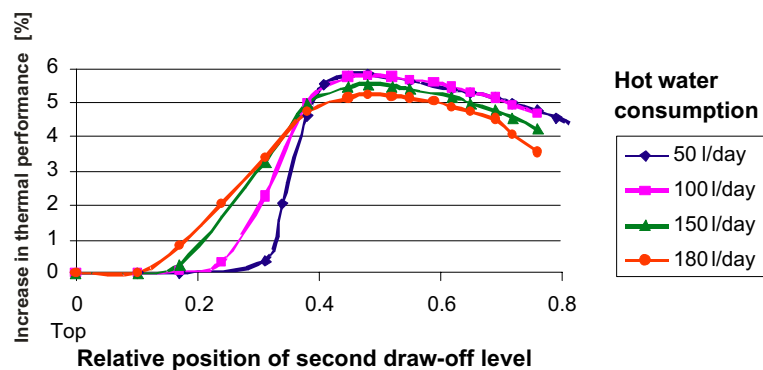


Fig. 5. Calculated increase in net utilized solar energy of the SDHW system by using two draw-off levels as a function of the position of the second draw-off level.

placed in the middle of the tank. It should be mentioned, that there is a need for development of an advanced control system before solar tanks in practice can supply the consumers with different draw-off temperatures.

### 3. Solar combisystems

Calculations of the yearly net utilized solar energy of a solar combisystem are carried out by means of TRNSYS developed by Klein et al. (1996) and Drück (2000). The solar combisystem taken into calculation is schematically shown in Fig. 6.

The solar heating system, which is a marketed system by SOLVIS Solar Systeme GmbH, was the best system investigated by Weiss (2003). The system has a compact heat storage unit with the following components integrated: A water tank with an auxiliary condensing natural gas burner, a domestic hot water flat plate heat exchanger with a pump, a solar collector loop and a solar heat exchanger. Thermal stratification is built up

in the heat storage in a good way, since SOLVIS inlet stratifiers ensure that the solar heat is transferred to the “right” level in the tank and that the water returning from the heating system enters the tank in the right level.

The volume of the tank is 650 l and the auxiliary volume heated by the natural gas burner is 136 l. The natural gas burner heats up the auxiliary volume to 57 °C. The solar collectors described in the previous section are also used in the calculations on the thermal performance of the solar combisystem. The solar collector area is 12.55 m<sup>2</sup>.

The water to the heating system is tapped from a level just above the lower level of the auxiliary volume.

The space heating demand of the house taken into calculation is 14970 kWh/year. The heating system is a traditional radiator system which, at an indoor temperature of 20 °C and an outdoor temperature of –12 °C, can supply the required heating power of the house with an inlet water temperature of 60 °C and an outlet water temperature of 50 °C. A daily hot water consumption of 150 l heated from 10 °C to 51 °C is assumed. Weather

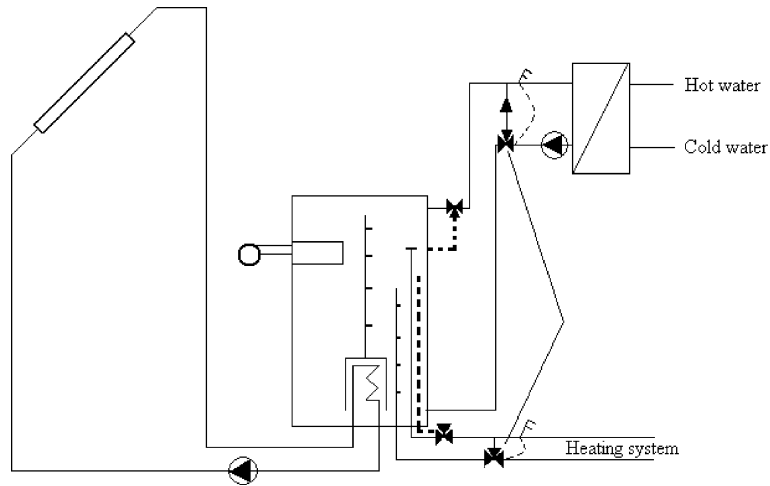


Fig. 6. Schematic illustration of solar combisystem taken into calculation.

data of the Danish Test Reference Year is used in the calculations. The draw-off level for the domestic hot water heat exchanger is placed at a relative position of 0.05 from the very top of the tank and the draw-off level for the space heating system is placed at a relative position of 0.23 from the very top of the tank.

Calculations of the yearly net utilized solar energy of the system are carried out for the standard system, for the system with two draw-off levels for the domestic hot water heat exchanger with different positions of the second draw-off level, for the system with two draw-off levels for the space heating system with different positions of the second draw-off level and for a system with two draw-off levels, both for the domestic hot water heat exchanger and for the space heating system.

Fig. 7 shows the calculated yearly net utilized solar energy of the system with two draw-off levels to the domestic hot water heat exchanger and the standard draw-off level to the heating system, as well as the yearly

net utilized solar energy of the system with two draw-off levels to the heating system and the standard draw-off level to the domestic hot water heat exchanger as functions of the position of the second draw-off level.

Fig. 8 shows the extra percentage net utilized solar energy for the solar combisystem by utilizing two draw-off levels to the domestic hot water heat exchanger as well as the extra percentage net utilized solar energy for the solar combisystem by utilizing two draw-off levels to the heating system as a function of the position of the second draw-off level. It is possible to increase the yearly thermal performance of the system by about 3%, either by using two draw-off pipes for the domestic hot water heat exchanger instead of one or by using two draw-off pipes for the heating system instead of one. The best position of the second draw-off level for the domestic hot water heat exchanger is in the middle of the tank, and the best position of the second draw-off level for the heating system is just above the middle of the tank.

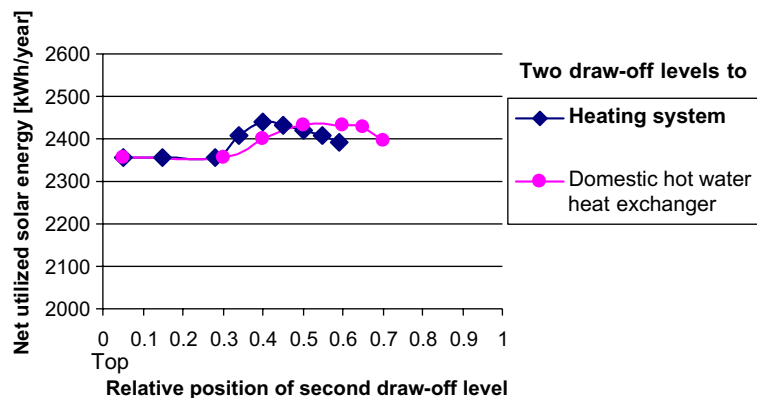


Fig. 7. Calculated yearly net utilized solar energy for the solar combisystem as a function of the position of the second draw-off level.

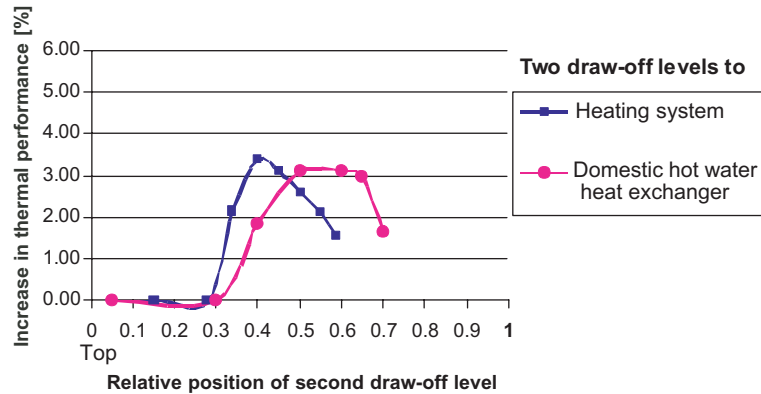


Fig. 8. Increase in net utilized solar energy for the solar combisystem by using two draw-off levels for the domestic hot water heat exchanger instead of one draw-off level and by using two draw-off levels for the heating system instead of one draw-off level as a function of the position of the second draw-off level.

Further calculations showed, that by using a second draw-off level, both to the domestic hot water heat exchanger and to the heating system, the yearly net utilized solar energy of the solar combisystem is increased by about 5% compared to the standard system. Also for this design, the second draw-off pipe for the domestic hot water heat exchanger is best placed in the middle of the tank, while the second draw-off pipe for the heating system is best placed just above the middle of the tank.

#### 4. Conclusions

The investigations showed that it is possible to increase the thermal performance of both SDHW systems and solar combisystems by using two draw-off levels from the solar tanks instead of one draw-off level at a fixed position.

The best position of the second draw-off level is for all the investigated systems in the middle or just above the middle of the tank. For the investigated SDHW system the increase in thermal performance of using a second draw-off level from the hot water tank is strongly influenced by the difference between the set point temperature of the auxiliary energy supply system and the required draw-off temperature. For increasing temperature difference the thermal advantage of the second draw-off level increases. For a realistic draw off hot water temperature of 40 °C and 45 °C and an auxiliary volume temperature of 50.5 °C the increase in thermal performance by the second draw-off level is about 6%.

For the investigated solar combisystem the increase in thermal performance by using one extra draw-off level, either for the domestic hot water heat exchanger or for the heating system, is about 3%, while an improvement of about 5% is possible by using a second

draw-off level both for the domestic hot water heat exchanger and for the heating system.

#### References

- Andersen, E., Jordan, U., Shah, L.J., Furbo, S., 2004. Investigations of the SOLVIS stratification inlet pipe for solar tanks. In: EuroSun 2004 Proceedings, Freiburg, Germany, vol. 1, 076–085.
- Drück, H., 2000. SOLVISMALX–Model for TRNSYS, Type 147. Institut für Thermodynamik und Wärmetechnik. Universität Stuttgart.
- Furbo, S., 1984. Varmelagring til solvarmeanlæg. Ph.D. Thesis, report no. 162. Thermal Insulation Laboratory, Technical University of Denmark.
- Furbo, S., Mikkelsen, S.E., 1987. Is low flow operation an advantage for solar heating systems? In: Bloss, W.H., Pfisterer, F. (Eds.), *Advances in Solar Energy Technology*, vol. 1. Pergamon Press, Oxford, pp. 962–966.
- Furbo, S., Berg, P., 1990. Calculation of the thermal performance of small hot water solar heating systems using low flow operation. In: *North Sun'90 Proceedings*, Reading, England.
- Furbo, S., Knudsen, S., 2004. Low flow SDHW systems based on mantle tanks—recent findings. In: *EuroSun 2004 Proceedings*, Freiburg, Germany, vol. 1, pp. 272–281.
- Furbo, S., Vejen, N.K., Shah, L.J., 2005. Thermal performance of a large low flow solar heating system with a highly thermally stratified tank. *Journal of Solar Energy Engineering* 127 (1), 15–20.
- Jenni Energietechnik AG, 2004. Available from: <[www.jenni.ch/html/Produkte/Armaturen/Heizungsgruppe%20zweistufig.htm](http://www.jenni.ch/html/Produkte/Armaturen/Heizungsgruppe%20zweistufig.htm)>.
- Klein, S.A., et al. 1996. TRNSYS 14.1, User Manual. University of Wisconsin, Solar Energy Laboratory.
- Knudsen, S., Furbo, S., 2004. Thermal stratification in vertical mantle heat exchangers with application to solar domestic hot water systems. *Applied Energy* 78/3, 257–272.

- Lorenz, K., 2001. Kombisolvärmsystem. Utvärdering av möjliga systemförbättringar. Report D59:2001. Institutionen för Installationsteknik, Chalmers Tekniska Högskola, Sweden.
- Shah, L.J., Furbo, S., 1998. Correlation of experimental and theoretical heat transfer in mantle tanks used in low flow SDHW systems. *Solar Energy* 64 (4–6), 245–256.
- Statens Byggeforskningsinstitut, 1982. Vejrdata for VVS og energi. Dansk referenceår TRY.
- van Koppen, C.W.J., Thomas, J.P.X., Veltkamp, W.B., 1979. The Actual Benefits of Thermally Stratified Storage in a Small and Medium Size Solar System. In: *Proceedings of ISES Solar World Congress, Atlanta, USA*, pp. 579–580.
- Weiss, W. (Ed.), 2003. *Solar heating systems for houses. A design Handbook for Solar Combinations*. James & James Ltd., Solar Heating and Cooling Executive Committee of International Energy Agency (IEA).



## **Bilag 9**

### **Investigations of medium sized solar combi systems**

Elsa Andersen og Simon Furbo.  
Paper til Eurosun 2006,  
Glasgow, UK



# INVESTIGATIONS OF MEDIUM SIZED SOLAR COMBI SYSTEMS

Elsa Andersen and Simon Furbo  
Department of Civil Engineering  
Technical University of Denmark  
DK-2800 Kgs. Lyngby  
Denmark  
E-mail: [ean@byg.dtu.dk](mailto:ean@byg.dtu.dk)

## ABSTRACT

A large variety of solar combi systems are on the market today. The best performing systems are highly advanced energy systems with thermal stratification manifolds, an efficient boiler and only one control system, which controls both the boiler and the solar collector loop (Weiss et al., 2003). However, it is still too early to draw conclusions on the design of solar combi systems. Among others, the following questions need to be answered: Is an external domestic hot water preparation more desirable than an internal domestic hot water preparation? What is the thermal advantage by using inlet stratifiers for different solar combi systems? Is an integrated boiler more desirable than a non integrated boiler? How does the design of the space heating system influence the thermal performance of different solar combi systems?

Theoretical investigations are carried out for different solar combi system types and sizes by means of the simulation program Trnsys (Klein et al., 1996) and the multiport store model (Drück, 2000). The work is carried out within the Solar Heating and Cooling Programme of the International Energy Agency (IEA SHC), Task 32 Advanced storage concepts for solar houses and low energy buildings.

## 1 INTRODUCTION

In the period 1998-2002 the IEA SHC, Task 26 Solar CombiSystems evaluated 21 solar combi systems which were on the European market. The evaluation comprised both the system costs and the thermal performance. It was found that most of the systems for one family houses had solar collectors of 10 m<sup>2</sup>- 30 m<sup>2</sup> with 0.3 m<sup>3</sup>- 3 m<sup>3</sup> tank volumes and that the best systems, regarding the performance/costs ratio, were the most advanced systems with thermal stratification manifolds, an efficient integrated boiler and only one control system, which controls both the boiler and the solar collector loop (Weiss et al., 2003).

A number of different tanks for Swedish solar combi systems were investigated experimentally by (Lorenz, 2001). Based on experimental as well as theoretical investigations on the optimum design of different heat storages by operating the space heating system as a high temperature system, a low temperature system or a low flow system were made. Among other things, it was concluded that the thermal performance could be improved with a low temperature SH system with stratification manifold in the heat storage for the return water.

A number of stratification inlet pipes, so called stratifiers, were investigated by (Andersen et al., 2005). It was found that thermal stratification can be built up and maintained in a very good way with certain stratifiers, among others with multilayer fabric stratifiers.

In the first part of the paper three differently designed medium sized solar combi systems are investigated. The systems have 1000 litre storage tanks and 20 m<sup>2</sup> solar collectors. In the second part of the paper it is investigated how the design of the space heating system and the control system in the solar collector loop influence the thermal performance of a solar combi system. Finally three different sizes of solar combi systems are investigated. The systems have 500 litre, 1000 litre and 1500 litres storage tanks with solar collector areas of 10 m<sup>2</sup>, 20 m<sup>2</sup> and 30 m<sup>2</sup> respectively.

## 2 INVESTIGATIONS OF DIFFERENTLY DESIGNED SOLAR COMBI SYSTEMS

A number of solar combi system types are investigated theoretically. Fig. 1 shows schematic illustration of the investigated solar combi system types. The investigation is based on three basically different system models, one model is based on a space heating storage with an external heat exchanger mounted in a side arm for domestic hot water preparation, one model is based on a domestic hot water tank with an internal heat exchanger spiral for the space heating system and one model is based on a hot water tank in tank storage. The three system models are referred to as model 1, 2 and 3 respectively. Further, the models are improved by introducing stratifiers in the solar collector loop and in the space

heating loop and in both the solar collector loop and the space heating loop. The variations in each model is numbered successively, see Fig. 1. The advantage of using stratifiers is that incoming water of any temperature is lead into the tank in a level where the temperature of the incoming water matches the temperature of the water in the tank. In this way thermal stratification in the tank is enhanced without destroying the already existing thermal stratification in the tank. In the present investigation, the thermal stratification is assumed to be built up in a perfect way without any mixing by the inlet stratifier. In this way the investigations show the maximum potential of stratification.

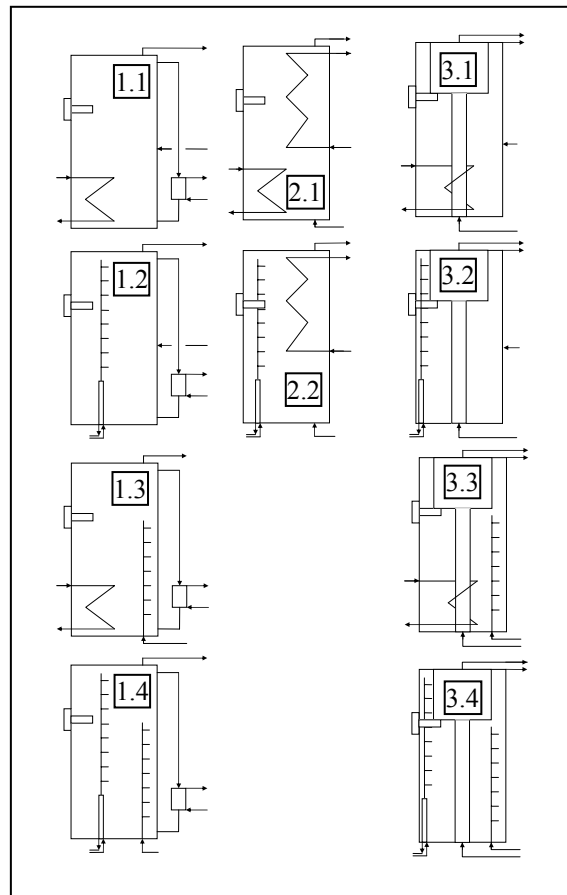


Fig. 1: Schematics of the three system models: model 1 (left), model 2 (middle) and model 3 (right) and the successively numbered variations of the system models.

## 2.1 Assumptions for the calculations

The solar combi systems are designed as described in Table 1. The Danish Design Reference Year, DRY is used as weather data (Skertveit et al., 1994). The daily hot water consumption is 100 litre and 200 litre. Domestic water is heated from 10°C to 50°C. Hot water is tapped at 7 am, noon and 7 pm in three equal portions with a volume flow rate of less than 2 l/min.

The temperature in the top of the heat storage of a solar heating is determined by the set point temperature of the auxiliary energy supply system and the temperature supplied from the solar collector during sunny hours. The set point temperature of the auxiliary volume is 57°C.

The required heating power and the flow and return temperatures for the space heating system for three one family houses of 150 m<sup>2</sup> with different degree of insulation are shown in Fig. 2. The heating demands of the three houses are about 30 kWh/(m<sup>2</sup> year), about 60 kWh/(m<sup>2</sup> year) and about 100 kWh/(m<sup>2</sup> year). The heating demands are referred to as LOA30, LOA60 and LOA100 respectively.

All positions for inlet to the tank and outlet from the tank are given as relative heights defined as: inlet height / total height of than where 0 equals the bottom of the tank and 1 equals the top of the tank.

The abbreviations spiralHX, fixSH, strSolar, strSH, 100 and 200 represent heat exchanger in the solar collector loop, fixed return inlet height from the space heating loop, stratifier in the solar collector loop, stratifier in the space heating loop, daily domestic hot water consumption of 100 litre and 200 litre respectively. The net utilized solar energy is defined as: energy for domestic hot water + energy for space heating – auxiliary energy. The system utilized solar energy is defined as: energy for domestic hot water + energy for space heating – auxiliary energy – energy for pump. The solar fraction is defined as: net utilized solar energy / the sum of energy for domestic hot water and energy for space heating. Finally, the performance ratio is defined as: net utilized energy for the system in question / net utilized solar energy for the system used as reference

Table 1: Data for the solar combi system used in the calculations.

<b>Solar collector</b>	
Solar collector area	20 m <sup>2</sup>
Start efficiency, $\eta_0$	0.756
Heat loss coefficients, $a_1 / a_2$	4.17 W/m <sup>2</sup> /K / 0.0095 W/m <sup>2</sup> /K <sup>2</sup>
Efficiency for small incidence angles, $\eta$ (E [W/m <sup>2</sup> ] is the total solar irradiance on the collector)	$\eta_0 - a_1 \cdot (T_m - T_a)/E - a_2 \cdot (T_m - T_a)^2/E$
Incidence angle modifier for beam radiation, $k_0$	$1 - \tan^4(\theta/2)$
Tilt, $\beta$ / Orientation	65° / South
<b>Solar collector loop</b>	
Outer/inner pipe diameter	20/18 mm
Length of pipe from/to solar collector to/from storage, indoor	5 m
Heat loss coefficient of pipe	4.2 W/m <sup>2</sup> /K
Solar collector fluid	40% (weight) propylene glycol/water mixture
Mass flow rate in solar collector loop, high / low	1.2 l/min/m <sup>2</sup> / 0.17 l/min/m <sup>2</sup>
Power of circulation pump	30 W
<b>Tank</b>	
Storage volume / auxiliary volume	1000 l (260 l DHW tank) / 190 l
Height/diameter	2 / 0.798 m
Heat loss coefficient, tank / sidearm / DHW heat exchanger	3.82 W/K / 0.39 W/K / 0.37 W/K
Heat transfer coefficient of external heat exchanger when stratifier in solar collector loop is used, UA	2000 W/K
Heat transfer coefficient of: spiral in solar collector loop / spiral in space heating system / tank in tank heat transfer	75 W/K per m <sup>2</sup> / 750 W/K / 278 W/K
Efficiency of auxiliary energy supply system	100%
Relative in-/outlet height of domestic hot water loop	0 / 1
Relative outlet height of space heating system (fixed inlet)	0.98
Relative in-/outlet height of spiral in solar collector loop	0.305 / 0.06
<b>Control system</b> – Differential thermostat control with one sensor in the solar collector and one in the tank	
Relative height of temperature sensor: spiral in solar collector loop / stratifier in solar collector loop	0.14 / 0.01
Start/Stop difference	10 K/0.5 K

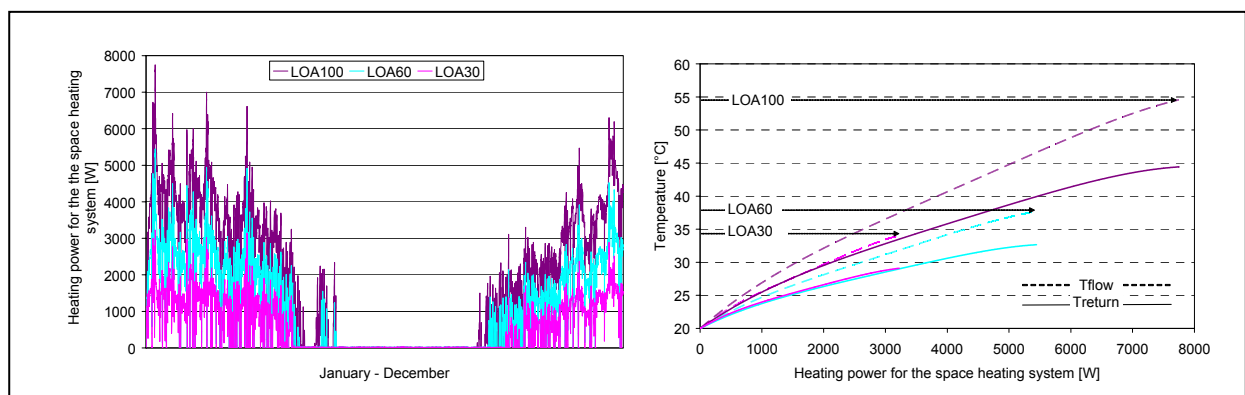


Fig. 2: Power for the space heating systems and flow and return temperatures in the space heating systems used in the calculations.

## 2.2 Results

The results are shown as the net utilized solar energy as function of the parameter varied. Further, the results are shown as the performance ratio as function of the parameter varied. The parameters varied are:

- Domestic hot water consumption
- Space heating demand
- Relative return inlet height from the space heating loop
- Control system in the solar collector loop, which are the position of the sensor in the tank and the stop temperature difference of the pump.

Fig. 3 shows the calculated yearly net utilized solar energy as function of the relative return inlet height from the space heating loop for model 1.1, model 2.1 and model 3.1 with a heat exchanger spiral in the solar collector loop and fixed return inlet height from the space heating loop. Further, the performance ratio relative to the optimal thermal performance of the system in question is shown. The space heating demand is varied in accordance with Fig. 2 and the daily domestic hot water consumption is 100 litre and 200 litre. Also the net utilized solar energy is shown for model 1.3 and model 3.3 with a stratifier in the space heating loop.

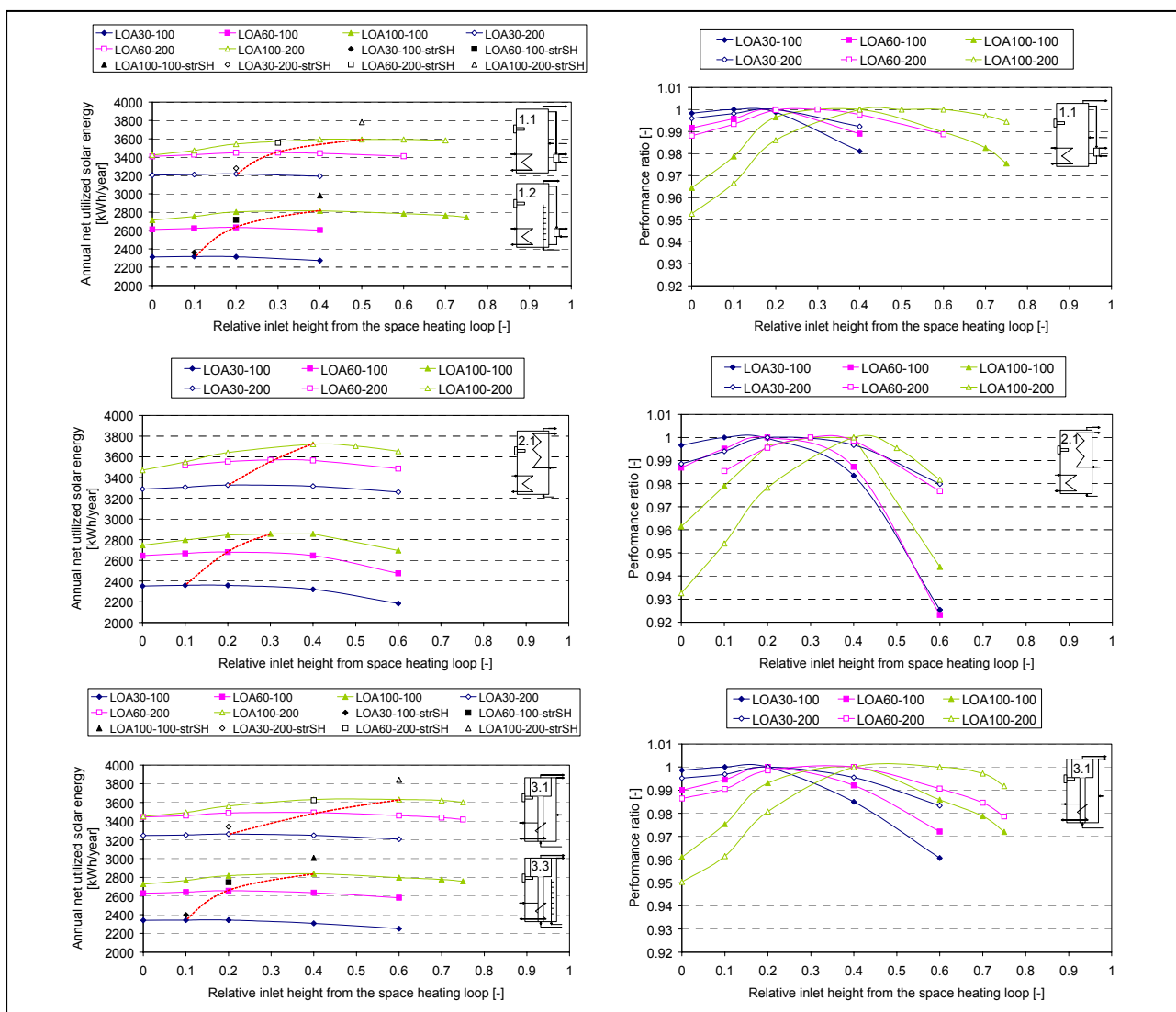


Fig. 3: Left: The annual net utilized solar energy as function of the relative return inlet height from the space heating loop for model 1.1, model 1.3, model 2.1, model 3.1 and model 3.3. Right: The performance ratio relative to optimal thermal performance of the system in question.

The figure show that the optimal inlet position from the space heating loop varies with the daily domestic hot water consumption and the space heating demand. For low space heating demand and thereby low return inlet temperatures the optimal inlet position is low. For increasing space heating demand and thereby increasing return inlet temperature, the

height of the optimal inlet position increases. Also the optimal return inlet position from the space heating loop increases for increasing domestic hot water consumption. This is due to a larger amount of cold water in the bottom of the tank which leaves the warmer water that matches the temperature of the return water from the space heating loop at a higher level in the tank.

The net utilized solar energy is reduced less than 1 % for all the system models if the relative return inlet position from the space heating loop is 0.3 and less than 2 % if the inlet position is between 0.2 and 0.4.

Fig. 4 shows the net utilized solar energy as function of the space heating demand and the domestic hot water consumption for model 1, model 2 and model 3 and the step by step improvement of the designs. Also the performance ratio relative to the least advanced model 1.1, model 2.1 and model 3.1 is shown. In all the calculations with a fixed return inlet height from the space heating loop, the optimal return inlet height shown in Fig. 3 is used.

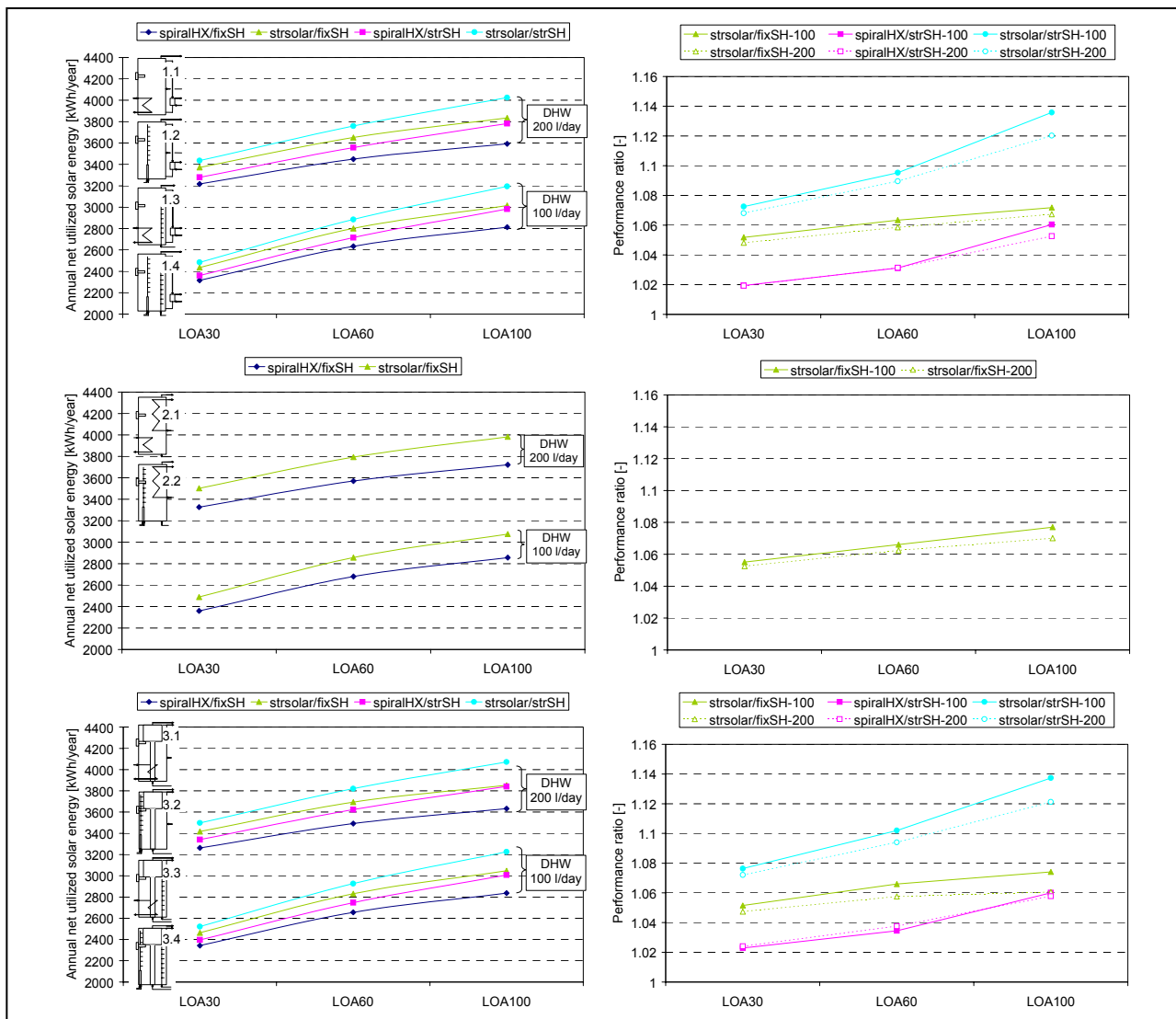


Fig. 4: Left: The annual net utilized solar energy as a function of the space heating demand and the domestic hot water consumption for model 1, model 2 and model 3 and the step by step improvement of the models. Right: The performance ratio relative to the thermal performance of the least advanced models, model 1.1, model 2.1 and model 3.1.

The figure shows that the thermal performance increases for increasing space heating demand and increasing domestic hot water consumption. Also, the figure shows that the thermal performance increases when the heat exchanger spiral is replaced with a stratifier in the solar collector loop and when an inlet stratifier is used for the returning water from the space heating system instead of a fixed return inlet position and that the thermal performance advantage is larger with a stratifier in the solar collector loop than with a stratifier in the space heating loop. Finally, it can be seen that the performance ratio of the system by using inlet stratifiers is almost the same regardless of the design of the solar combi system.

The additional gained net utilized solar energy by using stratifiers increases for increasing space heating demand. This is due to the return temperature from the space heating system which is higher for high space heating demands than for low space heating demands. Hence the variation in the return temperature from the space heating system is higher for high space heating demands than for low space heating demands and this leads to a better utilization of a stratifier.

The increase in net utilized solar energy by using a stratifier in the solar collector loop or in the space heating loop or in both the solar collector loop and in the space heating loop is in the range of 5 – 8 %, 2 – 6 % and 7 – 14 % respectively.

### 2.3 System comparison

In this section a comparison of the system models is facilitated. Fig. 5 shows the annual net utilized solar energy as function of the space heating demand and the domestic hot water consumption. The figure also shows the performance ratio where the reference system in all cases is the similar system model 1. In this way it can be seen how much better model 2.1 and model 3.1 perform than model 1.1 or how much better model 2.2 and model 3.2 perform than model 1.2 and so forth.

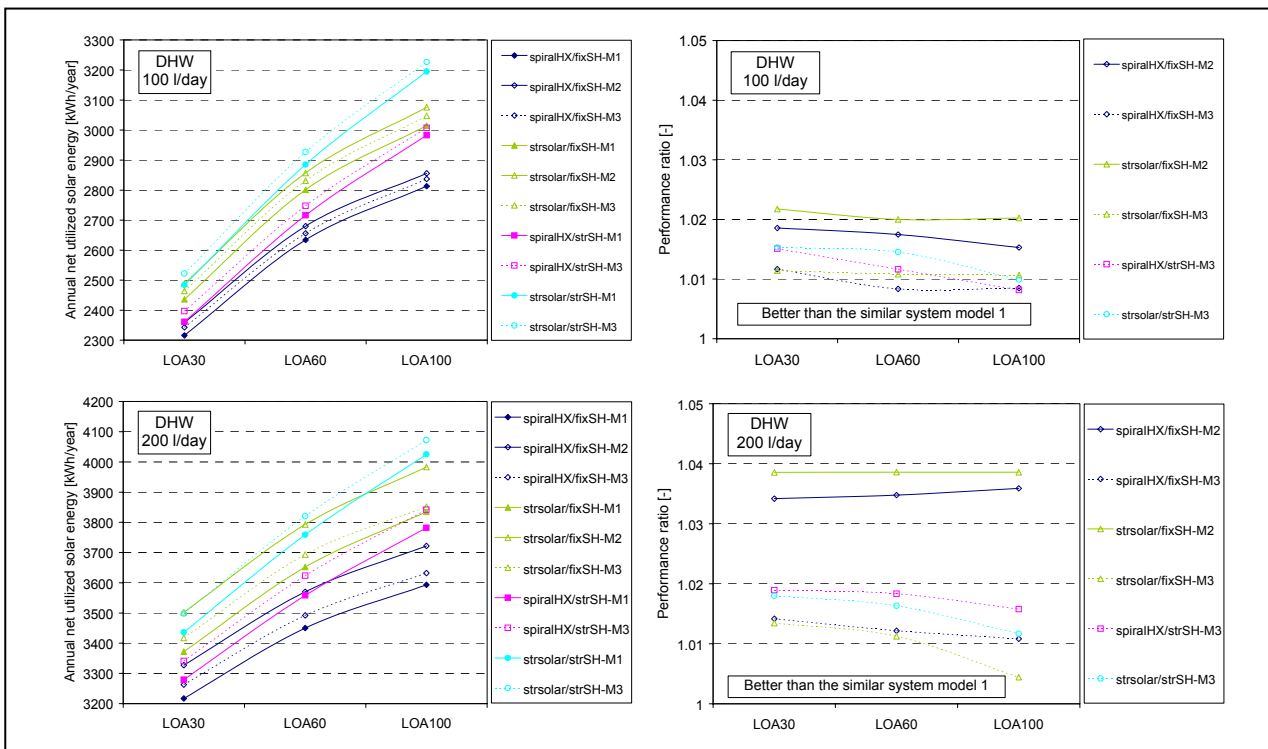


Fig. 5: Comparison of model 1, model 2 and model 3. Left: The annual net utilized solar energy as a function of the space heating demand and the domestic hot water consumption for model 1, model 2 and model 3 and the step by step improvement of the models. Right: The performance ratio relative to the thermal performance of the similar system model 1.

Figure 5 shows that model 1 has always the lowest thermal performance compared to the similar model 2 and model 3. Further, it can be seen that model 2 has the highest thermal performance compared to the similar model 1 and model 3 and that model 3 always perform better than model 1. The best performing system is the tank in tank system with inlet stratifiers in the solar collector loop and in the space heating loop.

The reason why model 2 is performing better than the similar model 1 and model 3 is most likely because the tank is a domestic hot water tank where the incoming cold water is directly utilized to cool the lower part of the tank. In model 1 the water returning from the domestic hot water heat exchanger to the tank is somewhat warmer than the cold water temperature. In model 3 the incoming cold water reaches a higher level in the heat storage after a domestic hot water draw off caused by the shape of the inner tank. The reason why model 3 is performing better than model 1 is most likely due to the higher tank heat loss coefficient of model 1 since the heat loss coefficients of the sidearm and the external domestic hot water heat exchanger are added to the tank heat loss coefficient. A further disadvantage for model 1 is that the set point temperature of the auxiliary volume must be about 10 – 15 K higher than the required hot water temperature to meet the hot water demand. The set point temperature in model 2 and model 3 only needs to be slightly higher than the required hot water temperature to meet the same demand. This effect is not investigated by calculations in this paper.

The performance ratio is mostly higher for high domestic hot water consumption than for low domestic hot water consumption and higher for low space heating demand. Model 2 and model 3 perform better than the similar model 1. With low domestic hot water consumption the performance increase is in the range of 1.5 – 2.2 % and 0.8 – 1.5 % respectively and with high domestic hot water consumption, in the range of 3.4 – 3.9 % and 0.4 – 1.9 % respectively.

### 3 FURTHER INVESTIGATIONS OF SOLAR COMBI SYSTEMS

In this section it is investigated how the space heating system influence the thermal performance of solar combi systems. Also the influence on the thermal performance by different operation conditions of the control system for the solar collector loop is investigated. The investigation is only carried out for system model.

#### 3.1 Space heating system

The size of the space heating system is varied for the house with heating load of about 60 kWh/(m<sup>2</sup>·year). Three sizes of space heating systems are taken into calculation: a small space heating system, a standard space heating system and a large space heating system. The flow and return temperatures for the space heating systems as a function of the heating power demand taken into calculation are shown in Fig. 6.

In Fig. 7 the annual net utilized solar energy as a function of the relative return inlet height from the space heating loop and the performance ratio relative to the optimal thermal performance of the system in question is shown. In Fig. 8 the performance ratio relative to the optimal thermal performance of the system with the standard space heating system is shown.

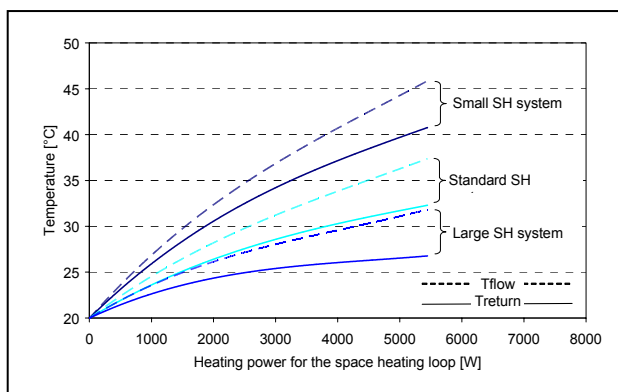


Fig. 6: The flow and return temperatures for the space heating systems as a function of the heating power demand.

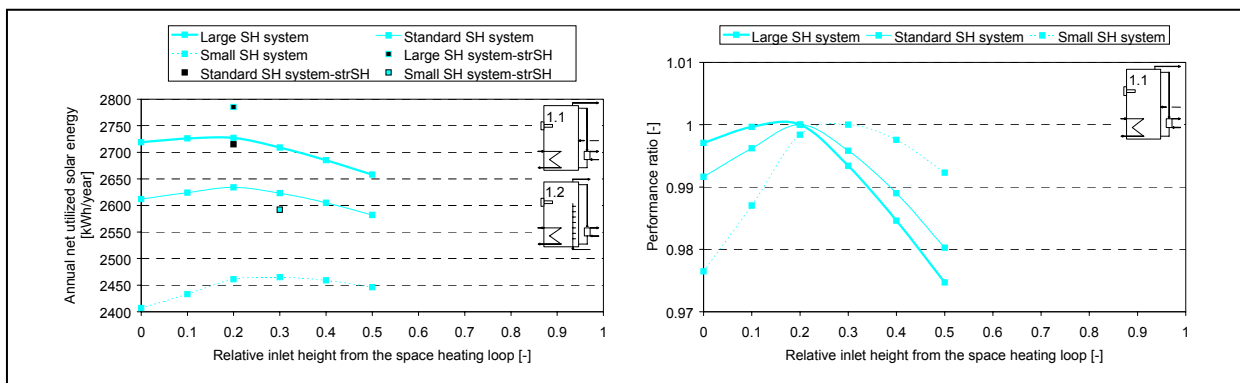


Fig. 7: Left: The annual net utilized solar energy as a function of the relative return inlet height from the space heating loop. Right: The performance ratio relative to the optimal thermal performance of the system in question.

Figure 7 shows that the annual net utilized solar energy is strongly influenced by the size of the space heating system. Also the optimal relative return inlet height from the space heating loop is influenced by the size of the space heating system. For small space heating systems, the optimal relative return inlet height increases while the optimal return inlet height increases for large space heating systems. Further, the figure shows the benefit of replacing the fixed inlet from the space heating loop with a stratifier and it can be seen that the largest improvement of the thermal performance is achieved

for small space heating systems. This is caused by the fact that the return inlet temperature varies most for small space heating systems.

The net utilized solar energy is reduced less than 1 % if the relative return inlet position from the space heating loop is between 0.2 and 0.3 and less than 2 % if the relative return inlet position is between 0.1 and 0.4.

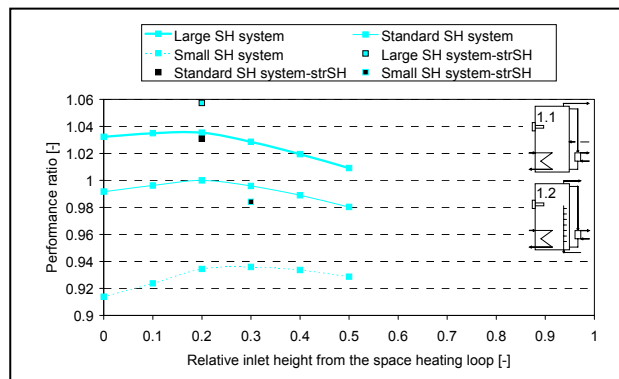


Fig. 8: The performance ratio as a function of the relative return inlet height from the space heating loop. The performance is relative to the optimal thermal performance of the system with the standard space heating system.

From Fig. 8 it can be seen that the thermal performance of solar combi systems is strongly influenced by the size of the space heating system.

The thermal performance of model 1.1 with the standard space heating system increases with about 3 % when a stratifier is used in the space heating loop instead of a fixed return inlet height. The thermal performance of model 1.1 and model 1.2 with the large space heating system is about 4 % and about 6 % higher than the thermal performance of model 1.1 with the standard space heating system. The thermal performance of model 1.1 and model 1.2 with the small space heating system is about 6 % and about 2 % lower than the thermal performance of model 1.1 with the standard space heating system.

### 3.2 Control system in the solar collector loop

The position of the temperature sensor mounted in the tank and the stop temperature difference that controls the operation of the pump in the solar collector loop is investigated for different conditions:

- Space heating demand
- Domestic hot water consumption
- Domestic hot water consumption pattern
- Fixed inlet height or stratified inlet from the space heating loop
- Volume flow rate in the solar collector loop

In Fig. 9 the different positions of the temperature sensor mounted in the tank is shown. The numbers next to the temperature sensors, seen to the right in the figure correspond to the relative height of the tank. The relative heights 0.3 and 0.065 correspond to the top and the bottom of the heat exchanger while the relative heights of 0.18, 0.14, 0.085 and 0.075 correspond to 1/2, 1/3, 1/10 and 1/20 of the heat exchanger height calculated from the bottom of the heat exchanger.

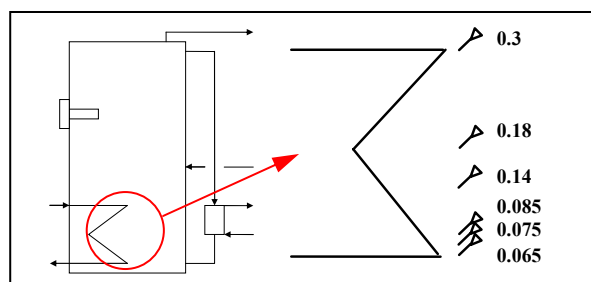


Fig. 9: Different positions of the temperature sensor in the tank.

Figure 10 shows the net utilized solar energy for model 1.1 as a function of the position of the temperature sensor in the tank and the stop temperature difference for the pump in the solar collector loop and the performance ratio relative to the

optimal thermal performance of the system in question. The space heating demand is 30, 60 and 100 kWh/(m<sup>2</sup>·year), the domestic hot water consumption is 100 l/day and domestic hot water is tapped at 7 am, noon and 7 pm. The volume flow rate is 1.2 l/(min·m<sup>2</sup>).

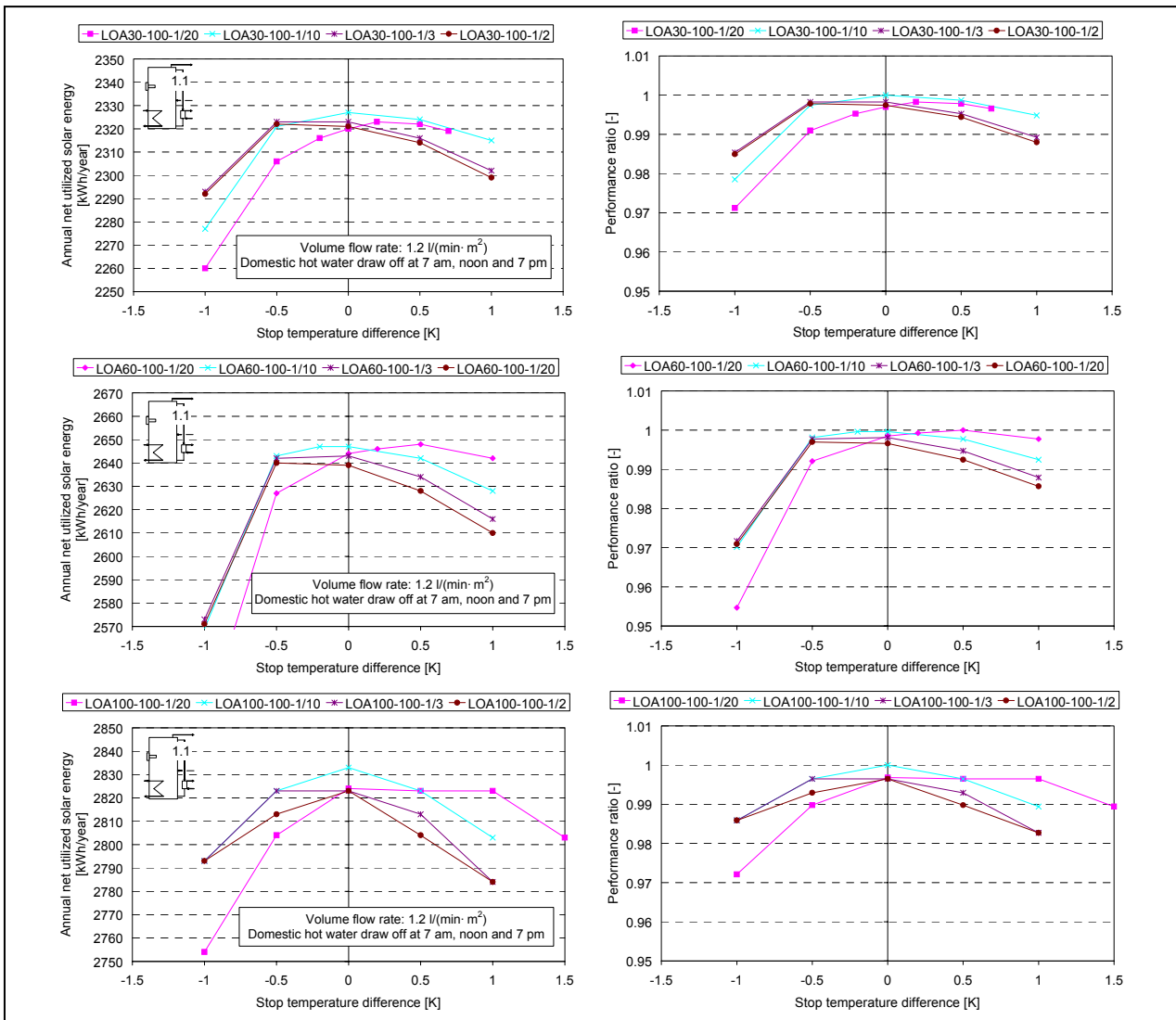


Fig. 10: Left: The annual net utilized solar energy as a function of the position of the temperature sensor in the tank and the stop temperature difference of the pump in the solar collector loop. Right: The performance ratio relative to the thermal performance of the system with the highest thermal performance.

From Fig. 10 it can be seen that the optimal position of the temperature sensor is 1/10 of the heat exchanger height from the bottom of the heat exchanger with a stop temperature difference of 0 K regardless of the space heating demand. Also it can be seen that for lower stop temperature differences the optimal position of the temperature sensor is higher than 1/10 of the heat exchanger height while for higher stop temperature differences the optimal position of the temperature sensor is lower than 1/10 of the heat exchanger height.

The net utilized solar energy is reduced less than 1 % if the stop temperature difference is between -0.5 K and 0.5 K and the temperature sensor is positioned between 1/20 and 1/2 of the heat exchanger height.

Figure 11 shows the net utilized solar energy for model 1.3 as a function of the position of the temperature sensor in the tank and the stop temperature difference for the pump in the solar collector loop and the performance ratio relative to the thermal performance of the system with the highest thermal performance. The space heating demand is 60 kWh/(m<sup>2</sup>·year), the domestic hot water consumption is 100 l/day and 200 l/day and domestic hot water is tapped at 7 am, noon and 7 pm. The volume flow rate in the solar collector loop is 1.2 l/(min·m<sup>2</sup>).

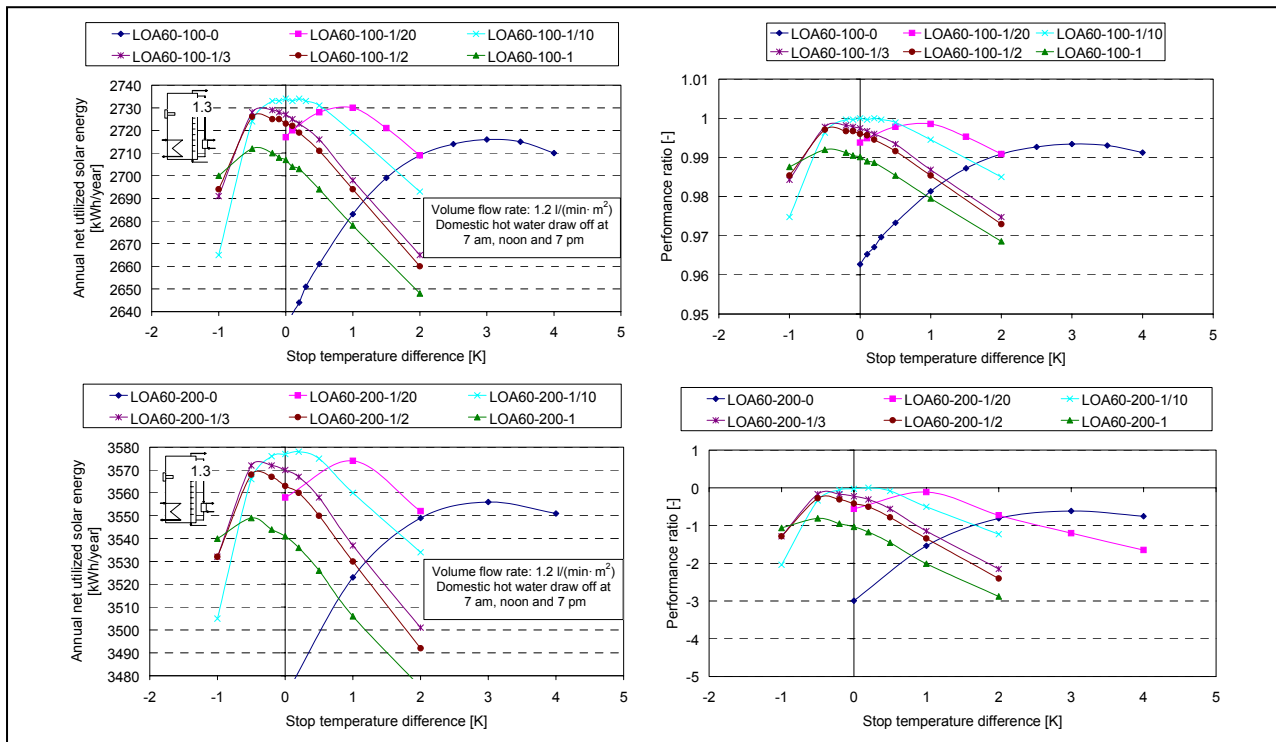


Fig. 11: Left: The annual net utilized solar energy as a function of the position of the temperature sensor in the tank and the stop temperature difference of the pump in the solar collector loop. Right: The performance ratio relative to the thermal performance of the system with the highest thermal performance.

From Fig. 11 it can be seen that the optimal position of the temperature sensor is 1/10 of the heat exchanger height with a stop temperature difference of between 0 K and 0.5 K regardless of the domestic hot water consumption. Also it can be seen that for lower stop temperature differences, the optimal position of the temperature sensor is higher than 1/10 of the heat exchanger height while for higher stop temperature differences the optimal position of the temperature sensor is lower than 1/10 of the heat exchanger height. Also it can be seen that the optimal stop temperature difference is increased in the system with stratified inlet from the space heating loop with about 0.5 K compared to the system with a fixed return inlet height from the space heating loop. This increase is probably due a destruction of the thermal stratification in the tank with stratifier in the space heating loop if the temperature from the solar collector is too low.

The net utilized solar energy is reduced less than 1 % if the stop temperature difference is between -0.5 K and 0.5 K and the temperature sensor is positioned between 1/20 and 1/2 of the heat exchanger height.

Figure 12 shows the net utilized solar energy for model 1.1 as a function of the position of the temperature sensor in the tank and the stop temperature difference for the pump in the solar collector loop and the performance ratio relative to the thermal performance of the system with the highest thermal performance. The space heating demand is 60 kWh/(m<sup>2</sup>·year), the domestic hot water consumption is 100 l/day and domestic hot water is tapped in the morning at 6 am, 7 am and 8 am or in the evening at 7 pm, 8 pm and 9 pm. The volume flow rate in the solar collector loop is 1.2 l/(min·m<sup>2</sup>).

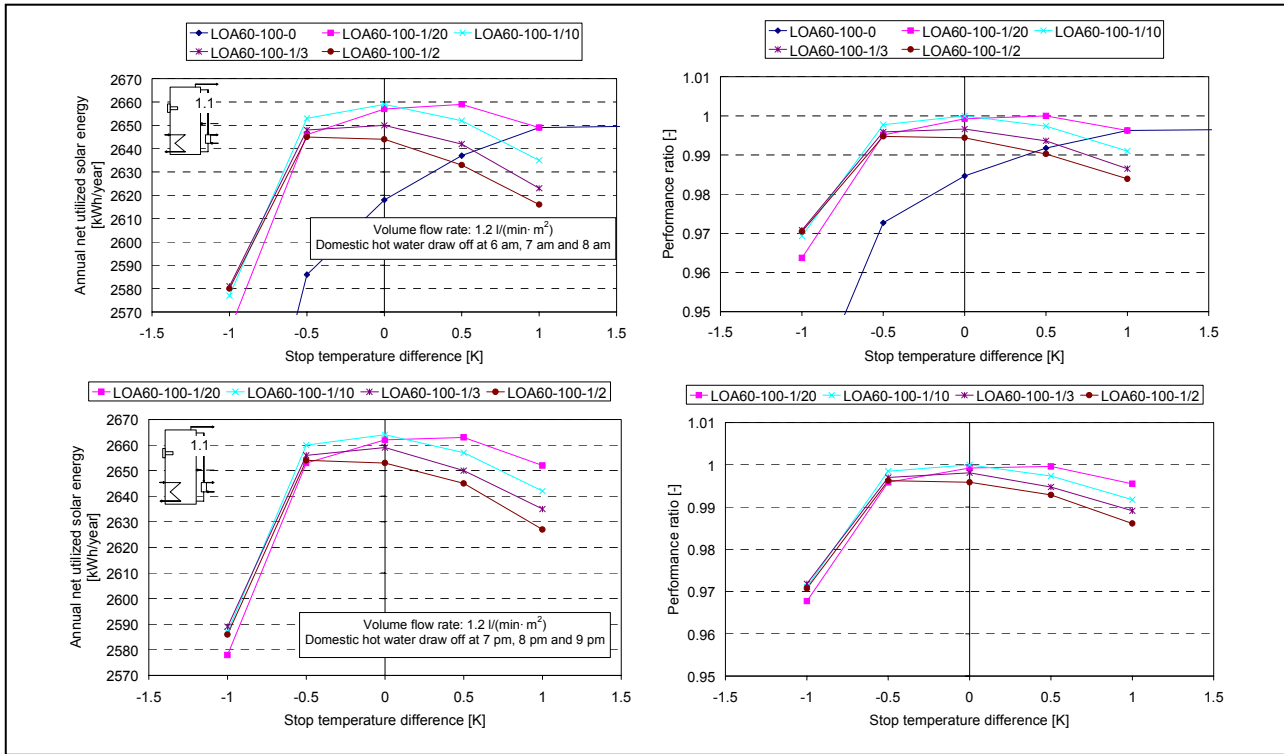


Fig. 12: Left: The annual net utilized solar energy as a function of the position of the temperature sensor in the tank and the stop temperature difference of the pump in the solar collector loop. Right: The performance ratio relative to the thermal performance of the system with the highest thermal performance.

From Fig. 12 it can be seen that the optimal position of the temperature sensor is again 1/10 of the heat exchanger height with a stop temperature difference of 0 K regardless of the domestic hot water consumption pattern. Also it can be seen, that for lower stop temperature differences the optimal position of the temperature is higher than 1/10 of the heat exchanger height while for higher stop temperature differences the optimal position of the temperature sensor is lower than 1/10 of the heat exchanger height.

The net utilized solar energy is reduced less than 1 % if the stop temperature difference is between -0.5 K and 0.5 K and the temperature sensor is positioned between 1/20 and 1/2 of the heat exchanger height.

Figure 13 shows the net utilized solar energy for model 1.1 and model 1.3 as a function of the position of the temperature sensor in the tank and the stop temperature difference for the pump in the solar collector loop. The space heating demand is 60 kWh/(m<sup>2</sup>·year), the domestic hot water consumption is 100 l/day and domestic hot water is tapped at 7 am, noon and 7 pm. The volume flow rate in the solar collector loop is 0.5 l/(min·m<sup>2</sup>) or 0.2 l/(min·m<sup>2</sup>).

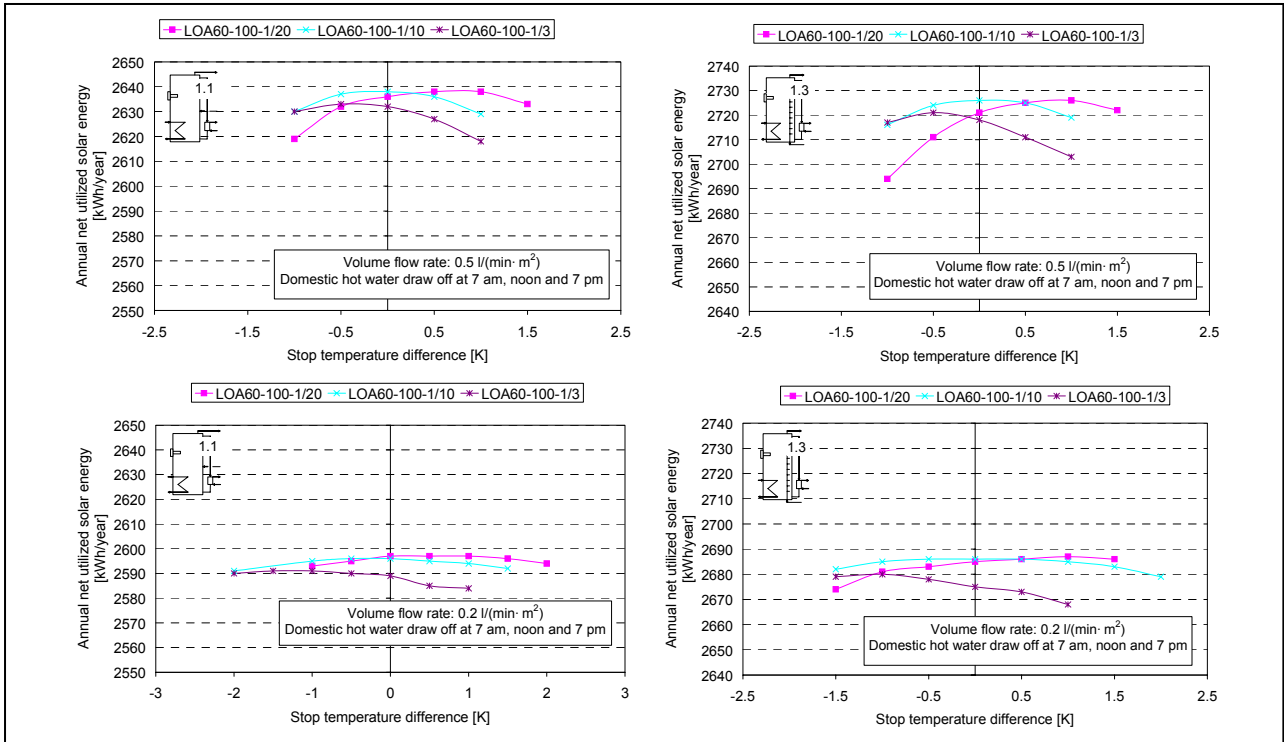


Fig. 13: The annual net utilized solar energy as a function of the position of the temperature sensor in the tank and the stop temperature difference of the pump in the solar collector loop for model 1.1 and model 1.3.

From Fig. 13 it can be seen that the optimal position of the temperature sensor is 1/10 of the heat exchanger height with a stop temperature difference of 0 K regardless of the volume flow rate in the solar collector loop. Also it can be seen that for lower stop temperature differences the optimal position of the temperature is higher than 1/10 of the heat exchanger height while for higher stop temperature differences the optimal position of the temperature sensor is lower than 1/10 of the heat exchanger height. Finally it can be seen that the net utilized solar energy is decreased when the volume flow rate in the solar collector loop is decreased.

Fig. 14 shows the net utilized solar energy for model 1.1 as a function of the position of the temperature sensor in the tank and the stop temperature difference for the pump in the solar collector loop. The space heating demand is 60 kWh/(m<sup>2</sup>·year), the domestic hot water consumption is 100 l/day and domestic hot water is tapped at 7 am, noon and 7 pm. The volume flow rate in the solar collector loop is 1.2 l/(min·m<sup>2</sup>) and the length of the pipe from/to the solar collector to/from the tank is 10 m and 15 m.

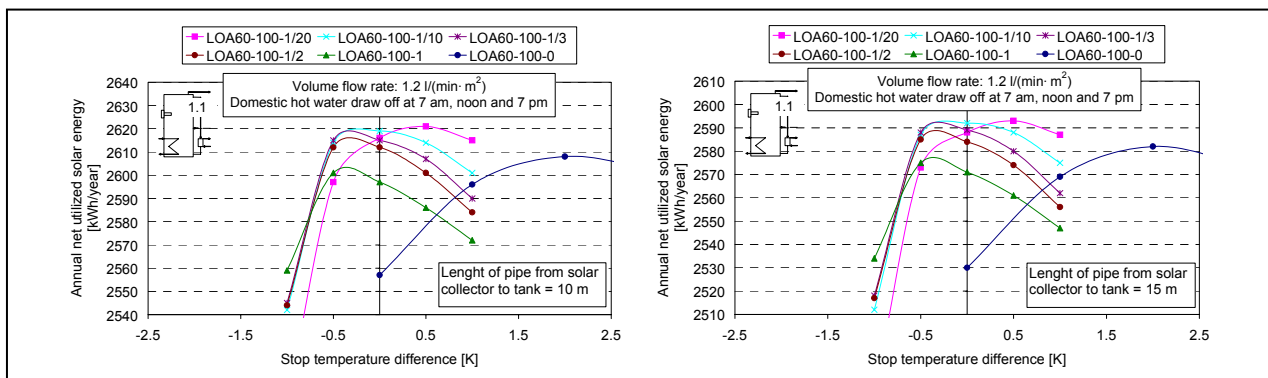


Fig. 14: The annual net utilized solar energy as a function of the position of the temperature sensor in the tank and the stop temperature difference of the pump in the solar collector loop.

From Fig. 14 it can be seen, that the optimal position of the temperature sensor is between 1/10 and 1/20 of the heat exchanger height with a stop temperature difference of 0 K or 0.5 K respectively. Further it can be seen that net utilized solar energy decreases when the length of the pipes in the solar collector loop increases. The pipe length does not influence the optimal position of the temperature sensor or the stop temperature difference. For lower stop temperature

differences the optimal position of the temperature is higher than 1/10 of the heat exchanger height while for higher stop temperature differences the optimal position of the temperature sensor is lower than 1/10 of the heat exchanger height.

Figure 15 shows the system utilized solar energy for model 1.1 as a function of the position of the temperature sensor in the tank and the stop temperature difference for the pump in the solar collector loop. The space heating demand is 60 kWh/(m<sup>2</sup>-year), the domestic hot water consumption is 100 l/day and domestic hot water is tapped at 7 am, noon and 7 pm. The volume flow rate in the solar collector loop is 1.2 l/(min·m<sup>2</sup>) and the length of the pipe from/to the solar collector to/from the tank is 10 m and 15 m.

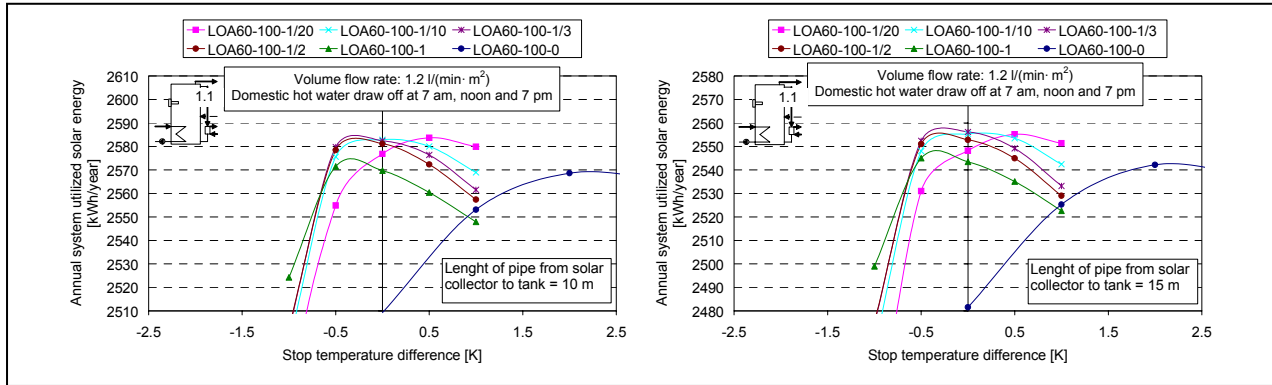


Fig. 15: The system utilized solar energy as a function of the position of the temperature sensor in the tank and the stop temperature difference of the pump in the solar collector loop.

From Fig. 15 it is obvious that the optimal position of the temperature sensor in the tank and the stop temperature difference are not influenced by including the energy consumption of the circulation pump in the calculated thermal performance.

Fig. 16 shows the net utilized solar energy for model 1.2 and model 1.4 as a function of the position of the temperature sensor in the tank and the stop temperature difference for the pump in the solar collector loop. The figure also shows the system utilized solar energy for with one pump and with two pumps in the solar collector loop. The space heating demand is 60 kWh/(m<sup>2</sup>-year), the domestic hot water consumption is 100 l/day and domestic hot water is tapped at 7 am, noon and 7 pm. The volume flow rate in the solar collector loop is 0.17 l/(min·m<sup>2</sup>). For the system with an external heat exchanger in the solar collector loop the volume flow rate is 0.17 l/(min·m<sup>2</sup>) on both sides of the heat exchanger..

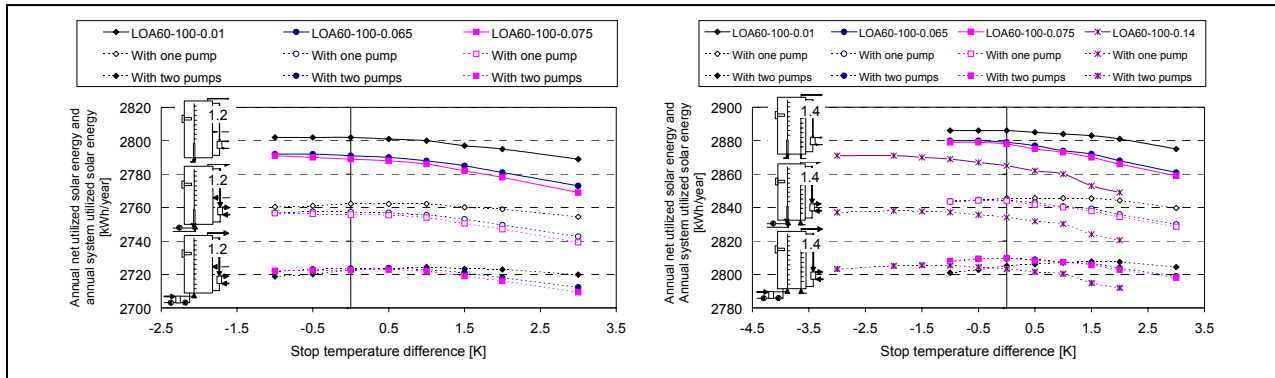


Fig. 16: The annual net utilized solar energy and the system utilized solar energy as a function of the position of the temperature sensor in the tank and the stop temperature difference of the pump in the solar collector loop.

From Fig. 16 it can be seen that the best position of the temperature sensor in the tank is at the bottom of the tank. Further it can be seen that the thermal performance is hardly influenced by the stop temperature difference in the range from -1 K to 2 K.

#### 4 THEORETICAL INVESTIGATIONS OF DIFFERENTLY SIZES SOLAR COMBI SYSTEMS

In this section it is investigated how the size of the solar combi system influences the thermal performance. The investigation is carried out for system model 1. The data for the models are described in Table 2. Data for the solar collector, the solar collector loop and the control system in the solar collector loop are described in Table 1.

In Fig. 17 the annual net utilized solar energy as function of the relative return inlet height from the space heating loop for different sizes of model 1 are shown. Further, the performance ratio relative to the optimal thermal performance of the system in question is shown.

Figure 16 shows the yearly net utilized solar energy as function of the space heating demand and the domestic hot water consumption for model 1 with 500 litre, 1000 litre and 1500 litre storage tanks and 10 m<sup>2</sup>, 20 m<sup>2</sup> and 30 m<sup>2</sup> solar collector areas respectively and the step by step improvement of the models. Also the performance ratio relative to the performance of the least advanced model 1.1 is shown. In all the calculations with a fixed return inlet height from the space heating loop, the optimal return inlet height shown in Fig. 17 is used.

Figure 17 shows the monthly net utilized solar energy for the three differently sized models 1 and the step by step improvement of the models. Also the monthly solar radiation per m<sup>2</sup> on the solar collector is shown. Finally, Fig. 19 shows the extra net utilized solar energy gained by replacing the heat exchanger spiral in the solar collector loop and the fixed return inlet height from the space heating loop with stratifiers. The calculations are made for a space heating demand of about 60 kWh/(m<sup>2</sup> year) with a domestic hot water consumption of 100 l/day.

In Table 3 the annual benefit of a stratifier in the solar collector loop or in the space heating loop or in both the solar collector loop and the space heating loop is shown.

Table 2: Data for the solar combi systems used in the calculations.

<b>Solar collector</b>	
Solar collector area	10 m <sup>2</sup> / 20 m <sup>2</sup> / 30 m <sup>2</sup>
<b>Tank</b>	
Storage volume	500 l / 1000 l / 1500 l
Auxiliary volume	190 l
Height of tank	1.5 m / 2 m / 2.5 m
Diameter of tank	0.652 m / 0.798 m / 0.874 m
Heat loss coefficient, tank	2.42 W/K / 3.82 W/K / 5.09 W/K
Heat loss coefficient, sidearm / DHW heat exchanger	0.39 W/K / 0.37 W/K
Heat transfer coefficient of external heat exchanger when stratifier in solar collector loop is used, UA	1000 W/K / 1500 W/K / 3000 W/K
Heat transfer coefficient of: spiral in solar collector loop	75 W/K per m <sup>2</sup>
Volume between temperature sensor and the lowest part of the auxiliary volume	50 l
Efficiency of auxiliary energy supply system	100%
Relative in-/outlet height of DHW	0 / 1
Relative outlet height of SH system (fixed inlet)	0.98
Relative in-/outlet height of spiral in solar collector loop	0.305 / 0.06

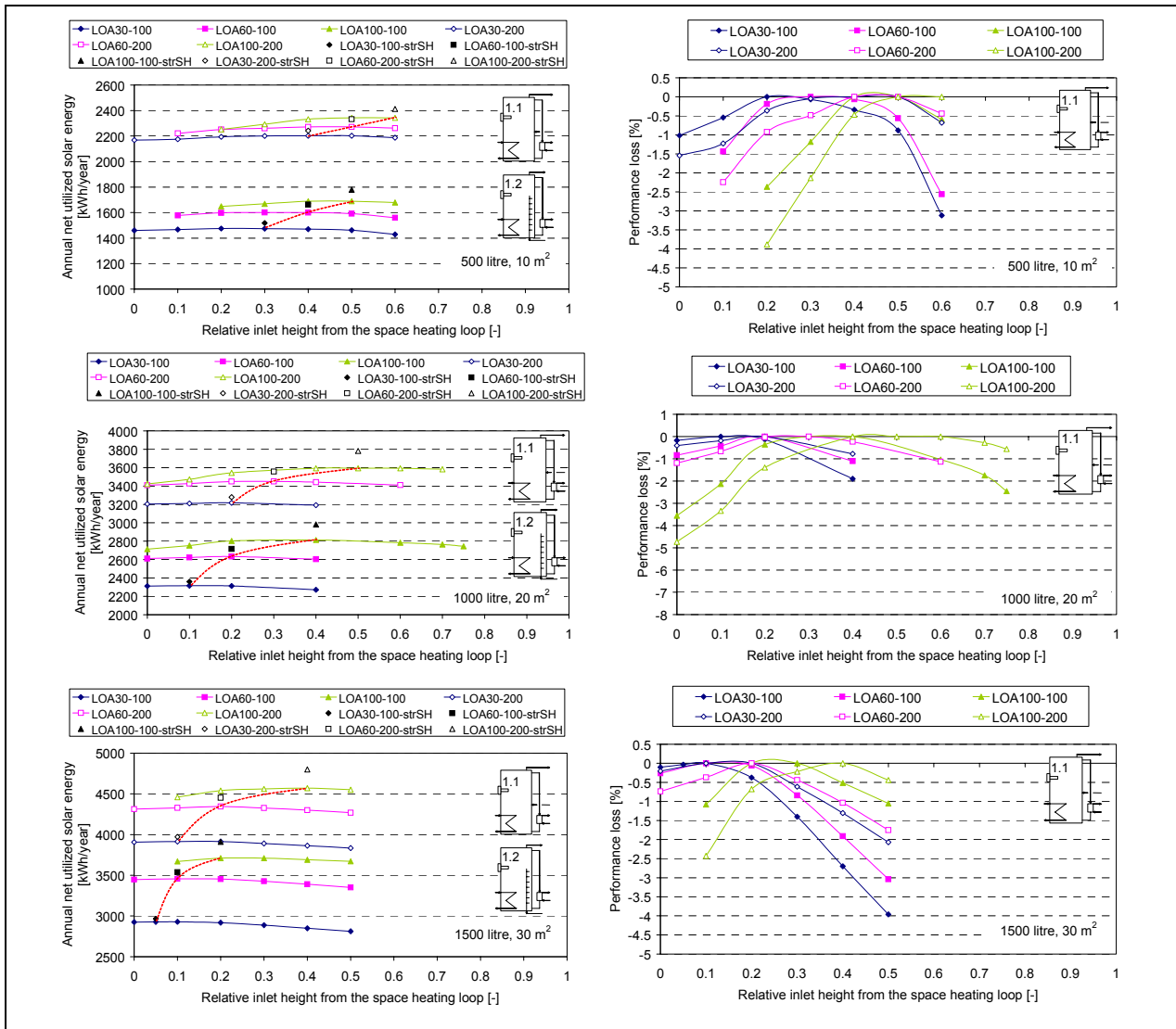


Fig. 17: Left: The Annual net utilized solar energy as a function of the relative return inlet height from the space heating loop for different sizes of model 1.1 and model 1.2. Right: The performance ratio relative to the optimal thermal performance of the system in question.

The figure show that the optimal inlet position from the space heating loop varies with the daily domestic hot water consumption and the space heating demand. For low space heating demand and thereby low return inlet temperatures from the space heating loop, the optimal inlet position is low. For increasing space heating demand and thereby increasing return inlet temperature from the space heating loop, the height of the optimal inlet position increases. Also the optimal return inlet position from the space heating loop increases for increasing domestic hot water consumption. This is due to a larger amount of cold water in the bottom of the tank which leaves the warmer water that matches the temperature of the return water form the space heating loop at a higher level in the tank.

The tendency is that the relative inlet position from the space heating loop is lower for larger systems than for smaller systems. However, the absolute inlet position as well as the volume below the inlet from the space heating loop is in the same range for all three systems.

For model 1 with 500 litre tank and 10 m<sup>2</sup> solar collector area, the thermal performance loss is less than 1 % for all the systems models if the relative return inlet position from the space heating loop is between 0.4 and 0.5 and less than 2 % if the relative inlet position is between 0.3 and 0.5. The best relative position of the inlet is 0.4.

For model 1 with 1000 litre tank and 20 m<sup>2</sup> solar collector area, the thermal performance loss is less than 1 % for all the system models if the relative return inlet position from the space heating loop is 0.3 and less than 2 % if the relative inlet position is between 0.2 and 0.4. The best relative position of the inlet is 0.3.

For model 1 with 1500 litre tank and 30 m<sup>2</sup> solar collector area, the thermal performance loss is less than 1 % for all the system models if the relative return inlet position from the space heating loop is 0.2 and less than 2 % if the relative inlet position is between 0.2 and 0.3. The best relative position of the inlet is 0.2.

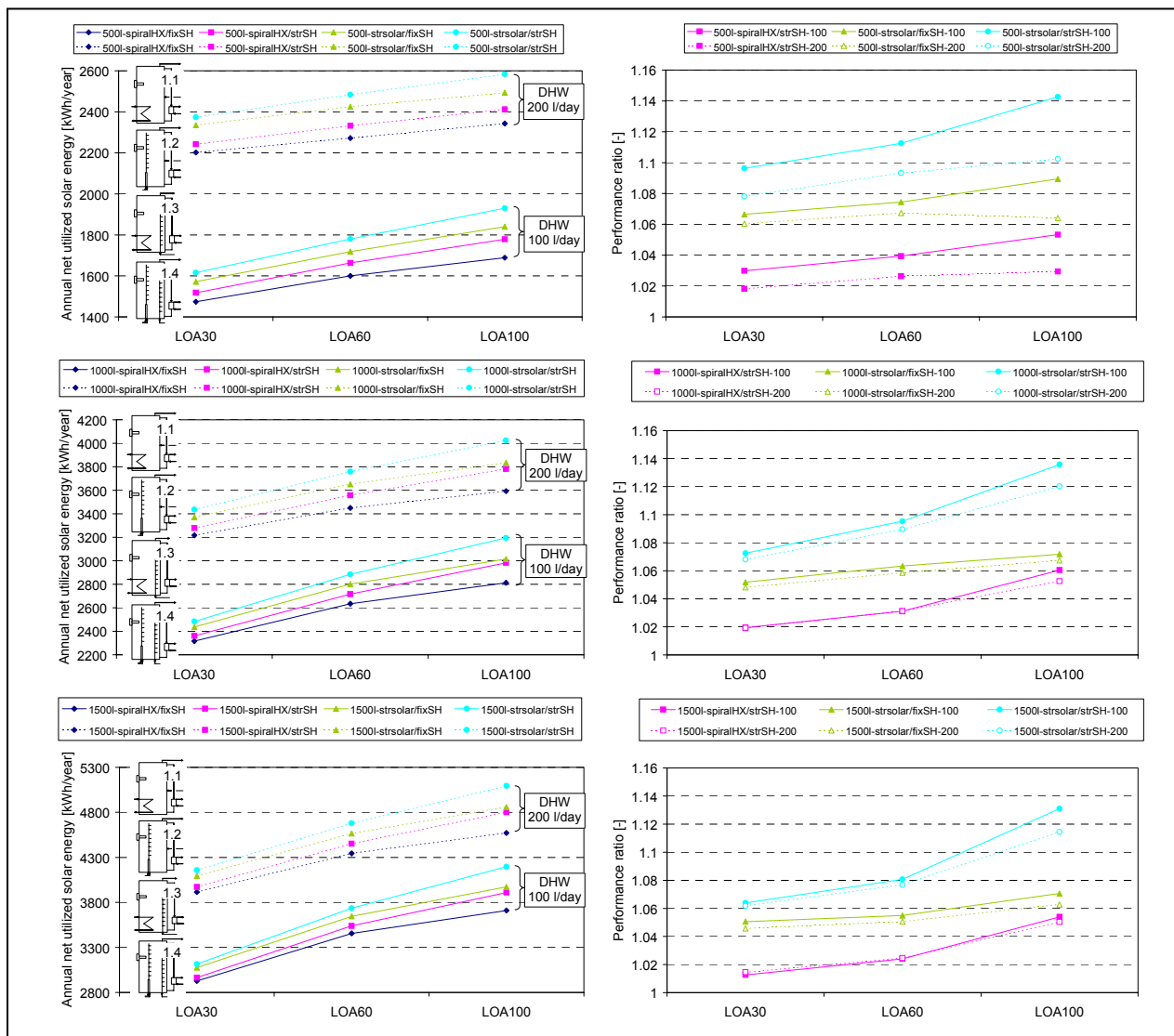


Fig. 18: Left: The annual net utilized solar energy as function of the space heating demand and the domestic hot water consumption for different sizes of model 1 and the step by step improvement of the model. Right: The performance ratio relative to the thermal performance of the least advanced model 1.1.

The figure shows that the thermal performance increases for increasing space heating demand and increasing domestic hot water consumption. Also, the figure shows that the thermal performance increases when the heat exchanger spiral in the solar collector loop and the fixed return inlet from the space heating loop are replaced with stratifiers and most when the heat exchanger spiral in the solar collector loop is replaced with a stratifier.

The performance ratio of the system by using inlet stratifiers is almost the same regardless of the size of the solar combi system.

The increase in net utilized solar energy by using a stratifier in the solar collector loop or in the space heating loop or in both the solar collector loop and in the space heating loop is in the range of 5 – 9 %, 1 – 6 % and 6 – 14 % respectively. The additional gained net utilized solar energy by using stratifiers is increasing for increasing space heating demand. This is due to the return temperature from the space heating system which is higher for high space heating demands than for low space heating demands. Hence the variation in the return temperature from the space heating system is higher for high space heating demands than for low space heating demands and this leads to a better utilization of a stratifier.

Figure 19 shows the monthly net utilized solar energy for the three different sizes of model 1.1, model 1.2, model 1.3 and model 1.4 and the extra monthly net utilized energy gained by the step by step improvement of model 1. The space heating demand is 60 kWh/(m<sup>2</sup>·year), the domestic hot water consumption is 100 l/day. In Table 3 the values are listed.

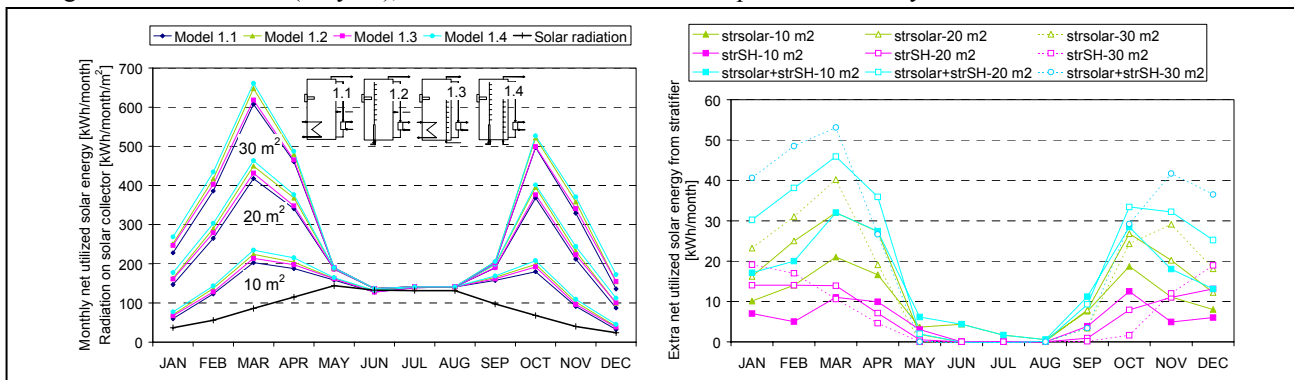


Fig. 19: Right: Monthly net utilized solar energy for the three differently sizes model 1.1, 1.2, 1.3 and 1.4 with solar collector areas of 10 m<sup>2</sup>, 20 m<sup>2</sup> and 30 m<sup>2</sup>. Left: Extra net utilized solar energy by introducing stratifiers.

From Fig. 19 it is obvious that the solar fraction is 100 % during the summer months and that the large amounts of solar radiation in this period is not utilized. Further, it is obvious that the increased performance of larger solar combi systems is due to higher utilization of the solar radiation during spring and autumn. Also the figure shows that small solar combi systems benefit from stratifiers in the space heating loop during a longer period than larger systems due to the lower solar fraction for small systems. For high solar fractions there is little or no benefit by using stratifiers.

Table 3: Extra net utilized solar energy with stratifier in solar collector loop or in space heating loop.

Solar collector area	10 m <sup>2</sup>	20 m <sup>2</sup>	30 m <sup>2</sup>
Net utilized solar energy for model 1.1	1600 kWh/year	2634 kWh/year	3456 kWh/year
Solar fraction for model 1.1	14.3 %	23.6 %	31 %
Extra net utilized solar energy for model 1.2	117 kWh/year	167 kWh/year	188 kWh/year
Solar fraction for model 1.2	14.9 %	24.3 %	31.7 %
Extra net utilized solar energy for model 1.3	63 kWh/year	82 kWh/year	84 kWh/year
Solar fraction for model 1.3	15.4 %	25.1 %	25.8 %
Extra net utilized solar energy for model 1.4	180 kWh/year	252 kWh/year	279 kWh/year
Solar fraction for model 1.4	15.9 %	32.6 %	33.5 %

From Table 3 it can be seen that large solar combi systems benefit more from stratifiers in the solar collector loop than small and medium sized systems although the additional benefit for large systems compared to the additional benefit for medium sized systems is much smaller than the additional benefit for medium sized systems compared to the additional benefit for small systems. The benefit from stratifiers in the space heating loop is largest for medium sized and large solar combi systems and only slightly larger than the benefit from stratifiers in small systems. Finally it is seen, that the extra net utilized solar energy for a system with stratifiers in both the solar collector loop and the space heating loop equals the sum of the extra net utilized solar energy of the system with only one stratifier in the solar collector loop and the system with only one stratifier in space heating loop.

## 5 CONCLUSIONS

Three basically differently designed solar combi system models are investigated theoretically. One model is based on a space heating storage with an external heat exchanger mounted in a side arm for domestic hot water preparation, one model is based on a domestic hot water tank with an internal heat exchanger spiral for the space heating system and one model is based on a tot water tank in tank storage. Further, it is investigated how stratifiers in the solar collector loop and the space heating loop and in both the solar collector loop and the space heating loop influence the thermal performance of the investigated systems. The solar combi system systems have a storage volume of 1000 litre with 20 m<sup>2</sup> solar collector area.

Also, three differently sized of solar combi systems are investigated. The different system sizes are: 500 litre, 1000 litre and 1500 litre with 10 m<sup>2</sup>, 20 m<sup>2</sup>, 30 m<sup>2</sup> respectively.

Apart from the above mentioned investigations, the investigation includes the size of the space heating demand, the domestic hot water consumption, the size of the space heating system and the control system for the solar collector loop.

It is found that:

- The thermal performance increases for increasing space heating demand and domestic hot water consumption.
- The thermal performance is strongly increased for increasing size of the space heating system.
- The thermal performance increases with 5 – 8 % if stratifiers are used only in the solar collector loop.
- The thermal performance increases with 2 – 6 % if stratifiers are used only in the space heating loop.
- The thermal performance increases with 7 – 14 % if stratifiers are used both in the solar collector loop and in the space heating loop
- The thermal performance increase by using stratifiers is highest for small space heating systems and for houses with large heating demands.
- The best performing solar combi system is based on a tank in tank storage with stratifiers both in the solar collector loop and the space heating loop.
- If the system has a direct return inlet from the space heating loop to the storage, the optimal relative inlet position from the space heating loop is lower for larger systems than for smaller systems, while the absolute inlet position as well as the volume below the inlet from the space heating loop is in the same range. The optimal volume below the inlet is between 200 litre and 300 litre, increasing with increasing tank size.
- In a tank with heat exchanger in the solar collector loop (high flow system), the best position of the temperature sensor in the tank for controlling the pump in the solar collector loop is 1/10 of the heat exchanger height calculated from the bottom of the heat exchanger with a stop temperature difference between 0 K and 0.5 K.
- In a tank with stratifier in the solar collector loop (low flow system), the best position of the temperature sensor in the tank for controlling the pump in the solar collector loop is in the bottom of the tank with a stop temperature difference between 0.5 K and 2 K.
- The domestic hot water consumption pattern does not influence the optimal settings of the control system in the solar collector loop.
- In a tank with stratifiers both in the solar collector loop and the space heating loop, the optimal stop temperature difference increases with about 0.5 K while the best position for the temperature sensor in the tank is unchanged compared to a system with heat exchanger spiral in the solar collector loop and fixed return inlet or a stratifier in the space heating loop.
- The increased performance of larger solar combi systems is due to higher utilization of the solar radiation during spring and autumn.
- Small solar combi systems benefit from stratifiers in the space heating loop during a longer period than larger systems due to a lower solar fraction.
- The extra net utilized solar energy for a system with stratifiers in both the solar collector loop and the space heating loop equals the sum of the extra net utilized solar energy of the system only with stratifier in the solar collector loop and the system only with stratifier in space heating loop.

## 6 REFERENCES

- (1) Andersen E., Furbo S., Fan J., Investigations of fabric stratifiers for solar tanks, Proceedings of ISES Solar World Congress 2005, Orlando, Florida, USA, 2005.
- (2) Drück H., MULTIPORT Store – Model, Type 140 for TrnSys. Institut für Thermodynamik und Wärmetechnik. Universität Stuttgart, 2000.
- (3) Klein S.A et al., TRNSYS 15, User Manual. University of Wisconsin Solar Energy Laboratory, 1996.
- (4) Skertveit, A., Lund, H., and Olseth, J. A., Design Reference Year, Report no. 1194 Klima, Det Norske Institutt, 1994.
- (5) Streicher W., Heimrath R., Sensivität von Systemparametern von solaren Kombisystemen – Analyse der simulierten Systeme des IEA SHC Task 26. Thermische Solarenergie Symposium, Bad Staffelstein, 2005.
- (6) Weiss et al., Solar Heating Systems for Houses, a Design Handbook for Solar Combisystems. James & James Ltd, London. ISBN 1 902916 46 8, 2003.